AD-A151 467

DESIGN AND ANALYSIS OF COMPOSITE ROADWHEELS
FOR LVTP7 AND M113A1

August 1984

KEITH BURGESS, JOHN PEPIN, and STEPHEN BIDDLE
Fiber Materials, Inc.
Biddeford, Maine 04005

FINAL REPORT   Contract No. DAAG46-83-C-0026

Prepared for

ARMY MATERIALS AND MECHANICS RESEARCH CENTER
Watertown, Massachusetts 02172-0001

85 03 20 001

The findings in this report are not to be construed as an official Department of the Army position, unless so designated by other authorized documents.

Mention of any trade names or manufacturers in this report shall not be construed as advertising nor as an official indorsement or approval of such products or companies by the United States Government

REPORT DOCUMENTATION PAGE		READ INSTRUCTIONS BEFORE COMPLETING FORM
1. REPORT NUMBER AMMRC TR 84-33	2 GOVT ACCESSION NO.	3. RECIPIENT'S CATALOG NUMBER
4. TITLE (and Subtitle) DESIGN AND ANALYSIS OF COMPOSITE ROADWHEELS FOR THE LVTP7 AND M113A1		5. TYPE OF REPORT & PERIOD COVERED Final Report – 20 May 83 to 20 Oct 83
		6. PERFORMING ORG. REPORT NUMBER
7. AUTHOR(s) Keith Burgess, John Pepin, and Stephen Biddle		8. CONTRACT OR GRANT NUMBER(s) DAAG46-83-C-0026
9. PERFORMING ORGANIZATION NAME AND ADDRESS Fiber Materials, Inc. Biddeford, Maine 04005		10. PROGRAM ELEMENT. PROJECT. TASK AREA & WORK UNIT NUMBERS D/A Project: 1L162105AH84 AMCMS Code: 612105.H840011
11. CONTROLLING OFFICE NAME AND ADDRESS Army Materials and Mechanics Research Center ATTN: DRXMR-K Watertown, Massachusetts 02172-0001		12. REPORT DATE August 1984
		13. NUMBER OF PAGES
14. MONITORING AGENCY NAME & ADDRESS(if different from Controlling Office)		15. SECURITY CLASS. (of this report) Unclassified
		15a. DECLASSIFICATION/DOWNGRADING SCHEDULE

16. DISTRIBUTION STATEMENT (of this Report)

Approved for public release; distribution unlimited.

17. DISTRIBUTION STATEMENT (of the abstract entered in Block 20, if different from Report)

18. SUPPLEMENTARY NOTES

19. KEY WORDS (Continue on reverse side if necessary and identify by block number)

Reinforced plastics	Fiberglass
Tracked vehicle	Graphite
Epoxy resins	Kevlar

20. ABSTRACT (Continue on reverse side if necessary and identify by block number)

(SEE REVERSE SIDE)

DD FORM 1473 1 JAN 73 EDITION OF 1 NOV 65 IS OBSOLETE

Block No. 20

ABSTRACT

Three composite design concepts are presented, a detailed analysis of one concept shows the feasibility of using advanced composites for the construction of LVTP7 and M113A1 roadwheels. The other two potential designs given may offer improved performance through lower internal shear stresses in the structure and lower cost manufacturing. Weight savings of about 30% were achieved with the composite designs. These designs will fit the existing vehicles with no modifications required.

While the manufacturing analysis shows that the composite wheels will be more expensive to manufacture than the aluminum wheels using current techniques, production efficiency and experience gained during prototype fabrication may result in a composite roadwheel which is more cost competitive. High production techniques such as injection molding with thermoplastics will not yield a wheel with the required performance or weight savings. Resin transfer molding, compression molding, and autoclave molding do offer some potential for economical manufacture and their merits are discussed.

i

FOREWORD

This final report was prepared by Fiber Materials,
Inc., Biddeford, Maine, for the U.S. Army Materials
and Mechanics Research Center, Watertown, Massachusetts
under contract DAAG46-83-C-0026. Mr. Keith Burgess
was the Program Manager and performed the manufacturing
analysis while Mr. John Pepin and Mr. Stephen Biddle
conducted the design and analysis work. Mr. Michael
Edwards assisted with computer code set-up and
Mr. Ted Grethe with graphics. The AMMRC COTR was
Mr. Peter G. Dehmer. This work was done during the
period of 20 May, 1983 to 20 October, 1983.

A-1

ii

TABLE OF CONTENTS

iii

iv

LIST OF FIGURES

LIST OF TABLES

1.0 INTRODUCTION

This report presents the design and analysis to establish feasibility and design criteria for reinforced plastic (RP) roadwheels for the LVTP7 and M113Al armored personnel carriers. The study includes the redesign of existing metal roadwheels using RP materials.

Additional goals of reducing weight and lowering production cost while retaining or increasing service life as compared to the current metal construction, were examined.

An analysis of the existing metal wheels was first undertaken to establish areas of high stress and deflection. The finite element analysis was used to evaluate these critical areas for the LVTP7 roadwheel. Because of the geometric similarities between the two roadwheels, knowledge of high stress regions for the LVTP7 roadwheel was used to infer critical areas of the M113Al wheel. Stress in these areas was then bounded by analyzing discrete ring and disc segments. The data acquired from this step were used to select materials, fiber architecture and geometry for the design of the composite roadwheels. A feasibility analysis was undertaken to determine whether or not reinforced composite materials could be used for this application. Various design alternatives were investigated along with manufacturing schemes. The composite roadwheels were designed and analyzed with respect to mechanical integrity, reliability, and environmental aging. A detailed manufacturing and cost analysis was undertaken to determine manufacturing methods, material costs, labor and tooling costs, and available volume for production. The report also makes recommendations concerning the practical feasibility of producing the composite roadwheels.

1

2.0 Analysis of Existing Roadwheels

2.1 LVTP7 Roadwheel

2.1.1 Finite Element Analysis Description

The static analysis of the LVTP7 roadwheel was performed using a finite element computer program called NISA (Numerically Integrated Elements for System Analysis) developed at the Engineering Mechanics Research Corporation.

The purpose of this analysis was to investigate the internal stresses and deformations of the wheel for two different loading conditions. These stresses were then used in the design of a composite roadwheel.

Note that a finite element analysis was conducted only on the LVTP7 roadwheel and not on the Ml13Al roadwheel. The design team felt that because of the similarities in the geometry and loading directions of the two wheels, only the LVTP7 roadwheel needed the fini' element analysis. Critical areas of the Ml13Al were inferre. from the results of the LVTP7 analysis and were investigated by solving loaded ring and disc problems to obtain stress upper bounds.

The following is a brief description of the process undertaken in construction of the finite element model. The geometry of the wheel had to be established in a form that could be easily coded into the program. From the engineering drawings, one repeatable sector or arc of the wheel, was broken up into 3-D finite elements, each containing 20 nodes as shown in Figure 2.1. The coordinates of each node of every element of the repeatable sector were determined from the drawings (in cylindrical coordinates), and listed as data in the input file of the program. Then the connectivities, or lines between nodes were established, thus defining each element. The result was a sector of the wheel containing 12 elements as shown in Figure 2.2. Using a system subprogram, this sector was reproduced in such a way as to generate the remainder of the model shown in Figure 2.3. Note that only half of the wheel needed to be modeled because of symmetry with respect to the vertical axis of both the geometry and loading boundary conditions.

2

It was intended that the elements be broken into more subelements, but difficulties with the mesh generating routine prevented this. At this point, the model has been generated but additional information was required before the program was executed. Since the wheel is mounted to an immovable hub, the displacements and rotations of the nodes at the mounting holes are zero. Also, because only half the wheel is present in our model, all the nodes along the interface between the existing model and the unmodeled half, had to be constrained to translate only along the wheel plane of symmetry. At this point, loading information was provided for two different load cases. The first load case, Figure 2.4, involved a uniform line load equivalent to 15,000 lbs; however, because only half the wheel was present in our model, only half of this load or 7,500 lbs was required for our analysis.

The second load case, Figure 2.5, involved a uniform line load equivalent to 1,901 lbs, as well as a uniform line load applied to the side of the wheel of 1,098 lbs located along the wear ring. As in the previous case, only half of these loads were used in the analysis because only half of the actual wheel was used as the model. This combination side and vertical loading was used to simulate the loads applied as the vehicle is traversing a 30° side slope.

At this point, the model was ready for execution. Stress plots were obtained for different views of the model. Contour plots of front, back and plane of symmetry cross-section views of maximum principle stress, minimum principle stress, Von Mises equivalent stress and maximum shear stress, were made and are given in Appendix 1. The results of these plots indicated areas of high stress. In the design of the composite wheel we used this information to minimize these areas of high stress and to develop a reliable lightweight composite replacement.

3

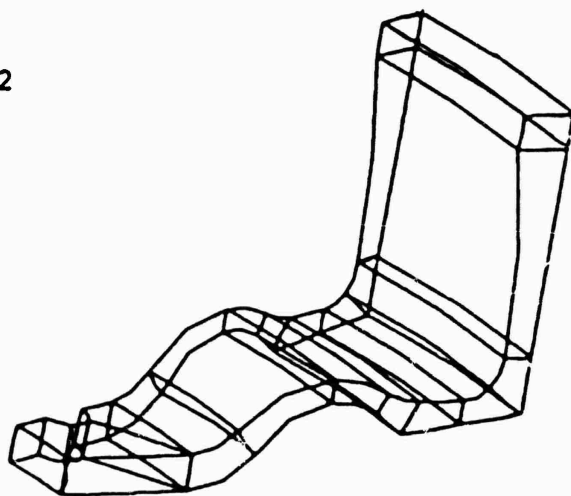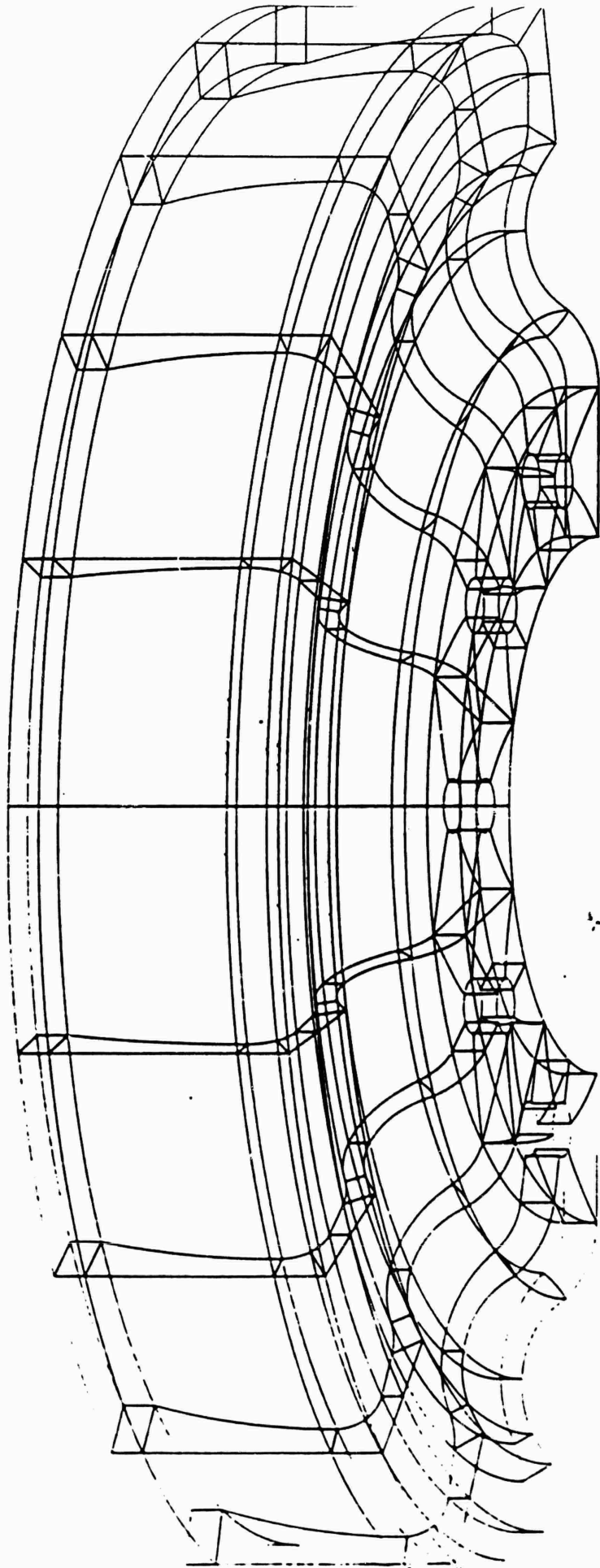3-D SOLID ELEMENT

FIGURE 2.1
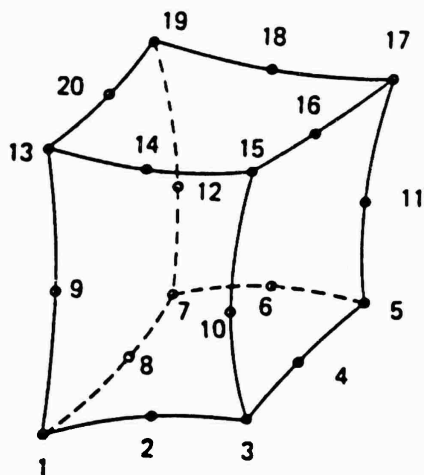
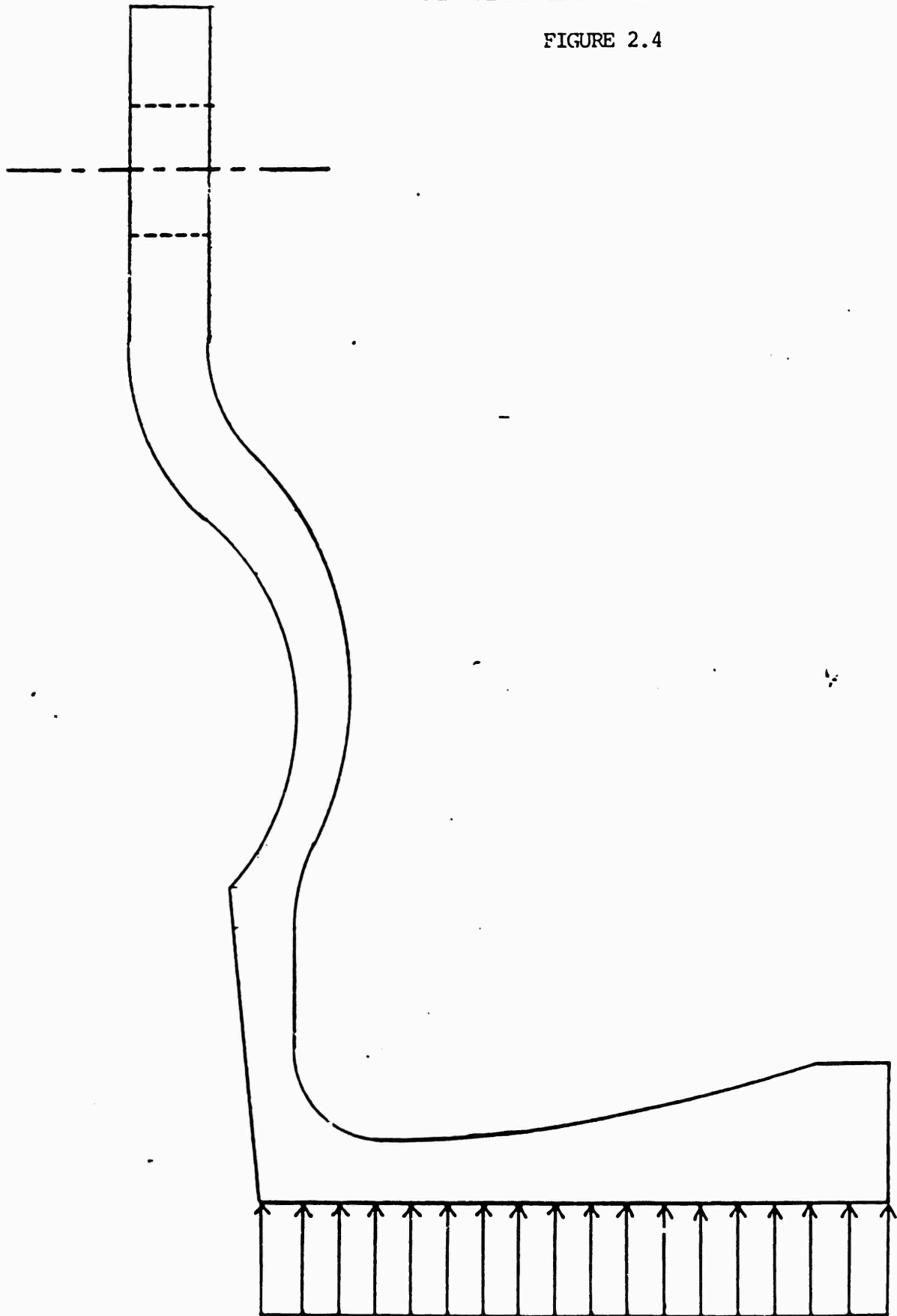

WHEEL SLICE

FIGURE 2.2

FINITE ELEMENT MODEL

FIGURE 2.3

VERTICAL LOAD CASE

MID PLANE CROSS SECTION VIEW

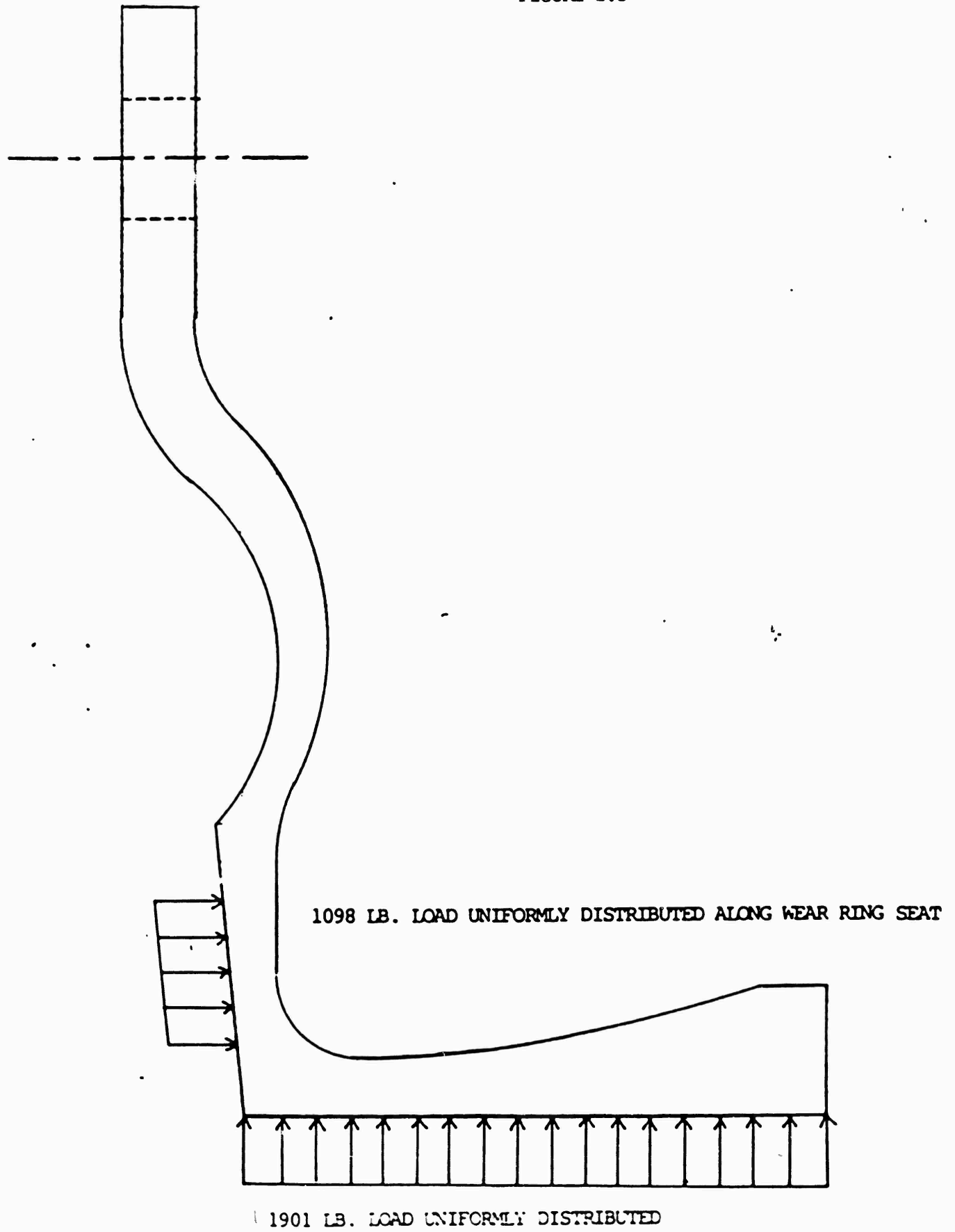FIGURE 2.4

15,000 LB. LOAD UNIFORMLY DISTRIBUTED

COMBINED VERTICAL AND SIDE LOAD CASE

MID PLANE CROSS SECTION VIEW

FIGURE 2.5

1098 LB. LOAD UNIFORMLY DISTRIBUTED ALONG WEAR RING SEAT
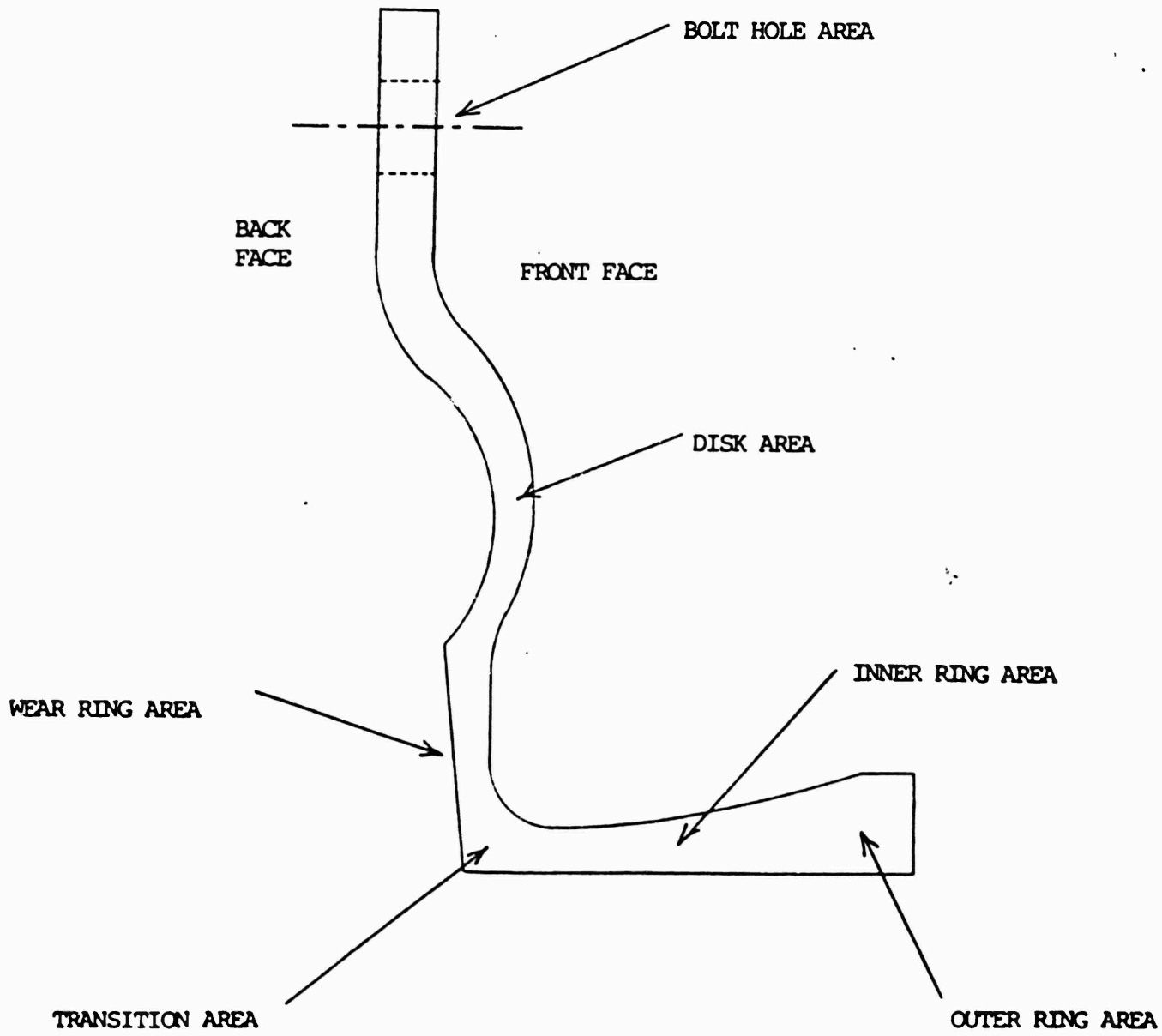
1901 LB. LOAD UNIFORMLY DISTRIBUTED

2.1.2 Analysis Results

Some unexpected results were obtained using the finite element analysis. In comparing the combined side and vertical load case with the vertical load case, the locations of the high stress levels occurred in the same areas. The side loading did not contribute to the bending stresses at the bolt hole areas as expected. The stress magnitudes were of course different because the applied loads were different. The vertical load case of 15,000 lbs imposed the highest stresses in the wheel, and as a result the investigation was focused on stresses and displacements of this loading case.
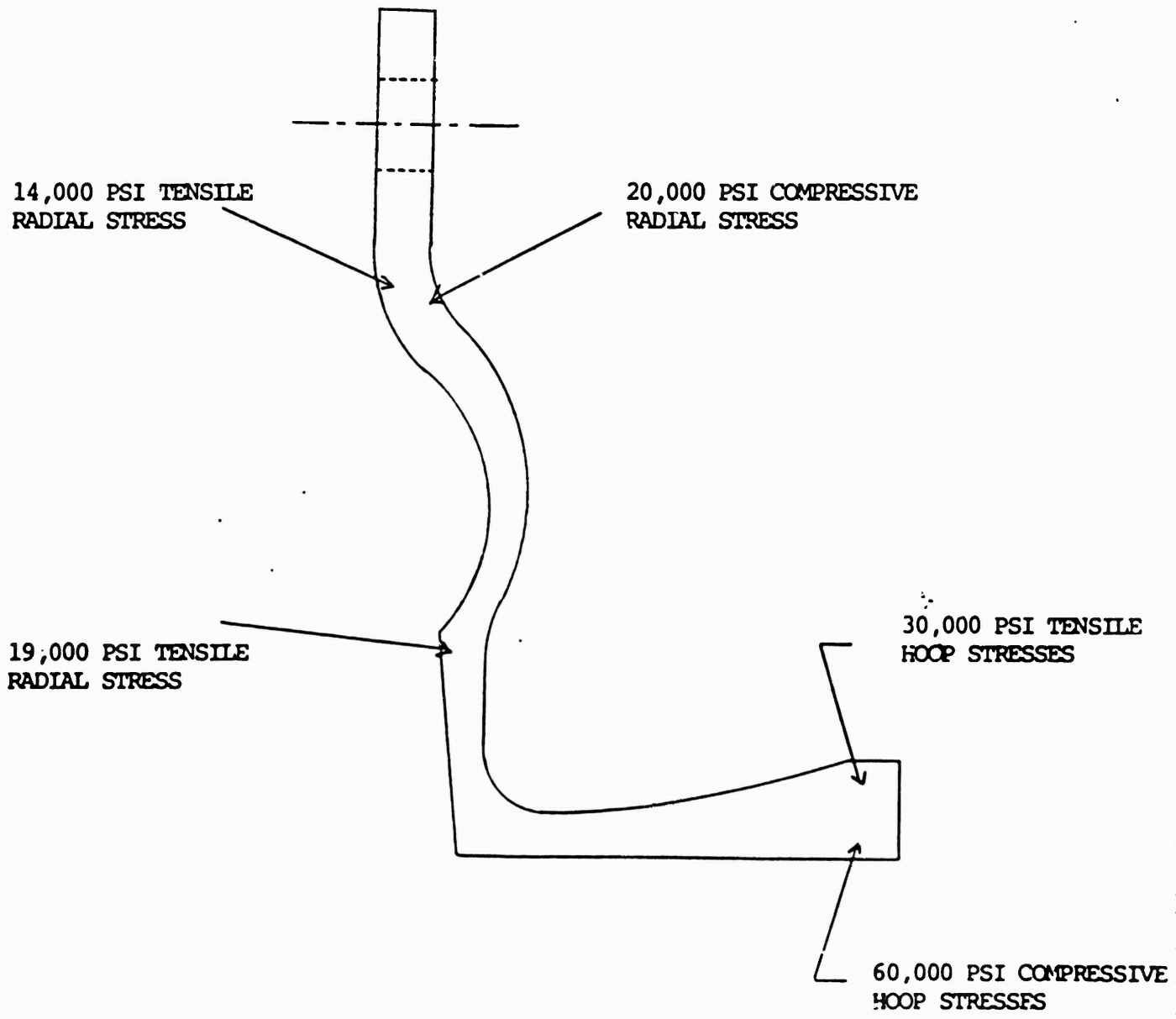
The most critical stresses imposed on the wheel occur in the outer ring area near the load application point (refer to Figures 2.6 and 2.7). These stresses are in the order of 60,000 psi compression on the lower portion of the outer ring area, and 30,000 psi tension on the upper portion. These are hoop stresses that act normal to radial planes. In the transition area high bending stresses had been expected due to the cantilever effect of the applied load acting along the inside and outside rim. The hoop stiffness was sufficient to minimize this cantilever effect, and the bending stresses in this region were not critical. Shear stress exists in the outer ring area, and oriented in the hoop direction. The magnitude of these stresses are 30,000 psi. As with the high normal stresses previously described, the shear stresses are caused primarily by the bending of the hoop or inner and outer ring portions of the wheel.

The deflections caused by the 15,000 lb vertical load were found to be high. As shown in the scale drawings of Figures 2.9 and 2.10, the tip of the outer rim area is displaced to the right and up about 0.2 inches. It should be emphasized that this deformed geometry is from a very severe, worst case type, loading condition. A deformed geometry, probably more representative of actual service conditions, is shown as circled dots on the end of the outer ring area of Figure 2.9. This corresponds to the combined vertical and horizontal load case.

8

BOLT HOLE AREA

BACK
FACE

FRONT FACE

DISK AREA

INNER RING AREA

WEAR RING AREA

TRANSITION AREA

OUTER RING AREA

NOMENCLATURE USED IN DESCRIBING THE LVTP7 WHEEL

FIGURE 2.6

9

14,000 PSI TENSILE
RADIAL STRESS

20,000 PSI COMPRESSIVE
RADIAL STRESS

19,000 PSI TENSILE
RADIAL STRESS

30,000 PSI TENSILE
HOOP STRESSES

60,000 PSI COMPRESSIVE
HOOP STRESSES

NORMAL STRESSES

MID PLANE CROSS SECTION

FIGURE 2.7

10

30,000 PSI SHEAR STRESS
DUE TO HOOP EFFECT
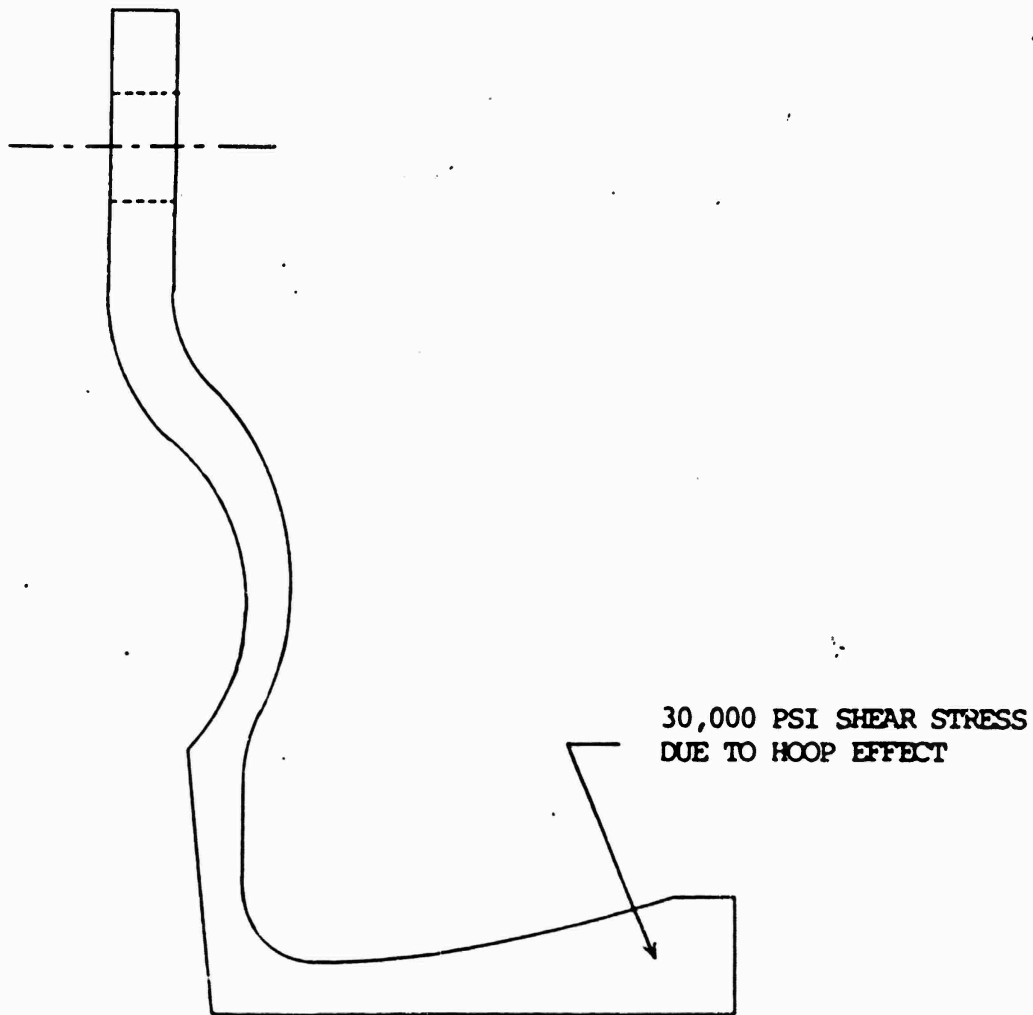
SHEAR STRESSES

MID PLANE CROSS SECTION

FIGURE 2.8

5.0 INCHES TO
CENTER OF
ROTATION
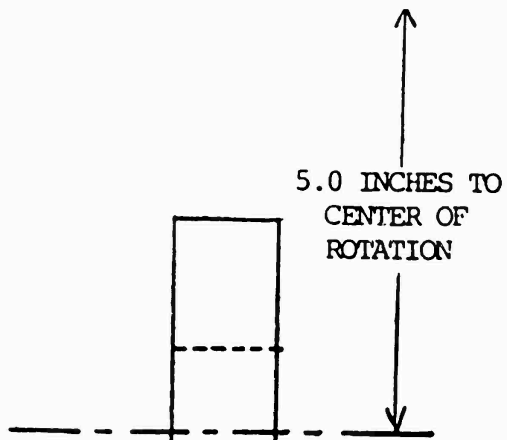
DEFORMED GEOMETRY

WHEEL MID PLANE CROSS SECTION

FIGURE 2.9

ACTUAL SIZE

--- DEFORMED GEOMETRY 15,000 LB. VERTICAL CASE
——— UNDEFORMED GEOMETRY
⊙   END POINT LOCATIONS OF DEFORMED GEOMETRY WITH
      VERTICAL AND SIDE LOAD CASE

12

DEFORMED GEOMETRY

FRONT SURFACE VIEW

FIGURE 2.10

42% OF ACTUAL SIZE

-- DEFORMED GEOMETRY

— UNDEFORMED GEOMETRY

APPLIED LOAD OF 15,000 LBS.

13

2.1.3 Alternative Analytical Approach

In order to establish an analytical approach to be used for the M113A1 roadwheel, each of the major stress areas on the LVTP7 was evaluated m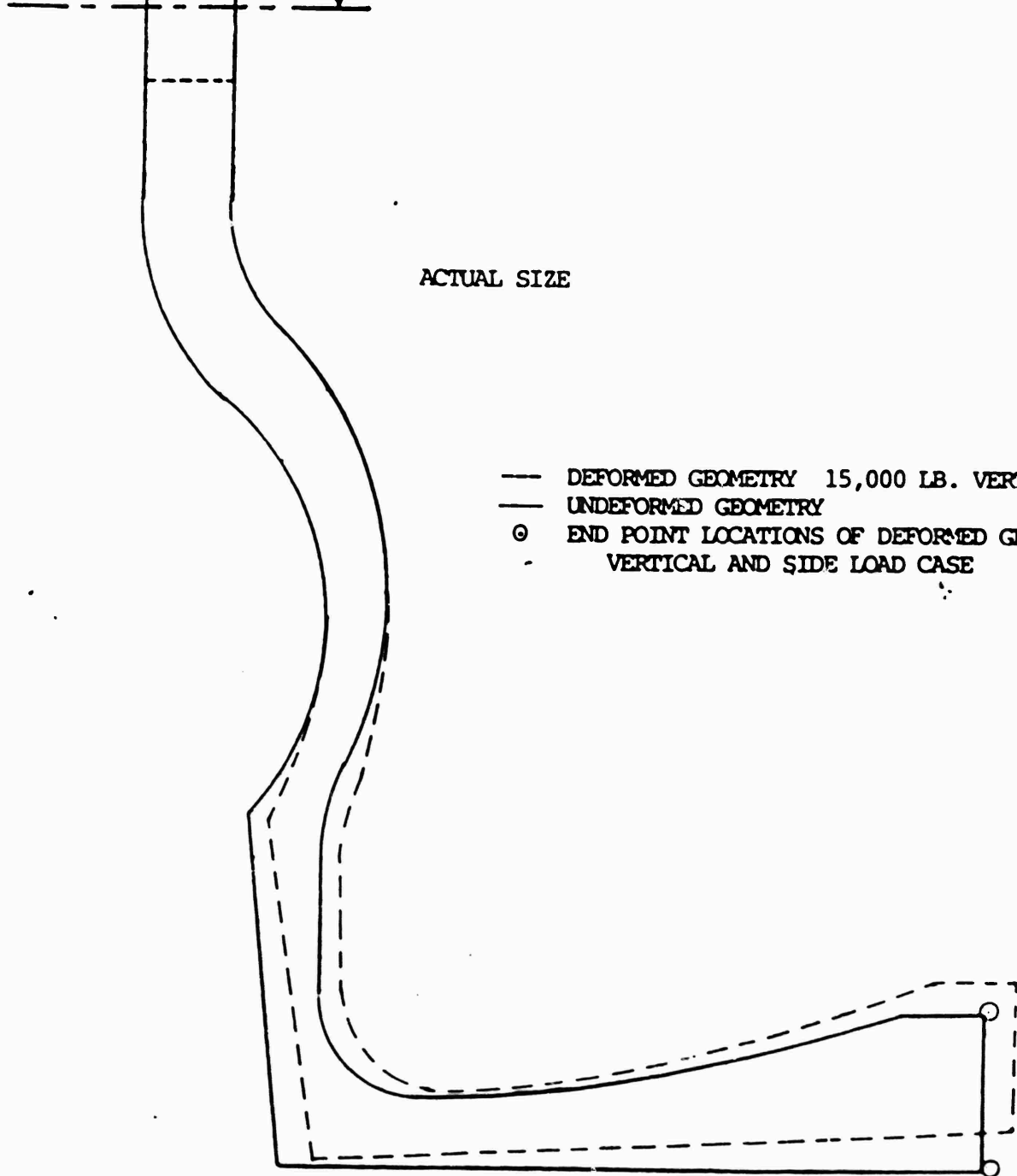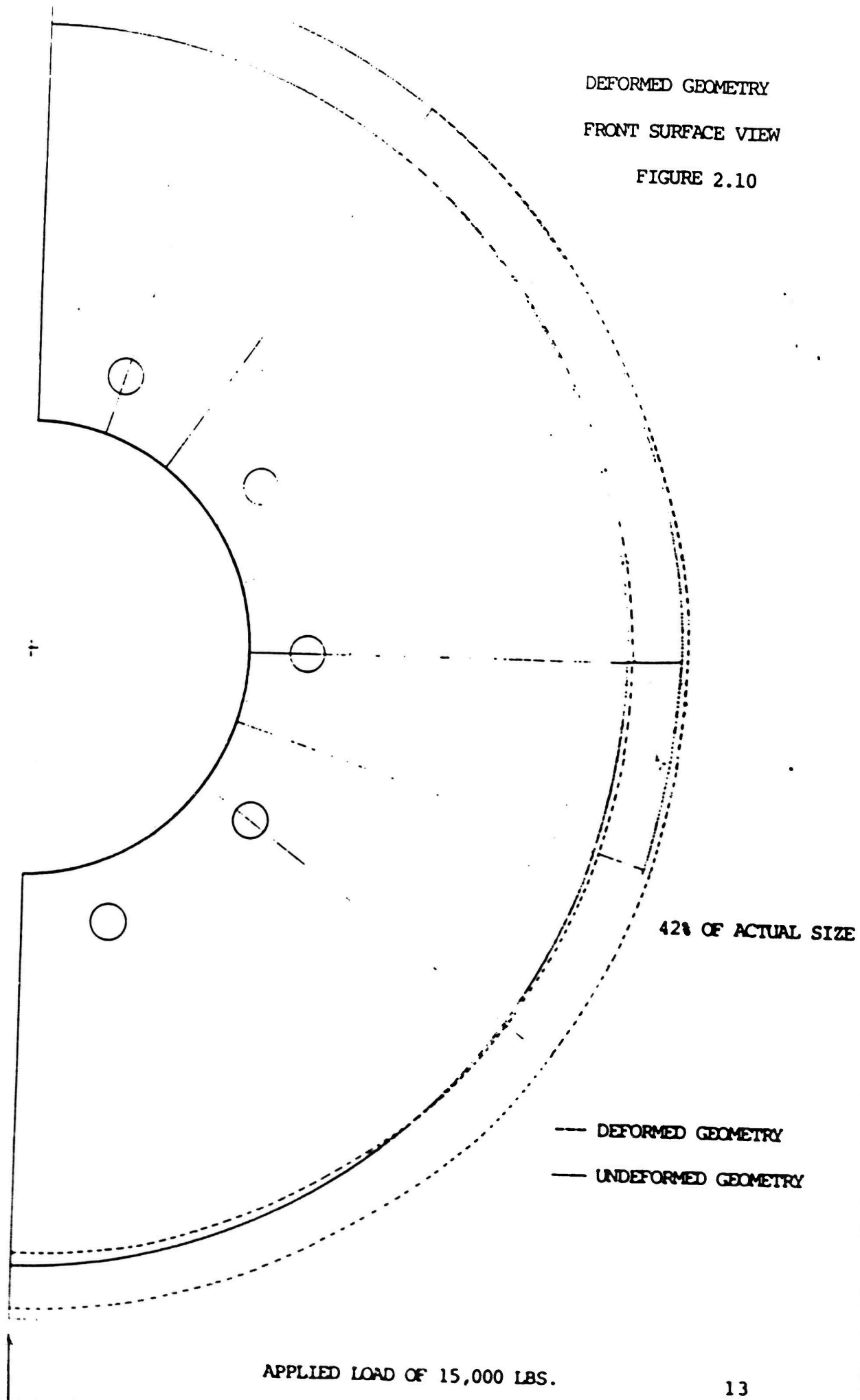anually and compared to the results of the Finite Element Method (FEM). The intent of this approach was to establish reasonable upper bounds for the predicted stresses in order to allow feasibility studies to be completed.

The approach used to establish the analytical methods was to first examine the output of the FEM analyses to observe the nature of the stresses and deformation of the wheel, and then to develop analytical models that incorporated these observations and yielded comparable results.

Stresses in the Disk Near the Bolt Circle The results of the FEM indicated that the curvature in the disks area did not contribute significantly to the strength of the disk. This was verified by calculating the stresses by assuming that the disk was flat and fixed at the edges by the rim. Case #21 from page #368 of Roark's "Formulas for Stress and Strain" (5th Edition) was used.

Based on the FEM, the stresses were

Compression	20,000 psi
Tension	14,000 psi

Notation:

σ	=	calculated stress
a	=	effective outer radius of the disk = 11.75"
b	=	restrained inner radius of the disk = 6.12"
β	=	factor per Roark
M	=	applied moment
F	=	force on bottom of wheel = 15,000#
t	=	thickness at radius location "b" = .531
m	=	moment arm = 3.06"

14

$$b/a = 0.521$$

$$\beta = 1.06 \quad \text{(per Roark)}$$

$$M = Fm = 45,900 \text{ in lb}$$

$$\sigma = \frac{\beta M}{at^2} \quad \text{(per Roark)}$$

$$\sigma = 15,000 \text{ psi (versus an average of 17,000 by FEM)}$$

Compressive stresses due to radial support loads in the disk were estimated by assuming that, at the point in question, the effective width of the disk was equal to two-thirds of the restrained inner diameter of the disk. This resulted in a compressive stress.

$$\sigma = 15,000/(2/3 \times 2 \text{ b} \times \text{t} = 3100 \text{ psi}$$

The total of the stresses was then found by adding the above values

$$\sigma = 15,000 - 3000 = 12,000 \text{ in tension}$$

$$\sigma = 15,000 + 3000 = 18,000 \text{ in compression}$$

These values are comparable to the FEM values of 14,000 and 20,000 respectively.

<u>Stresses in the Outer Rim</u> The FEM results indicated
that the principal stresses in the outer rim were circum-
ferential and caused by deflecting the outer rim section
into a non-circular shape. This result is reasonable in
that the bending stiffness of the rim (in the hoop direction)
is substantial compared to the bending restraint of the disk.
The result of this is a deflection of the outer edge of the
rim both towards the axis and towards the disk (the disk
behaves like a simple support to the rim). The above condi-
tion was approximated by calculating the bending stress in a
rim of 1/2 of full width, i.e., the outer half of the rim.
Half of the load was assumed to be carried by the disk and
the other half by the rim.

In order to account for the interaction between the
disk and the rim, the disk was assumed to be providing
distributed support to the rim. This support was applied
over 90° of rim which coincided with the deflection nodes
as shown in Figure 2.10.

Based on the FEM, the stresses were

Compression   60,000 psi

Tension   30,000 psi

Roark's 5th edition, page 226, case #8 was used for the
following calculations:

Notation:

θ = 135°

F_r = Force on the rim = 7,500#

R = Radius of the rim = 11.4"

I = Moment of inertia through the section centoid = 0.081 in^4

C = Distance to extreme fiber = 0.45"

K = Constant per Roark (K_{Mc})

w = Effective loading of the rim

σ_r = Calculated stress

F = 2 w R sin θ

w = 466 #/in

K = -0.149 for θ = 135°

M = K (wR^2)

M = 9000 in. lb. at θ = 180°

σ = $\frac{Mc}{I}$

σ = 50,000 psi (verses an average of 45,000 psi per FEM)

16

2.2 M113A1 Roadwheel

2.2.1 Analysis Method

From the finite element method (FEM) of the LVTP7 road-wheel, specific areas and values of high stress were located. Since the basic geometry of the two wheels is similar, critical areas of the M113A1 can be identified from the previous analysis. These areas were:

1. Hoop stress in the outer rim.

2. Radical bending stresses in the disk near the bolt circle.

3. Circumferential shear stresses in the outer rim.

By applying the methods used in section 2.1.3, the stresses can be calculated for the M113A1 roadwheel. All notation corresponds to section 2.1.3.

Stresses in the Disk Near the Bolt Circle

a = 10.8"   F = 4245#
b =   4.1"   m = 1.87"

b/a=   0.38

B =- 1.92

M = 8,450 in. lb.

σ = 50,000 psi (bending stresses)

Compression Stresses:

σ = 4525/(2/3 x 2 x 4.1 x 0.31)

σ = 2700 psi = approximately 3000

Combined Stresses:

σ = 50,000 + 3,000 = 53,000 compressive
σ = 50,000 - 3,000 = 48,000 tensile

17

Stresses in the Outer Rim

I = 0.0832

c = 0.86 (inside)

c = 0.384 (outside)

w = 305#/in.

$M = K (wR^2)$

M = -5010 in. lb.

$\sigma = \dfrac{Mc}{I}$

σ = 49,000 psi tension on inside edge

σ = 23,000 psi compression on outside edge

Bearing Stresses at Bolt Holes Bearing stresses at the bolt holes were conservatively estimated by assuming all the load on two bolts.

d = bolt diameter

t = laminate thickness

$\sigma = (F/2)/(d/t)$

$\sigma = (4525/2)/(0.685 \times 0.31)$ = 11,000 psi

3.0 Feasibility Analysis

Based on the analyses of the metal roadwheels and on factors peculiar to composites, the feasibility of using composites was reviewed prior to developing the design of the laminates.

Strength The character of the stresses and strains devleloped in a wheel very quickly eliminate thermoplastics and short fiber composites. High modulus composites are required to limit the rim deflections and to provide resistance to fatigue. A composite consisting of primarily carbon/epoxy will be considered in more detail due to the combination of light weight, high strength and high stiffness.

Wear Ring Attachment Holes subjected to bending or axial loading in a composite material are subject to high stress concentrations in the vicinity of the hole area. The wear righ on both of the existing wheels is rivited in place. On the composite wheel design however, the wear rings would be held in place using an adhesive. The first major consideration in the selection of an adhesive for the composite wheels was strength. The required adhesive strength was determined by calculating the rivet shear strength, and comparing this value to the adhesive shear strength assuming the entire mating surface of the wear ring is bonded to the wheel.

Adhesives that easily possess the required shear strength characteristics when bonded to steel are: cyanoacrylate, and epoxy. If a thermoset adhesive is used, the softening point temperature must be lower than the softening point of the graphite epoxy wheel. To remove the wear ring for routine replacement, it must be heated carefully and stripped off. The surface of the wheel must be abraded and cleaned, and the new wear ring abraded and degreased before replacement. Adhesive must be applied to the mating surface of the wear ring and pressed into place. It would then be cured for a specific time and temperature depending on the adhesive used.

It was assumed that the main mode of failure for the existing rivets that fasten the wear ring to the wheel is shear. The method of analysis for the replacing these rivets with an epoxy based adhesive is to determine the maximum shear forces the existing rivets can support, and then calculate the shear requirements for the adhesive.

For this analysis, the ultimate shear stress for the rivets is assumed to be 49,000 psi as per Mil-HDBK-5C. This is based on Monel rivets per Table 8.1.2(b).

LVTP7 roadwheel-

for the rivets D = 0.385 inches   15 rivets per wheel

$$A_r = \frac{\pi D^2}{4} = 0.116 \ in^2$$

Maximum load supported per rivet (F/r) - $S_{su}A$

$$F/r - 49,000 \times 0.116 - 5,684 \ lbs.$$

Di = 19.375 inches (inside diameter of wear ring)
Do = 22.875 inches (outside diameter)
    Area of wear ring; Aw = $\frac{\pi}{4} (Do^2 - Di^2)$

$$= 116.1 \ in^2$$

Theoretical wear ring area supported by each rivet

$$A/r = \frac{Aw}{\# \ of \ rivets}$$

$$\frac{116.1 \ in^2}{15}$$

$$A/r = 7.7 \ in^2$$

the required shear strength of the adhesive is $\frac{F/r}{A/r}$

$$\frac{F/r}{A/r} = \tau = \frac{5,684 \ lbs}{7.74 \ in^2}$$

$$\underline{\tau = 734 \ psi} \quad \text{(required shear strength of adhesive)}$$

20

M113A1 roadwheel—

for the rivets D = 0.25 inches   18 rivets per wheel

$$Ar = \frac{\pi D^2}{4} = 0.049 \text{ in}^2$$

$$F/r = S_{su}A$$
$$= 49,000 \times 0.049$$

$$F/r = 2401 \text{ lbs.}$$

$$Di = 16.69 \text{ in.}$$

$$Do = 21.81 \text{ in.}$$

$$Aw = \frac{\pi}{4}(Do^2 - Di^2)$$
$$Aw = 154.8 \text{ in}^2$$

$$A/r = \frac{Aw}{\# \text{ of rivets}}$$

$$= \frac{154.8 \text{ in}^2}{18}$$

$$A/r = 8.6 \text{ in}^2$$

$$\frac{F/r}{A/r} = \frac{2401 \text{ lbs.}}{8.6 \text{in}^2}$$

$$\tau = 279 \text{ psi (required shear strength}$$
$$\text{of adhesive)}$$

Based on this review, it is concluded that the wear
plates can be bonded due to the low strengths required. In
the event that riveting is desired, then this option may
be available depending on the actual strength requirements.
The primary consideration against rivets is that close
tolerances are required to avoid fatigue damage to the
composite. Shock and impact loads were not evaluated and
may affect these conclusions.

Fatigue Considerations - Requirements given for the
wheel show a cyclic environment to about $.5 \times 10^5$ cycles.
High strength unidirectional graphite/epoxy can be cycled
in tension to up to 130 ksi for a half million cycles
(from reference 3, Figure 1.2.5-17). This cyclic stress
level corresponds to about .6% strain in tension. Since
these composite wheel designs attempt to align fibers with
principle stress directions, effects of cyclic loading on
in-plane properties will be small. However, the inter-
laminar shear strength drops to 55% of its static value
after a half million cycles while the stiffness remains
close to 90% (Figure 1.2.5-25, reference 3). Given this
fact, the resin systems used, a working level interlaminar
shear strength of 4 ksi must be obtained.

Reliability and Environmental Effects - Reliability and
maintainability of the composite wheels is a function of
several factors such as preventing damage from heavy impact.
A glass reinforced plastic (GRP) outer protective covering
will sacrificially protect the wheel from abrasion and small
scale impact.

The titanium sleeve in the holes was chosen to protect
the graphite laminate holes from wear and corrosive contact
with bolts.

Environmental effects such as heat, moisture, and high
strain rate change the mechanical properties of graphite
epoxy composites. Heat and moisture studies that have been
conducted show that these environmental effects are matrix
dependent. The graphite fibers are affected little by
temperature or humidity increases while the epoxy matrix is

22

susceptible to these environmental influences; hence, the longitudinal properties (those in the direction of the fibers) for a unidirectional composite remain fairly constant. The tensile strength is, in fact, found to be slighly higher in the longitudinal direction after being subjected to a heat and moisture environment as shown by Figure 3.9. This is presumably due to uneven tension on the fibers and the behavior of the matrix material near broken fibers. Properties for the transverse direction (perpendicular to the longitudinal direction) are degraded by heat and moisture as shown in Figure 3.10. The transverse strength decreases with an increase of either temperature of humidity, caused by a weakening of the epoxy matrix material. The transverse modulus becomes less temperature dependent with an increase in moisture content. Figure 3.11 shows that the axial shear modulus is the property most affected by humidity, temperature, and strain rate. In addition, the shear modulus is dependent on the level of the applied shear stress. As expected with polymeric materials, the stiffness decreases with increasing temperature and moisture content. Also, the stiffness increases with increasing applied strain rate. Figs 3.1, 3.2 & 3.3 are based on Ref (8).

For this particular application, environmental effects will be minimal. The operating temperatures are moderate enough for thermal degradation effects to be insignificant. For thermal cycling between room temperature and 270°F for 500 cycles, (much more demanding than this application), the data shows only a slight decrease in interlaminar shear strength with other physical properties unaffected.

Physical aging effects are also slight. Aging is primarily a matrix bound phenomena. The graphite fibers are unaffected by aging, and so for a unidirectional composite, the properties in the longitudinal direction are unaffected. Available data suggests that a 10% decrease of interlaminar shear strength and transverse strength can be expected in 10 years.

23
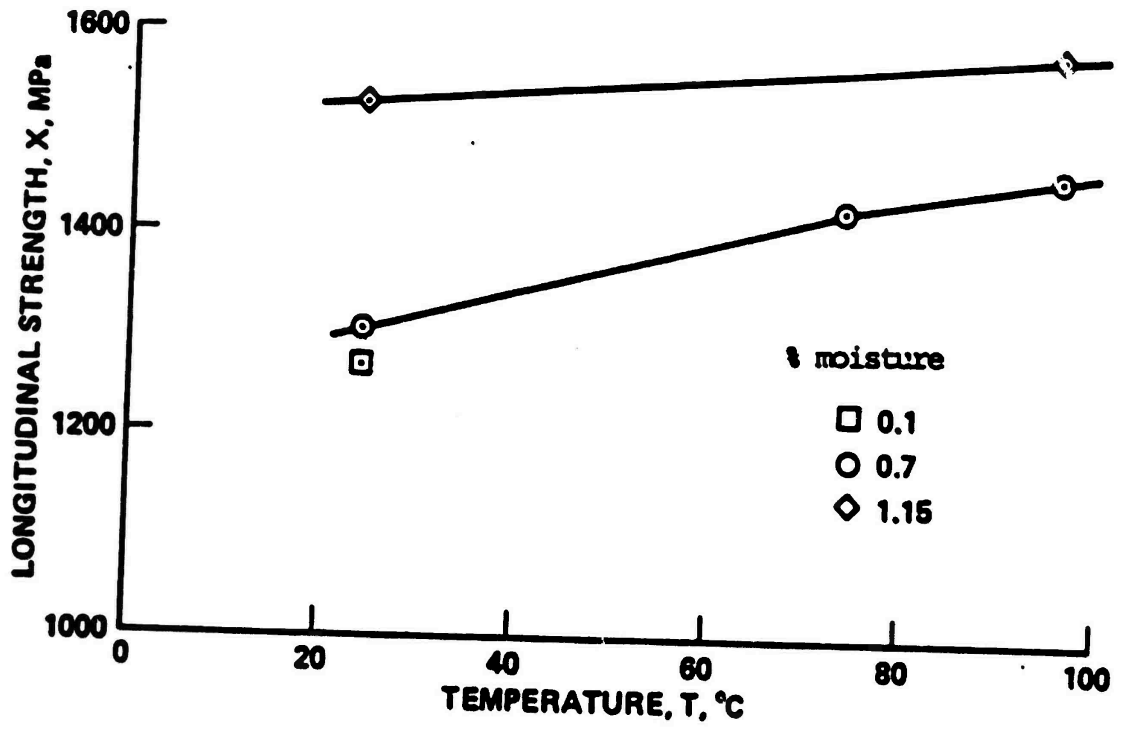
VARIATION OF AXIAL STRENGTH WITH
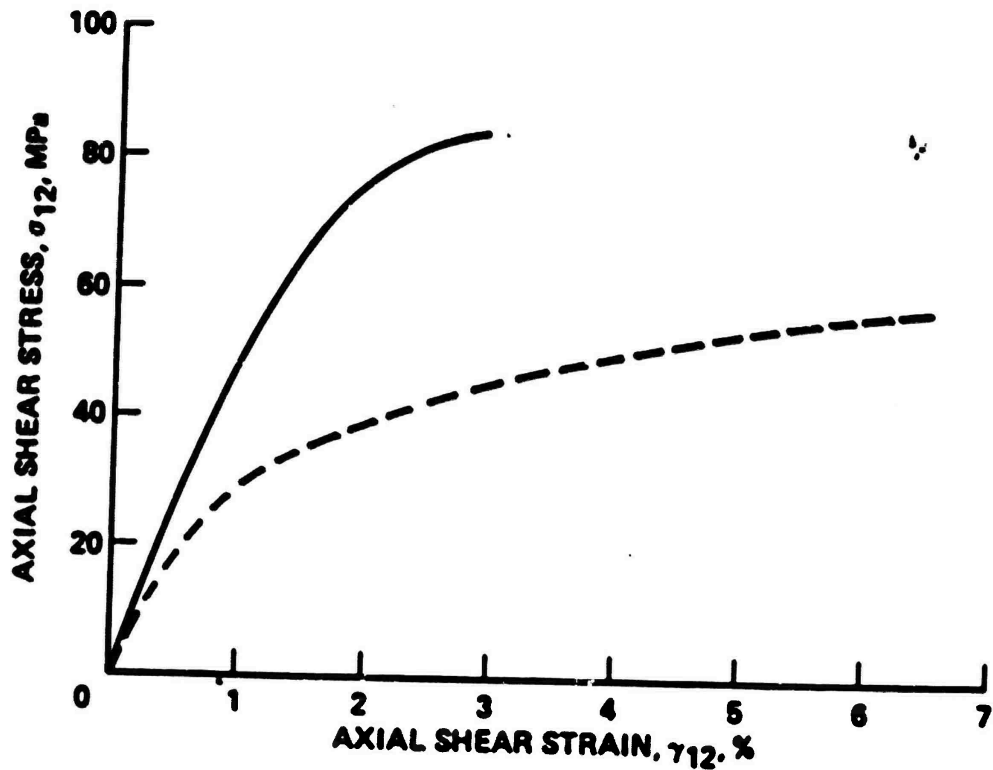TEMPERATURE AND MOISTURE CONTENT

FIGURE   3.1

24
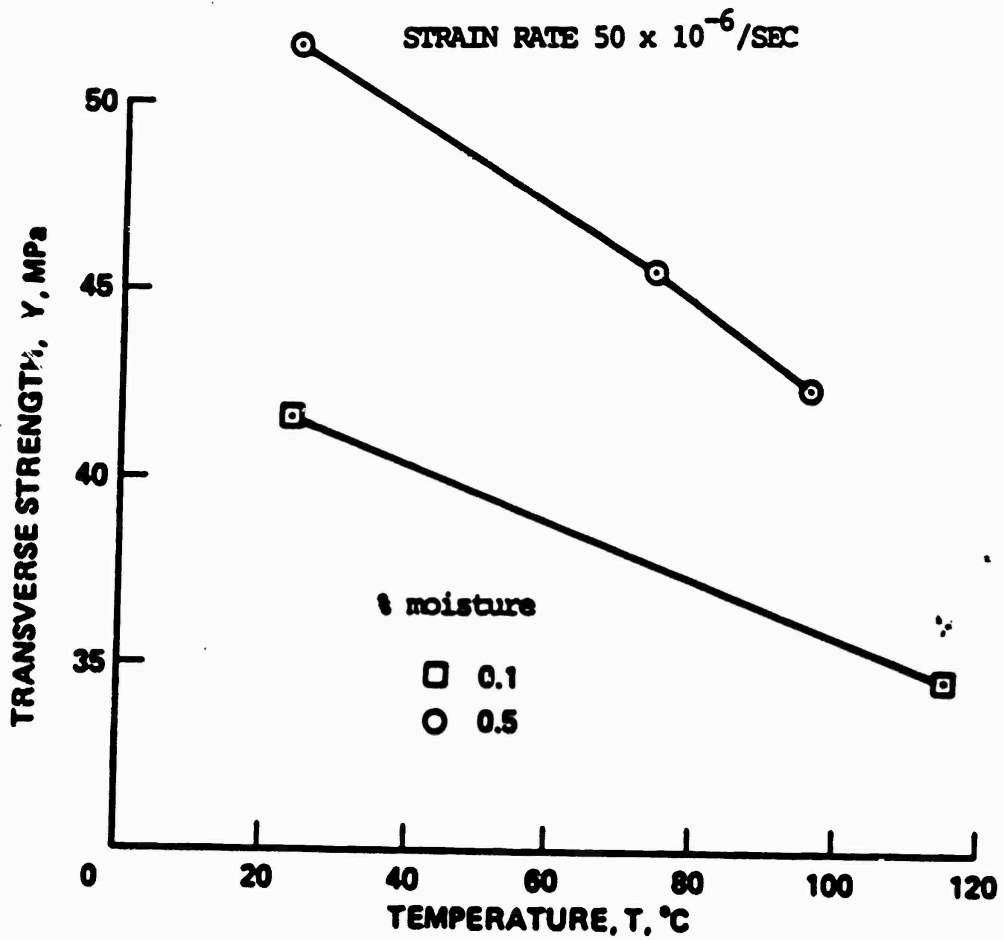
EFFECT OF TEMPERATURE AND MOISTURE CONTENT
ON TRANSVERSE STRENGTH

FIGURE   3.2

- - - - STRAIN RATE 50×10^{-6}/SEC
    TEMPERATURE   96°C
    MOISTURE CONTENT   1.15%

------ STRAIN RATE 2000×10^{-6}/SEC
    TEMPERATURE   24°C
    MOISTURE CONTENT   0.1%

AXIAL SHEAR STRESS-STRAIN CURVES FOR TWO LOADING CONDITIONS

FIGURE 3.3

4.0 Design of Composite Wheels

4.1 LVTP7 Roadwheel Design

4.1.1 Design Criteria

The design of the composite roadwheel was based on the maximum wheel load of 15,000 lbs. in the vertical direction. The finite element analysis showed that this condition was the worse loading case causing high stresses in the wheel rim and bolt hole areas. A margin of safety of 1.25 was established for the composite roadwheel design. To allow for design uncertainty in composite degradation due to moisture, environmental factors, and damage tolerance, the ultimate composite stress shall be 1.25 times that stress encountered at the 15,000 lb. vertical load in any area of the wheel.

The basic structural material selected for this design is a high strength, intermediate modulus graphite fiber such as T-300 in an epoxy resin matrix.

Several factors were considered in the selection.

1. Graphite/epoxy is lightweight over glass and has better compressive properties than Kevlar. Many areas of this wheel experience high compressive stresses.

2. High stiffness.

3. Good data base from which to design.

4. Good fatigue properties compared to glass.

Glass and Kevlar composites will be used as secondary materials to protect the graphite laminate from impact, abrasion and contact with metals.

The strain at selected areas of the wheel will be compared to the aircraft industry standard of .6% allowable for a graphite/epoxy laminate. Typically, the maximum tensile strain of a T-300 unidirectional composite is .8% while for a ±45 angle ply laminate it is 2.2%. The .6% allowable reflects, again, the general lack of firm knowledge about the onset of delamination and the tolerance of the structure to delamination growth.

The thickness of the laminate in the bolt hole area was kept the same as the aluminum to preserve the symmetry and alignment of the wheels when mounted. This is required in order to maintain the same center line between a set of roadwheels without resorting to two different designs.

4.1.2 Composite Design Considerations Resulting from Alumunim Wheel Analysis

First, the deformation and stress state of the aluminum wheel are reviewed to determine how the selective reinforcement of a structural composite can best be used. Figures 2.9 and 2.10 show a cross section and end view of the wheel with the deformed shape at maximum wheel load shown in dotted lines. Several deformation mechanisms are evident.

1. Rim distortion out-of-round leading to beam loading type stresses in radial planes of the rim. A hoop compression of the rim is also taking place leading to a hoop compressive stress.

2. Out-of-plane bending of the wheel disc causing flexural stresses through the thickness of the disc.

3. Cantilever type bending of the rim along the line of high pressure contact with the ID of the rubber tire.

Each type of deformation results in a stress state within all points of the wheel. By limiting the magnitude of certain types of deformation using selective orientation of the reinforcing fibers, stress magnitudes can be reduced in critical areas. For example, the flexural stiffness of

28

of the rim cross sections (EI) offer resistance to
out-of-round deformation of the rim. Using preferential
reinforcement of the hoop direction in the rim, the rim
flexural stiffness will be increased over that of the
aluminum. This will both lower the hoop stresses in the
rim and flexural stresses in the corner joint between the
rim and disc.
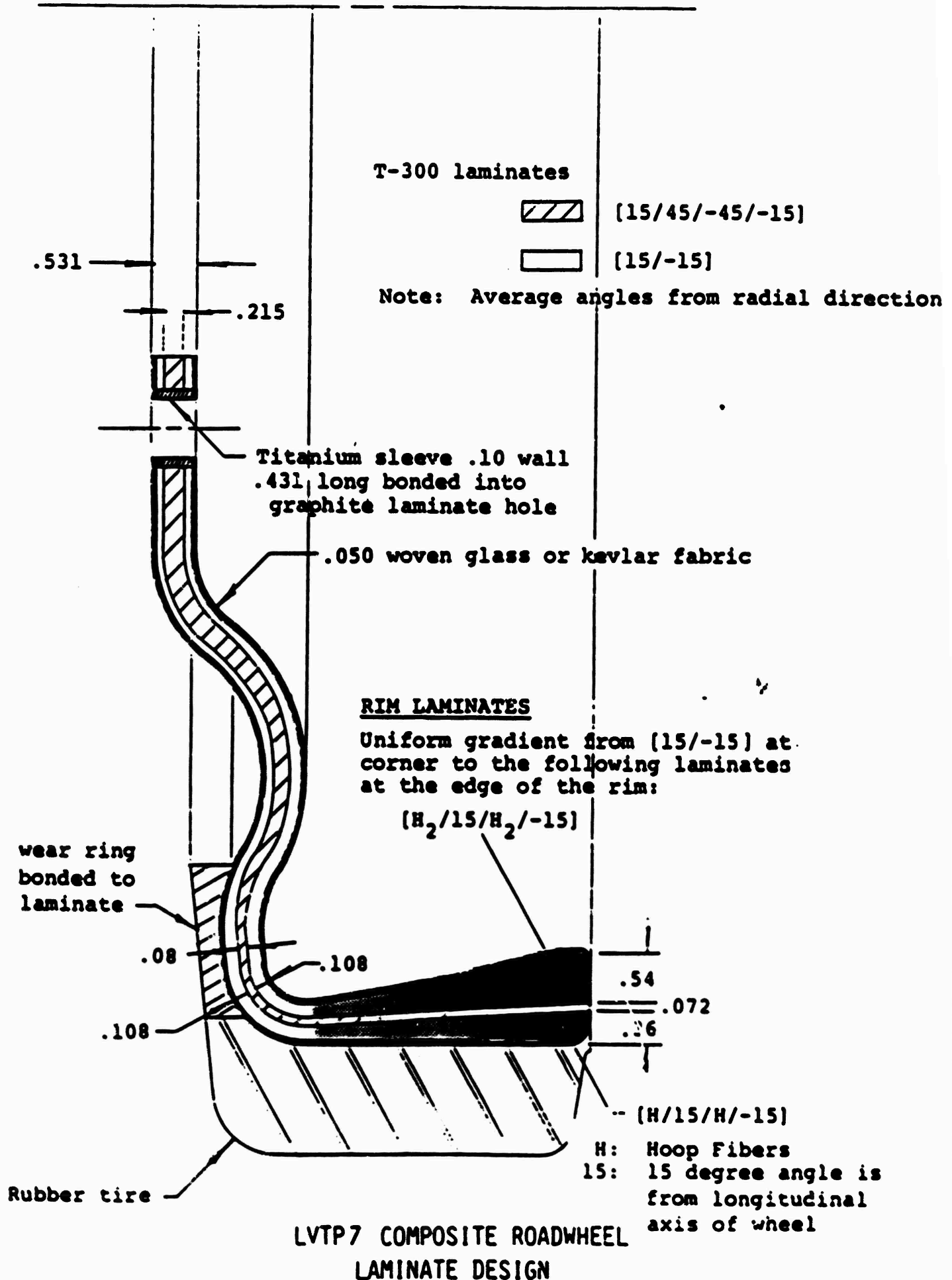
4.1.3 Composite Design Conc pt for LVTP7 Roadwheel

To design the composite wheel as a laminate with much
the same envelope as the aluminum wheel, it is important
to reduce deformations of the rim as much as possible to
avoid high interlaminar shear stresses in the rim itself
and in the transition corner between the rim and disc.
Also, since the primary loading of the wheel disc is
compression and tension in the radial direction and
flexure out-of-plane, the primary reinforcement of the
wheel disc is radial. Figure 4.3 shows the lamina orien-
tations selected for each area of the wheel. They exhibit
the preferential radial and hoop reinforcement as well as
multi-axial reinforcement around the bolt holes. Dimensions
of the wheel are shown in drawing #740-0008 found in
Appendix 3.

4.1.4 LVTP7 Composite Design Analysis

The analysis of the composite wheel is performed by
checking the strain and laminate stress in critical areas
of the wheel. This is done by making upper bound assumptions
on the internal loading in these areas.

The laminate rim shown in Figure 4.3 is strongly
reinforced in the hoop direction with a 2:1 ratio of hoop
to ± 15° fibers in the ID of the rim and 1:1 ratio at the
OD. To prevent possible shear failure on a 45° plane from
the horizontal plane, ± 15° fiber reinforcement of 50% was
maintained and the rim outer corner was rounded to a radius
of .25 inches. The hoop flexural stiffness of this composite
laminate rim is 1.72 times that of the aluminum rim at the
outer edge as shown by the calculation of Appendix 2. This
reduces the change in diameter of the rim by the same factor
and will more effectively transmit the bearing load into
the wheel disc. This load is transmitted through shear
at the rim/disc interface, and, if transmitted uniformly,
would result in a shear stress of 470 psi. The actual
gradient of interlaminar shear stress from the contact
point along the wheel disc should be established by subscale
test.

29

FIGURE 4.3

T-300 laminates

| [15/45/-45/-15] |
| [15/-15] |

Note: Average angles from radial direction

.531

.215

Titanium sleeve .10 wall
.431 long bonded into
graphite laminate hole

.050 woven glass or kevlar fabric

RIM LAMINATES

Uniform gradient from [15/-15] at
corner to the following laminates
at the edge of the rim:

$[H_2/15/H_2/-15]$

wear ring
bonded to
laminate

.08

.108

.108

.54

.072

.?6

$[H/15/H/-15]$

H: Hoop Fibers
15: 15 degree angle is
from longitudinal
axis of wheel

Rubber tire

LVTP7 COMPOSITE ROADWHEEL
LAMINATE DESIGN

The disc laminate is primarily a ± 15° to the mid-radial angle ply with a core of [15/45/-45/15]. The core is required for bearing strength around the holes while the ± 15° cross ply supports the radial tension, compression and flexure stresses. From reference 3, Figure 2.4.2-26 and Figure 4.4, a conservative value of the ultimate bearing stress for this laminate is 50 ksi for a single lap, bolted - only joint. This is confirmed by bearing test results at FMI on an eight harness satin cross ply laminate. Unclamped pin bearing resulted in bearing stresses of 48.5 ksi in the fill and 62.1 ksi in the warp direction. The margin of safety of 1.25 results in a 40 ksi bearing strength allowable. At this level, each hole should be capable of supporting 15,000 lbs. in clamped bearing.
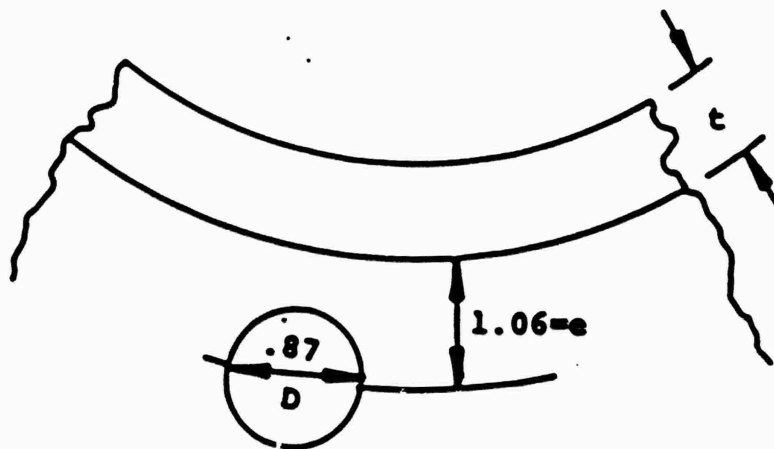
GEOMETRIC PARAMETERS NEAR A HOLE

Figure 4.4

$$D = .87 \text{ in.}$$
$$E = 1.06 \text{ in.}$$
$$e/D = 1.25 \text{ in.}$$
$$D/t = .87/.431 = 2.02$$

An important parameter in the bolt hole area of the wheel is the maximum in-plane strain which may be expected. To estimate its value, a force of 7500 lbs. is assumed to

be distributed uniformly along the length of the diameter - .87 inches. The strain in a symmetric laminate is given by (Reference 1):

$$\varepsilon_1 = a_{11} N_1 + a_{12} N_2 + a_{16} N_6$$

$$\varepsilon_2 = a_{21} N_1 + a_{22} N_2 + a_{26} N_6$$

$$\varepsilon_6 = a_{61} N_1 + a_{62} N_2 + a_{66} N_6$$

where: $\varepsilon_{1,2,6}$ = components of rotated longitudinal, transverse, and shear strain.

a_{ij} = laminate compliance components

N_i = stress resultants; average stress multiplied by laminate thickness.

When N_1 = 8620 lbs./in. and assuming it to be the major contributor to strain in the 1 direction, that strain becomes:

$$\varepsilon_1 \approx a_{11} N_1 = (8620 \text{ lbs./in.}) (1.642 \times 10^{-7} \text{ in./lb.})$$

$$\varepsilon_1 \approx .0014$$

where a_{11} is taken from Table 4.1.

Another component of strain in the disc is due to bending of the disc out of its original plane. The maximum bending moment per unit width of laminate was estimated in two ways. First, the maximum radial stress of a circular plate twisted from a central hole (Figure 4.5) is calculated in section 2. This model gives a conservative answer which is desired at this stage of design.

32
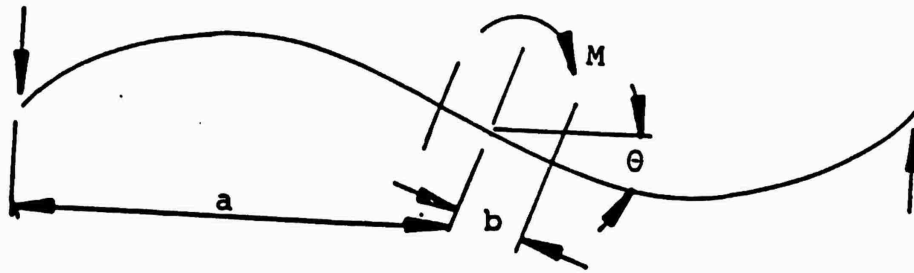
BENDING OF A DISC WITH A CENTRAL HOLE

FIGURE 4.5

$$\sigma_r = \frac{\beta M}{at^2}$$

b/a = .426

β = 2.062

M = 42600 in.-lbs. from the 15,000 lb. loading boundary condition

t = .431 in.

$$\sigma r = \frac{(2.062)(42600)}{(11.75)(.431)^2}$$

$$\sigma_r = 40244 \text{ psi}$$

The moment per unit width caused by the stress gradient through the thickness would be from the flexure formula,

$$\sigma_r = \frac{My}{I}$$

$$M = \frac{\sigma_r I}{y} = \frac{(40244)[\frac{(1)(.431)^3}{12}]}{.215}$$

M = 1248 in.-lbs./in.

33

Secondly, if it is assumed that the moment is evenly distributed along a chord line of the disc passing horizontally through the center of the lowest bolt hole, the resulting moment distribution becomes 42,600 in.-lbs./22 in. = 1,936 in.-lbs./in.

To obtain the strain due to this moment, the curvature must first be found. The moment-curvature relation for a symmetric laminate is given by,

$$k_1 = d_{11} M_1 + d_{12} M_2 + d_{16} M_6$$

$$k_2 = d_{21} M_1 + d_{22} M_2 + d_{26} M_6$$

$$k_6 = d_{61} M_1 + d_{62} M_2 = d_{66} M_6$$

where: k_i = laminate curvature,

M_i = bending moment per unit laminate depth,

d_{ij} = components of flexural compliance of a symmetric laminate

We assume that the primary bending moment M_1 is large compared to its transverse counterpart M_2 and the twisting moment M_6. Then;

$$k_1 = d_{11} M_1$$

$$k_1 = [9.14 \times 10^{-6} (lb.-in.)^{-1}] \times [1936 \; in.-lbs./in.]$$

$$k_1 = .0177 \; in^{-1}$$

$$\varepsilon_{1b} = k_1 \; (1/2 \; laminate \; thickness)$$

$$\varepsilon_{1b} = (.077 \; in^{-1})(.215 \; in.)$$

$$\varepsilon_{1b} = .0038$$

The assumptions made to arrive at this strain were conservative in that the entire bending moment was assumed to have been absorbed by the wheel disc neglecting the contribution of the rim. The actual bending moment in the disc laminate will decrease from the center outward along the chord line since the flexural rigidity varies with angle as shown by the values for d_{11} (γ) in Table 4.1.

Adding the in-plane and bending strains yields

$$\epsilon_1 \text{ total} = \epsilon_1 + \epsilon_{1b} = .0014 + .0038 = .0052$$

which is still within the .006 guideline.

4.2 M113A1 Composite Roadwheel Design

4.2.1 Design Considerations

The baseline composite design for this roadwheel shown in Figure 4.6 is similar to the LVTP7 wheel. It incorporates a laminate for the disc portions and a rim with preferential reinforcement in the hoop direction. Again, the worst loading case for this wheel is the maximum vertical load of 4,525 lbs. and the design is based on this load condition. The dimensioned drawing #740-0009 for this wheel is again found in Appendix 3.

Since the stresses in this roadwheel are not as high as for the LVTP7 wheel, a uniform laminate [15/45/-45/-15] was chosen for the entire disc area. The 15 and 45° angles are nominal angles at the mid radius of the wheel. As this laminate turns the corner into the rim it becomes mixed with layers in the hoop direction until, at the outer portion of the rim, there are two hoop layers for every layer from the disc laminate. This again is to reduce hoop deformation which prevents high interlaminar shear stresses at the loading point by distributing the load more evenly at the disc/rim interface. The high hoop fiber volume was maintained even at the contact surface unlike the LVTP7 wheel. This is due to the lower contact load and large radius of curvature at the rim outer corner. The thickness of the structural disc laminate is maintained at .31 in. to retain bending stiffness. It will be shown in the following analysis that a .21 in. thick laminate with a .050 abrasion covering on each side was not acceptable from a disc bending standpoint. The structural material chosen for this wheel is again a high strength graphite/epoxy with an impact abrasion covering of Kevlar or glass/epoxy.

35

COMPONENTS OF IN-PLANE
AND FLEXURAL STIFFNESS FOR LAMINATE
IN THE BOLT HOLE AREA OF THE LVTP7 WHEEL
TABLE 4.1

	γ(deg)	0	15	30	45	60
A_{11}	lb/in	6.846 E+06	6.289 E+06	5.077 E+06	3.641 E+06	2.389 E+06
A_{22}		1.293 E+06	1.612 E+06	2.529 E+06	3.905 E+06	5.394 E+06
A_{12}		9.817 E+05	1.100 E+06	1.248 E+06	1.278 E+06	1.159 E+06
A_{66}		1.248 E+06	1.366 E+06	1.514 E+06	1.544 E+06	1.425 E+06
A_{16}		-1.173 E+05	-9.051 E+05	-1.338 E+06	-1.337 E+06	-1.015 E+06
A_{26}		-1.462 E+04	-5.972 E+05	-1.133 E+06	-1.439 E+06	-1.323 E+06
a_{11}	in/lb	1.642 E-07	1.879 E-07	2.592 E-07	4.027 E-07	6.043 E-07
a_{22}		8.679 E-07	7.911 E-07	6.003 E-07	3.903 E-07	2.417 E-07
a_{12}		-1.245 E-07	-9.796 E-08	-3.819 E-08	-4.947 E-09	-3.148 E-08
a_{66}		8.029 E-07	9.090 E-07	1.148 E-06	1.281 E-06	1.175 E-06
a_{16}		1.397 E-08	8.167 E-08	2.004 E-07	3.441 E-07	4.013 E-07
a_{26}		-1.528 E-09	2.810 E-07	4.512 E-07	3.596 E-07	2.020 E-07
D_{11}	lb-in	1.196 E+05	1.062 E+05	7.926 E+04	5.032 E+04	2.852 E+04
D_{22}		1.348 E+04	1.853 E+04	3.348 E+04	5.872 E+04	8.885 E+04
D_{12}		1.143 E+04	1.559 E+04	2.160 E+04	2.345 E+04	1.929 E+04
D_{66}		1.554 E+04	1.970 E+04	2.571 E+04	2.755 E+04	2.339 E+04
D_{16}		-3.436 E+03	-2.096 E+04	-2.856 E+04	-2.519 E+04	-1.605 E+04
D_{26}		-7.626 E+02	-9.209 E+03	-1.949 E+04	-2.786 E+04	-2.780 E+04
d_{11}	lb-in^{-1}	9.140 E-06	1.226 E-05	2.104 E-05	3.682 E-05	5.713 E-05
d_{22}		8.077 E-05	7.234 E-05	5.346 E-05	3.290 E-05	1.792 E-05
d_{12}		-7.655 E-06	-4.996 E-06	5.108 E-08	2.439 E-06	-2.200 E-07
d_{66}		6.485 E-05	7.548 E-05	9.567 E-05	1.052 E-04	9.459 E-05
d_{16}		1.646 E-06	1.071 E-05	2.341 E-05	3.613 E-05	3.894 E-05
d_{26}		2.272 E-06	2.850 E-05	4.058 E-05	3.550 E-05	2.114 E-05

.108 [15/-15]
.215 [15/45/-45/-15]
.108 [15/-15]
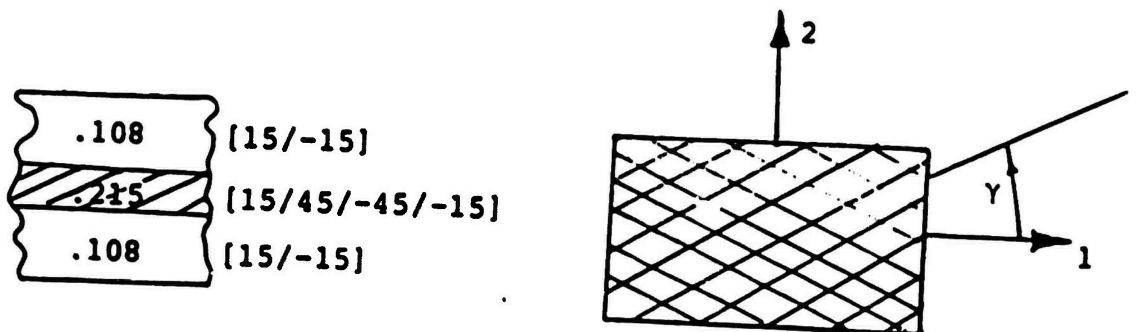
$[D_{ij}]$ and $[d_{ij}]$ denote flexural stiffness and compliance.

$[A_{ij}]$ and $[a_{ij}]$ denote in-plane stiffness and compliance.

COMPONENTS OF IN-PLANE
AND FLEXURAL STIFFNESS FOR LAMINATE
AT OUTER RADIUS OF WHEEL DISC
TABLE 4.2

	γ(deg)	0	15	30	45	60
A_{11}	lb/in	7.415 E+06	6.839 E+06	5.372 E+06	3.625 E+06	2.174 E+06
A_{22}		1.020 E+06	1.300 E+06	2.174 E+06	3.625 E+06	5.372 E+06
A_{12}		8.336 E+06	9.817 E+05	1.278 E+06	1.426 E+06	1.278 E+06
A_{66}		1.099 E+06	1.248 E+06	1.544 E+06	1.692 E+06	1.544 E+06
A_{16}		0.0	-1.056 E+06	-1.641 E+06	-1.599 E+06	-1.128 E+06
A_{26}		0.0	-5.429 E+05	-1.128 E+06	-1.599 E+06	-1.641 E+06
a_{11}	in/lb	1.485 E-07	1.758 E-07	2.761 E-07	4.738 E-07	7.418 E-07
a_{22}		1.080 E-06	9.825 E-07	7.418 E-07	4.738 E-07	2.761 E-07
a_{12}		-1.214 E-07	-8.630 E-08	1.608 E-08	1.902 E-08	-1.608 E-08
a_{66}		9.096 E-07	1.050 E-06	1.331 E-06	1.471 E-06	1.331 E-06
a_{16}		0.0	1.113 E-07	2.817 E-07	4.657 E-07	5.250 E-07
a_{26}		0.0	3.545 E-07	5.250 E-07	4.657 E-07	2.817 E-07
D_{11}	lb-in	1.241 E+05	1.154 E+05	8.858 E+04	5.617 E+04	3.025 E+04
D_{22}		1.150 E+04	1.496 E+04	2.723 E+04	5.035 E+04	8.151 E+04
D_{12}		1.017 E+04	1.279 E+04	2.007 E+04	2.472 E+04	2.209 E+04
D_{66}		1.427 E+04	1.689 E+04	2.417 E+04	2.882 E+04	2.620 E+04
D_{16}		2.625 E+03	-1.853 E-04	-3.054 E+04	-2.932 E+04	-1.939 E+04
D_{26}		2.856 E+02	-7.101 E+03	-1.677 E+04	-2.698 E+04	-3.082 E+04
d_{11}	$(lb-in)^{-1}$	8.716 E-06	1.075 E-05	2.003 E-05	3.841 E-05	6.298 E-05
d_{22}		9.375 E-05	8.535 E-05	6.421 E-05	4.033 E-05	2.212 E-05
d_{12}		-7.670 E-06	-4.491 E-06	1.441 E-06	4.194 E-06	1.015 E-06
d_{66}		7.035 E-05	8.307 E-05	1.068 E-04	1.178 E-04	1.051 E-04
d_{16}		-1.450 E-06	9.909 E-06	2.631 E-05	4.301 E-05	4.782 E-05
d_{26}		-4.654 E-07	3.095 E-05	4.637 E-05	4.203 E-05	2.678 E-05

.180 [15/-15]

.071 [15/45/-45/-15]

.180 [15/-15]

FIGURE 4.6

.41

.31

Titanium sleeve .10 in. wall
.31 in. long bonded into
graphite laminate hole

.050 Woven glass
or kevlar fabric

[15/45/-45/-15]$_n$

Graphite epoxy

laminate

Increasing proportion
of hoop fibers from
disc toward edge of
rim to a maximum of
[H$_2$/15/H$_2$/45...]

Note: Average
angles from radial
direction

1.08

Wear ring
bonded to
laminate

Rubber tire

M113A1 COMPOSITE ROADWHEEL
LAMINATE DESIGN

39
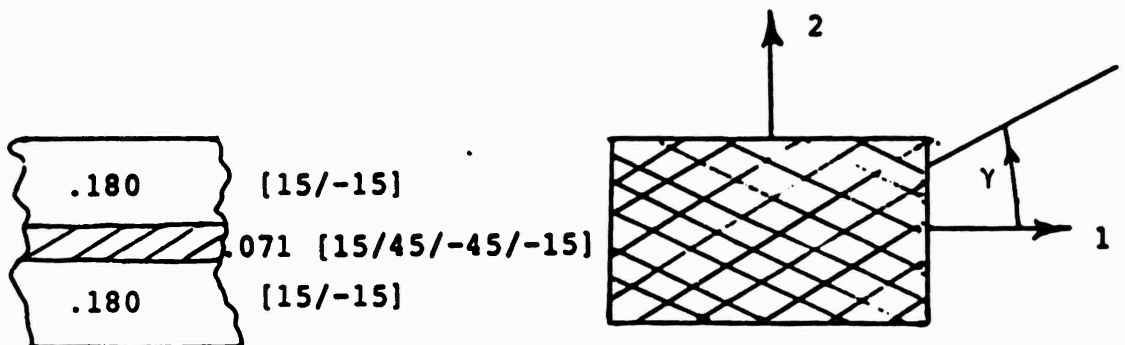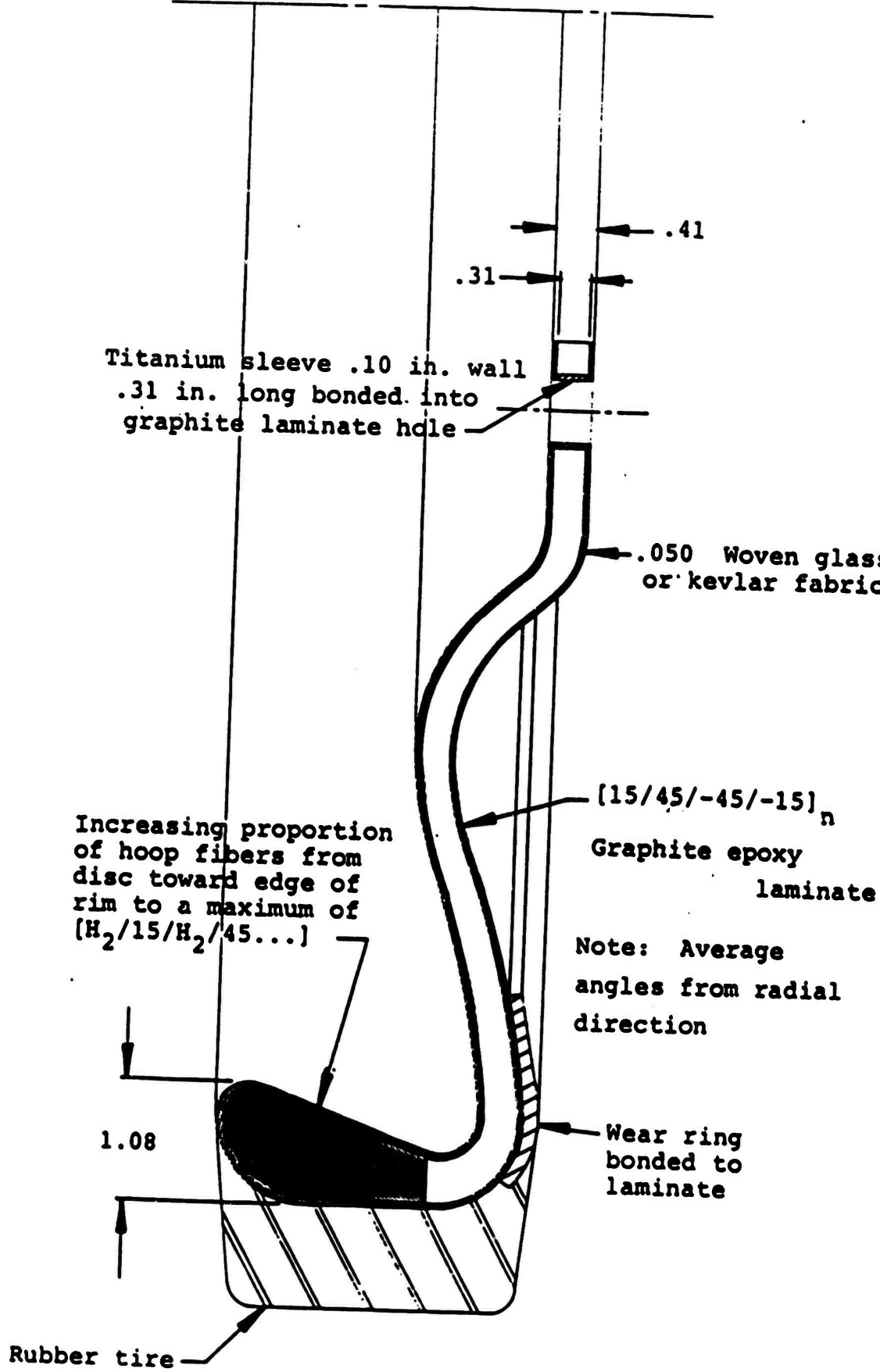
4.2.2 Analysis of Critical Areas

Rim   The hoop flexural rigidity of the composite
rim was compared to that of the aluminum rim by approxi-
mating the outer rim of the composite wheel by a set of
rings with rectangular cross sections. The hoop flexural
rigidity of the outer .75 in. of the aluminum rim was
calculated previously as

$$EI_{.75al} = 1.25 \times 10^6 \text{ lb-in}^2$$

while the entire aluminum rim including the transition
to the disc was

$$EI_{2.91al} = 2.22 \times 10^6 \text{ lb-in}^2$$

The 2:1 hoop laminate chosen has about twice the flexural
rigidity in the hoop direction as an equivalent aluminum
ring. The equivalent EI of the composite rim was found by
calculation of the [D] matrix for the cross-sections of
each of two rings .375 in. wide. The flexural rigidity
of the outer .75 in. of the composite rim was found to be

$$EI_{.75gr} = 5.72 \times 10^6 \text{ lb-in}^2$$

This value assumes that the hoop bending moment is the
major contributor to change in hoop curvature. This value
is more than twice the rigidity for the full width aluminum
rim.

The maximum strain in the hoop direction resulting
from rim flexure was found using the maximum moment M_1 =
12111 in.-lbs., calculated in section 2 for the full
width of the roadwheel. Assuming the entire moment is
supported by the outer .75 in. of the composite rim we have
for the curvature from the inverse of equation ($k_1 = d_{11}M_1$),

$$M_1 = D_{11}k \qquad (3.6)$$

$$k_1 = (12111 \text{ in-lbs/in})/(7.621 \times 10^6)\text{in-lbs}$$

$$k_1 = .00159 \text{ in}^{-1}$$

39

To get the strain ε_H, the curvature is multiplied by the distance from the neutral axis to the outer fiber which for this case is taken as .61 in. from the previous calculation of flexural stiffness.

$$\varepsilon_H = (.61 \text{ in.}) \ (.00159 \text{ in}^{-1})$$

$$\varepsilon_H = .00097$$

This strain level is well within the boundary of .006.

__Holes__   The bearing stress at the holes assuming all the load of 4,525 lbs is supported at one hole is

$$\sigma_b = \frac{(4,525 \text{ lbs})}{(.7 \text{ in}) \ (.31) \text{in}} = 20,852 \text{ psi}$$

Even this condition is well within the clamped bearing capability of the disc laminate (referring again to reference 3 Figure 2.4.2-26).

The maximum in-plane strain near a hole is estimated by assuming all the load is taken by one hole and uniformly distributed across its diameter of .7 in.

$$\varepsilon_{1 \text{ disc}} = a_{11} \ N_1$$

where a_{11} = 3.081 x 10^{-7} in/lb from Table 4.3
N_1 = 6,464 lbs/in

$$\varepsilon_{1 \text{ disc}} = .002$$

__Bending of the Disc__. As before $\sigma = \beta M/(at^2)$ will be used to estimate the maximum local bending moment within the disc.

$$\sigma_r = \frac{\beta M}{at^2}$$

$$M = (4,525 \text{ lbs}) \ (.66 + \frac{2.91}{2} \text{ in})$$

$$M = 9,570 \text{ in-lbs}$$

40

COMPONENTS OF IN-PLANE AND FLEXURAL STIFFNESS
FOR THE LAMINATE IN THE DISC AREA OF THE
M113A1 ROADWHEEL
TABLE 4.3

γ (deg)		0	15	30	45	60
A_{11}	lb/in	3.970 E+06	3.879 E+06	3.568 E+06	2.995 E+06	2.252 E+06
A_{22}		1.337 E+06	1.599 E+06	2.252 E+06	2.995 E+06	3.568 E+06
A_{12}		9.845 E+05	8.992 E+05	7.285 E+05	6.431 E+05	7.285 E+05
A_{66}		1.176 E+06	1.091 E+06	9.199 E+05	8.346 E+05	9.199 E+05
A_{16}		0.0	-1.812 E+05	-4.221 E+05	-6.581 E+05	-7.178 E+05
A_{26}		0.0	-4.769 E+05	-7.178 E+05	-6.581 E+05	-4.221 E+05
a_{11}	in/lb	3.081 E-07	2.971 E-07	3.049 E-07	4.049 E-07	6.081 E-07
a_{22}		9.146 E-07	8.224 E-07	6.081 E-07	4.049 E-07	3.049 E-07
a_{12}		-2.268 E-07	-1.752 E-07	-7.193 E-08	-2.030 E-08	-7.193 E-08
a_{66}		8.503 E-07	1.057 E-06	1.470 E-06	1.676 E-06	1.470 E-06
a_{16}		0.0	-2.724 E-08	8.376 E-08	3.032 E-07	4.415 E-07
a_{26}		0.0	3.305 E-07	4.415 E-07	3.032 E-07	8.376 E-08
D_{11}	lb-in	3.197 E+04	2.919 E+04	2.557 E+04	2.109 E+04	1.605 E+04
D_{22}		1.064 E+04	1.357 E+04	1.984 E+04	2.680 E+04	3.166 E+04
D_{12}		7.837 E+03	7.755 E+03	6.435 E+03	5.199 E+03	5.282 E+03
D_{66}		9.371 E+03	9.288 E+03	7.969 E+03	6.732 E+03	6.815 E+03
D_{16}		-2.093 E+03	-3.092 E+03	-3.855 E+03	-4.667 E+03	-4.714 E+03
D_{26}		-7.604 E+02	-4.711 E+03	-6.807 E+03	-5.999 E+03	-3.096 E+03
d_{11}	lb-in^{-1}	3.855 E-05	4.041 E-05	4.348 E-05	5.617 E-05	8.021 E-05
d_{22}		1.148 E-04	1.018 E-04	7.347 E-05	4.676 E-05	3.392 E-05
d_{12}		-2.795 E-05	-2.235 E-05	-9.739 E-06	-2.726 E-06	-8.325 E-06
d_{66}		1.084 E-04	1.308 E-04	1.812 E-04	2.093 E-04	1.869 E-04
d_{16}		6.340 E-06	2.118 E-06	1.272 E-05	3.651 E-05	5.171 E-05
d_{26}		3.076 E-06	4.418 E-05	5.805 E-05	3.977 E-05	9.646 E-06

[15/45/-45/-15]$_{16s}$

32 layers total

symmetric graphite/epoxy laminate

.31 in. thick
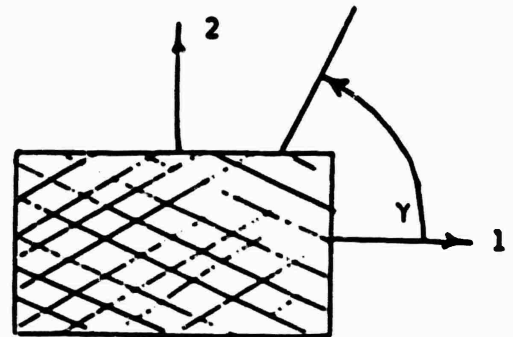
$$a = 10.97 \text{ in.}$$

$$b = 2.63 \text{ in.}$$

$$t = .31 \text{ in.}$$

for $b/a = 2.39$ $\quad \beta = 3.8$

$$\sigma_r = 34,495 \text{ psi} = \frac{M_{local} Y}{I}$$

$$M_{local} = \frac{(1) \ (.31)^3}{(12)(.155)} (34,495) \ \frac{\text{in-lbs}}{\text{in}}$$

$$M_{local} = 552 \text{ in-lbs/in}$$

The alternate approach of assuming that the entire imposed bending moment is supported along a chord line passing through the bolt hole closest to the ground yields.

$$M_{local} = \frac{9,570 \text{ in-lbs}}{11 \text{ in}} = 870 \text{ in-lbs/in}$$

Using this larger value to determine strain due to bending

$$k_1 = \frac{M_{local}}{D_{11}}$$

$$k_1 = \frac{870 \text{ in-lbs/in}}{3.197 \times 10^4 \text{ in-lb}}$$

$$k_1 = .0272 \text{ in.}^{-1}$$

$$\epsilon_{bend} = (.155) \ (.0272) = .0042$$

If a laminate thickness of .21 in. were used

$$D_{11} = 1.038 \times 10^4 \text{ in-lbs}$$

and the distance from the neutral axis to the laminate outer fiber would be .105 in.

The maximum strain would then be

$$\epsilon_{bend \ .21} = (.105 \text{ in.}) (\frac{870 \text{ in-lbs/in}}{1.038 \times 10^4 \text{ in-lbs}} = .0088$$

This value is higher than the .006 allowable so the thinner laminate cannot be used given the assumptions made.

4.3 Additional Design Concepts

Two other design approaches are presented to show that a variation in geometry with application of a lightweight core material may allow more efficient load introduction into the composite structure. In design with structural composite materials, introducing the load into the laminates or 3D structures is usually the biggest problem. In this case the vertical load is imposed along a narrow band at the high pressure contact area of the rim with the rubber tire. In the previous designs this vertical load was supported by a stiff rim which transmitted the vertical load to the disc through shear at the corner of the disc/rim interface. The distribution of this shear stress from the point of load application along the rim is best determined through prototype testing. The two alternate designs -- the Laminated Cone Concept of Figure 4.7 and the Double Walled Core Concept of Figure 4.8 -- are attempts to introduce the compressive loading directly into the disc of the wheel. This eliminates a potentially high interlaminar shear stress at the corner of the wheel.

The laminated cone concept is shown for the M113A1 roadwheel in Figure 4.7. Its structure is a stack of four (or perhaps more) laminates on the order of .10 in. thick. In the bolt hole area, they are bonded together to form a thick laminate but separate and flare out to form four separate discs at the OD of the wheel. To prevent buckling of the separated laminates and also transmit shear loading from one laminate to the other, the spaces between laminates are filled with a lightweight core material such as Rohacell foam. Typical properties of this foam core are given in Table 4.4. The laminates are built up slightly at the edges to provide a wider bearing surface. Assuming each carries a nominal 1,000 lb. compressive load distributed over a .20 x .25 surface, the resulting stress would be 20 ksi-- a feasible level for the [±15 ±45] laminate. Since transmitting the bearing loads into the laminate discs through shear would be difficult for the foam core or rubber, an overwrapped rim is added. This can be a [0, ±45] laminate with the 0° direction parallel to the wheel axis to support bending between the disc laminate bearing points.

One possible disadvantage of this concept is that the direct bearing load introduction reduces the global compliance of the wheel as a whole. Depending on fiber orientations within the lamina, it can become very stiff causing problems in a shock loading environment.

43

LAMINATED CONE CONCEPT
Figure 4.7

.31

Graphite/Epoxy
Laminates

Light Weight Core

Overwrapped Rim
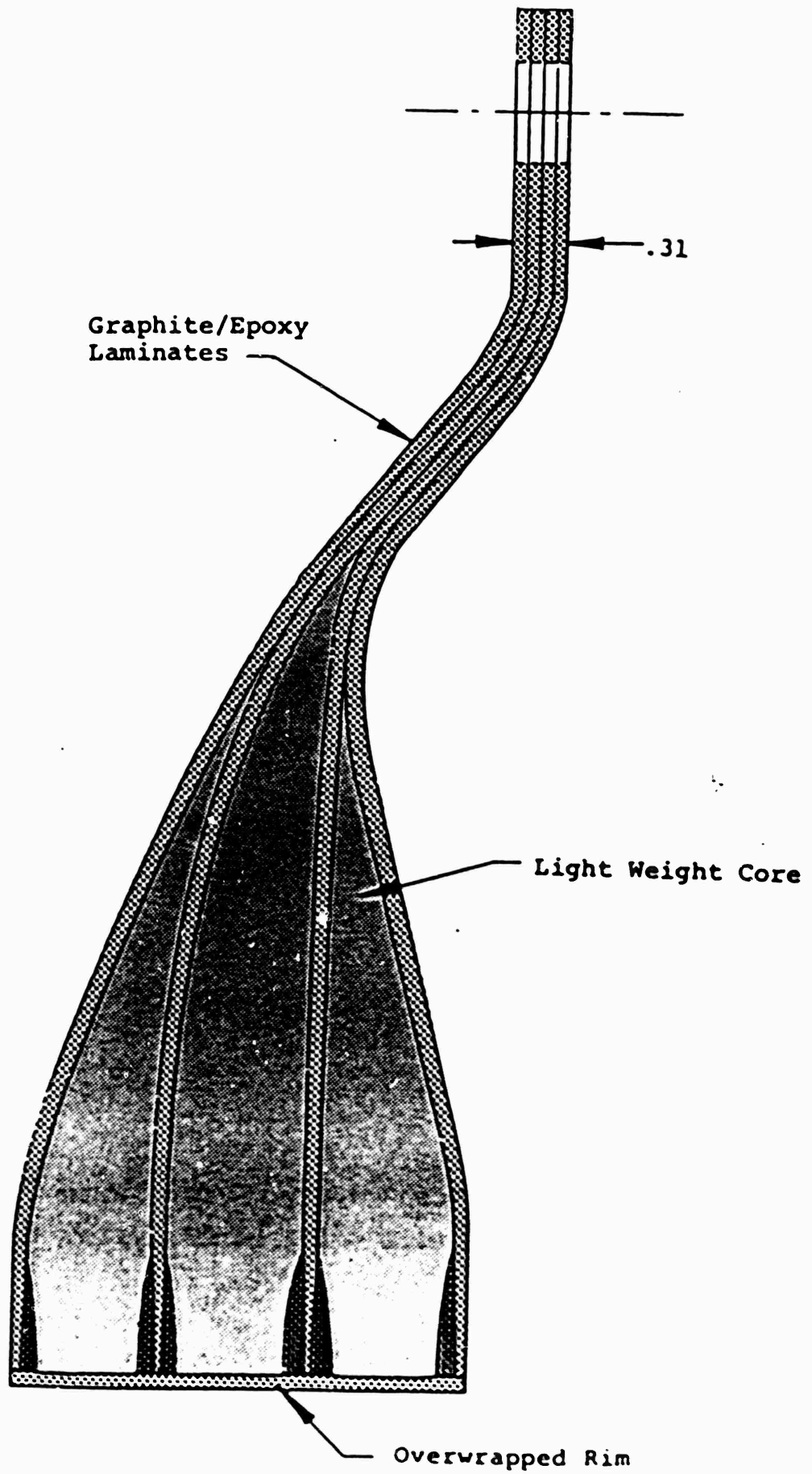
DOUBLE WALLED CORE

DESIGN CONCEPT

FIGURE 4.8
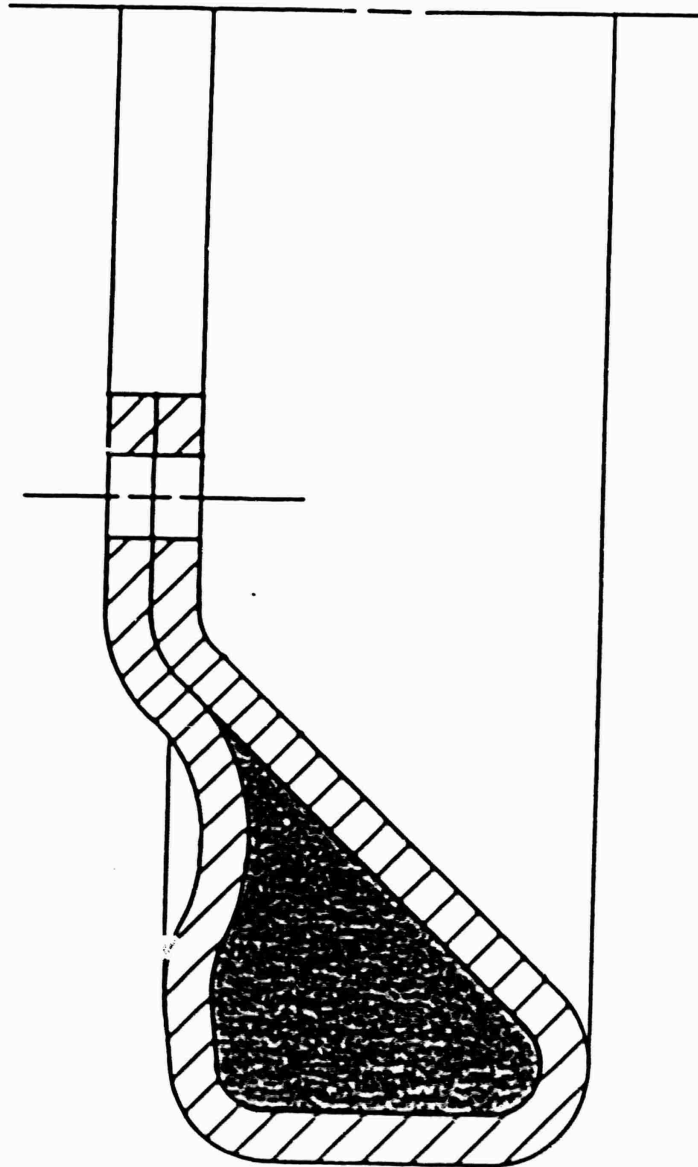
Typical Mechanical Properties of Rohacell® Foam Core
Table 4.4

Density 7 lb/ft^3

Max. tensile stress 525 psi

Max. flexural stress 738 psi

Max. compressive stress 511 psi

Max. shear stress 341 psi

Young's Modulus 25,560 psi

Shear Modulus 7,100 psi

Max. strain to failure 3%

The second alternate concept, the double walled core, involves the features of both the pure laminated and laminated cone concepts. The core is again required to prevent buckling of the laminated skins whose thickness would be typically half the thickness of the laminate in the bolt hole area. The interlaminar shear distribution in the contact area is again an area of concern and is best resolved by subscale or proto-type testing. From a design point-of-view, this concept has the potential advantages of slightly higher overall compliance and possibly lower shear stresses at the corners depending on the interaction between the core and the covering laminates. In both this and the laminated cone concept, the wheel's bending rigidly about a horizontal axis through the wheel center is increased over the pure laminated design.

Table 4.5 gives a comparision of the weights for the existing wheels and estimated weights for the composite wheels. It shows a weight savings of 17 lbs or 27% for the LVTP7 wheel. The laminate design for the M113A1 wheel saves 5 bls over the aluminum wheel while the laminated cone design for this wheel saves 10 lbs or 28%. The difference is due to a more efficient use of the structural material in the laminated cone design.

46

WEIGHT COMPARISONS

TABLE 4.5

LVTP7 Existing Wheel	wt. (lbs.)
Aluminum Wheel	38.63
Wear Ring	8.23
Rubber Tire	15.14
	62.00 lbs.

LVTP7 Laminate Design Composite	
Graphite/Epoxy Structure	19.18
Glass Cover	3.00
Wear Ring	8.23
Rubber Tire	15.14
	45.55 lbs.

M113A1 Existing Wheel	
Aluminum Wheel	22.35
Wear Ring	6.13
Rubber Tire	7.52
	36.00 lbs.

M113A1 Laminate Design	
Graphite/Epoxy Structure	15.25
Glass Cover	3.00 (approximate)
Rubber Tire	7.52
Wear Ring	6.12
	31.89 lbs.

M113A1 Laminated Cone Concept (w/.10 in. rim)	
Graphite/Epoxy Structure	8.15
Rohacell Foam	2.10
Wear Ring	6.12
Rubber Tire	7.52
	23.89 lbs.

47

5.0 Manufacturing Analysis

5.1 Fabrication Concepts

A review was conducted of the available fabrication concepts that might be used to produce a fiber reinforced composite roadwheel. Each concept was examined relative to the advantages and disadvantages in general and to the suitability for the design concept presented in section 4.0.

(a) Injection Molding

Advantages	- very low labor cost
	- good part consistency
	- good toughness properties
	- intricate shape capabilities
Disadvantages	- poor thermal properties
	- low physical strength of materials
	- difficult to control fiber orientation caused by resin flow
	- tooling costs
Conclusion	The method is not acceptable due to poor environmental properties, low stress allowable around bolt holes, and poor shear stress capabilities.

(b) Resin Transfer Molding (RTM)

Advantages	- lower material cost that prepeg
	- two finished surfaces
	- low cost tooling
Disadvantages	- resin systems have moderate shear strength
	- physicals are limited by moderate fiber volume
Conclusion	The method is not acceptable for this application due to poor physicals resulting from the moderate fiber volume and from the poor properties of the low viscosity resins.

48

(c)   Press Molding

    Advantages   – more economical than autoclave
                        molding for large volume
                      - two finished surfaces
                      - high fiber volume
                      - allows high quality resins to be
                        used

    Disadvantages   - shape is limited due to the
                        requirements for positive draft
                        for the molds
                      - the mold surface should be as
                        near to perpendicular to the ram
                        stroke as possible
                      - the long cure cycle of the high
                        quality epoxy resins will limit
                        output to about one part every
                        two hours

    Conclusion   The advantages relative to auto-
                      clave molding do not appear to
                      warrant the required expenses for
                      the tools and the large number of
                      presses

(d)   Autoclave Molding

    Advantages   - very good part quality
                      - economical tooling
                      - high fiber volume
                      - allows high quality resins to be
                        used

    Disadvantages   - one finished surface
                      - some increased labor due to
                        vacuum bagging
                      - material costs tend to be high

    Conclusion   The method meets the requirements
                      for the part quality both in terms
                      of resin quality and fiber volume

(e)   Filament Winding

    Advantages   - lowest cost for materials
                      - lowest labor cost

    Disadvantages   - fiber orientation has limitations
                      - fiber placement has limitations

49

Conclusion   Filament winding is not suitable due
                  to the inability to achieve control
                  over both the fiber orientation and
                  wall thickness on the disc face.

5.2 Selected Fabrication Method

Only two of the five fabrication methods for the AMMRC
Composite Roadwheel application were deemed practical.
Injection molding and transfer molding are unsuitable
because of their insufficient physical properties as a result
of the lower fiber content necessary to apply these processing
methods.

Press molding and autoclave molding were the two options
that allowed for very high fiber content with resultant
higher physical properties. Both methods however, involve
higher quality and therefore higher priced prepeg. Autoclave
molding is the most practical method of the two. Press mold-
ing offers no significant benefits over autoclave molding
other than a part with finished surfaces on both sides.

Autoclave molding requires far less tooling costs than
 press molding. The extra time required to apply a vacuum
bag would be about 1/2 hour resulting in extra labor costs
of roughly $5. Against this cost increase of approximately
¼ of 1 percent, the autoclave process has the further benefit
of being more easily adapted to variations in production rate
due to the capability of curing several wheels at one time.

5.2.1 Process Description

The fabrication process that would be used for the
design concept shown in Figure 4.3 is based on using unidirec-
tional prepeg for material to be placed on ±15 degree angles
or for the hoop wraps on the rim. The ±45 degree material
would be made from balanced weave (5H) prepeg pattern cut
on the bias. Placement of the prepeg on the male mold will
require that the material be cut in pie-shaped sections
with a maximum of about four inches. This is necessary in
order to form the material over the rim of the wheel as it
is a 3-D curve and the prepeg is a 2-D material. Approxima-
tely 2000 pieces will be required for each wheel. The hoop
wrap material on the rim would be applied as a continuous
tape by winding it on the mold. Application of vacuum bags,
bleeders and curing cycles would be in accordance with
current practice.

The male molds would be constructed composites
and would be made in several pieces to allow for part
molding with negative draft.

50

5.3 Cost Analyses

Estimates were made for the tooling and manufacturing costs for 30 and 24,000 unit quantities (20,000 for the M113A1). The estimates were based on production during a one-shift day with 250 production days.

5.3.1 LVTP7 Estimates

Estimates for both LVTP7 and the M113A1 were based on similar production methods and materials.

LVTP7 Estimate

Item	30 Units	24,000 Units
Tooling Master	8,900	8,900
Glass/Epoxy Molds (one)	3,100	-
Glass/Epoxy Molds (100)	-	168,000
Engineering	29,000	40,000
C/Ep Prepreg (26.7#ea.)	29,790	23,830,000
Glass/Epoxy Prepreg (7.1#ea.)	4,560	3,648,000
Production Labor (20 hrs./pc)	12,000	-
(13.4 hrs./pc)	-	6,432,000
Total Costs	$87,350	$ 34,126,900
Cost/Wheel	$ 2,912	$ 1,422

M113A1 Estimate

Item	30 Units	20,000 Units
Tooling Master	8,900	8,900
Glass/Epoxy Molds (one)	3,100	-
Glass/Epoxy Molds (80)	-	143,000
Engineering	29,000	40,000
C/Ep Prepreg (23#ea.)	25,660	17,108,000
Glass/Ep Prepreg (4.5#ea.)	2,890	1,927,000
Production Labor (17 hrs./pc)	10,200	-
(11.2 hrs./pc)	-	4,480,000
Total Costs	$79,750	$23,706,900
Cost/Wheel	$ 2,658	$ 1,185

The above cost estimates are based on the following cost factors:

Shop labor rate   = $20/hr.
Engineer rate   = $60/hr.
G & A on Material = 30%
Fee   = 10%
Material Waste   = 50%

51

5.4 Alternative Design Concept

The four plate concept shown in Figure 4.7 was examined for possible cost savings. Due to the predominance of the effects of material cost, this concept results in an estimated cost reduction of approximately 15%.

Tooling	300,000
Engineering	55,000
Material	12,354,000
Labor	7,200,000
Total	$19,909,000
Cost/Wheel	$ 995 ea.

$$\frac{1185-995}{1185} = 16\%$$

5.5 Alternative Materials

Due to the high material costs, other resin systems were considered. Use of a 250°F curing system would reduce the prepreg cost from $26/# to about $22/# but it was not done at this time due to the task of resistance to heat. The $26/# value is on the low side for 350°F curing systems.

5.6 Materials Qualifications

The prepreg materials will be certified to the manufacturers' specifications and will be tested for tensile and shear strength per ASTM standards for carbon/epoxy laminates.

52

6.0 Conclusions and Recommendations

The results of this study indicate that advanced composite materials are a feasible alternate material for roadwheel construction from a performance point-of-view. That is, the objective of significant weight saving while maintaining the current level of reliability/maintainability of aluminum wheels can be met. Economical manufacture of these roadwheels, however, is doubtful. A continuous graphite fiber composite was chosen as the structural material from the necessity to meet both static structural, fatigue and weight savings goals. Manufacturing analysis showed that the wheel cost is largely material cost dependent due to the conservative analyses done in this study; there is a possibility that further cost reductions could be achieved by additional analysis or testing.

It is recommended that the demonstrator wheels be manufactured as originally planned; however, results of this design and analysis task indicate the need for limited subscale and prototype testing to verify analytical results and establish an optimum design. If promising results are obtained with the demonstrator program, a manufacturing technology program should be undertaken to reduce the single part cost for the large scale production run.

6.0 REFERENCES

1. Tsai, S. W. and Hahn, H. T., Introduction to Composite Materials, Technomic Publishing Company, 1980.

2. Koo, F. H. and Kliger, H. S., "Development of Carbon Fiber-Resin Composite Material For Advanced ABM Structures", AMMRC CTR 75-17, September 1975.

3. Advanced Composites Design Guide, Advanced Development Division, AFML, January 1973, Revisions to-date.

4. Roark, R.J., and Young, W. C., Formulas for Stress and Strain, Fifth Edition, McGraw-Hill Book Company, 1975.

5. Timoshenko and Young, Elements of Strength of Materials, Fifth Edition, D. Van Nostrand Company, 1968.

6. Katz, I., Adhesive Materials, Revised Edition, Foster Publishing Company, 1971.

7. Cagle, C.V., Handbook of Adhesive Bonds, McGraw-Hill Book Company, 1973.

8. Lifshitz, J.M., Strain Rate, Temperature and Humidity Influences on Strength and Moduli of a Graphite/Epoxy Composite, NASA TM-81247, Jan. 1981

APPENDIX 1

LVTP7 ROADWHEEL STRESS CONTOURS

VERTICAL LOAD CASE

MID PLANE CROSS SECTION VIEW

FIGURE A1.1
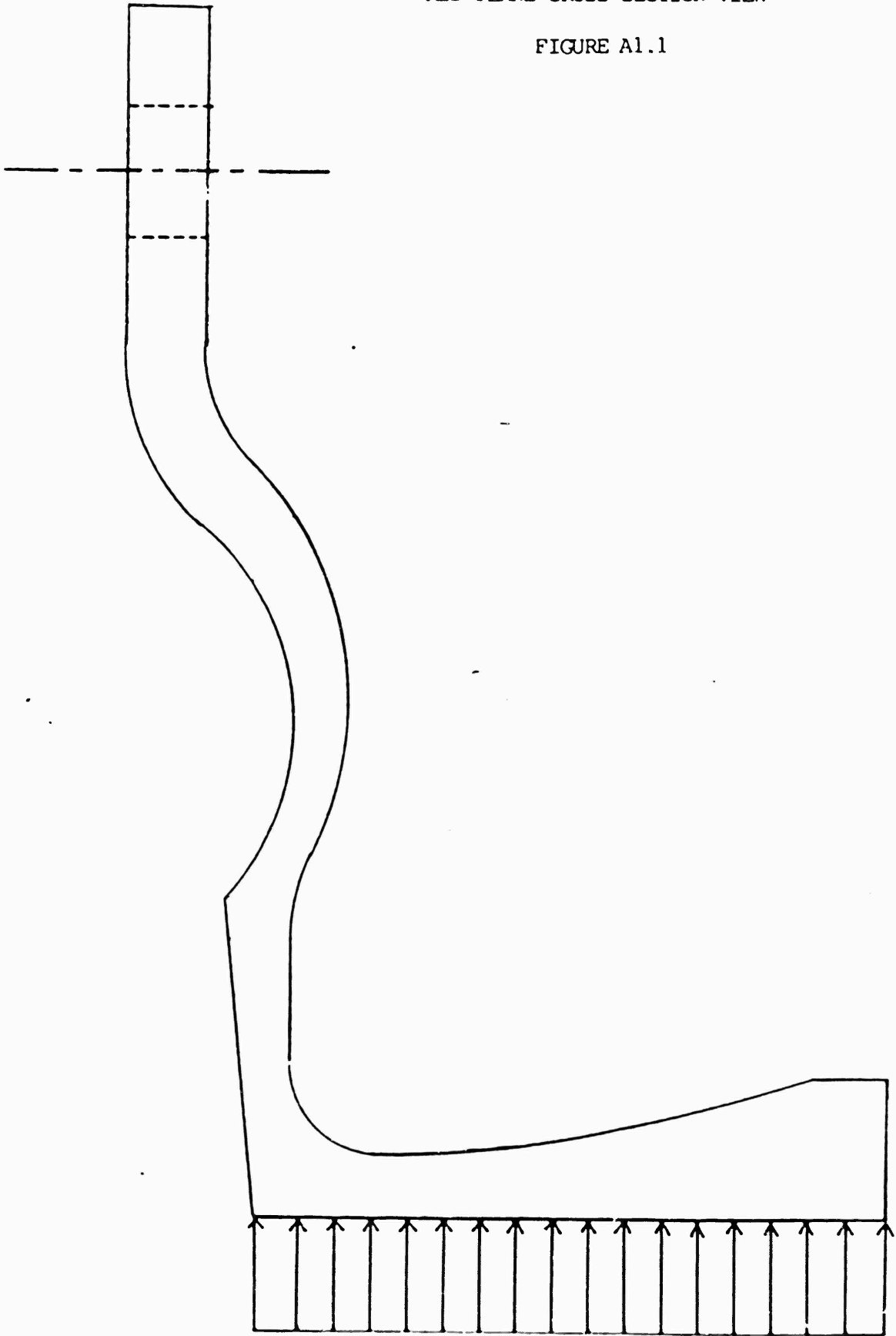
15,000 LB. LOAD UNIFORMLY DISTRIBUTED
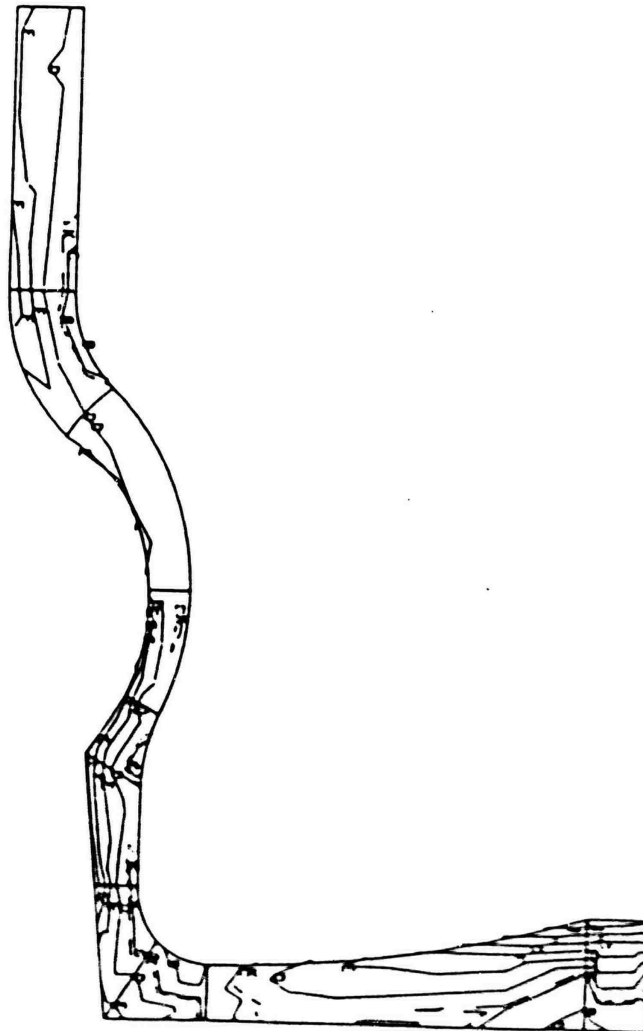
LEGEND

A = -1.115E+4 psi
B = -5.107E+3
C = -1.050E+3
D = +3.968E+3
E = +9.035E+3
F = +1.405E+4
G = +1.913E+4
H = +2.416E+4
I = +2.922E+4
J = +3.427E+4
K = 0.000E 0

MAXIMUM PRINCIPAL STRESS CONTOURS

MID PLANE CROSS SECTION
VERTICAL LOAD CASE
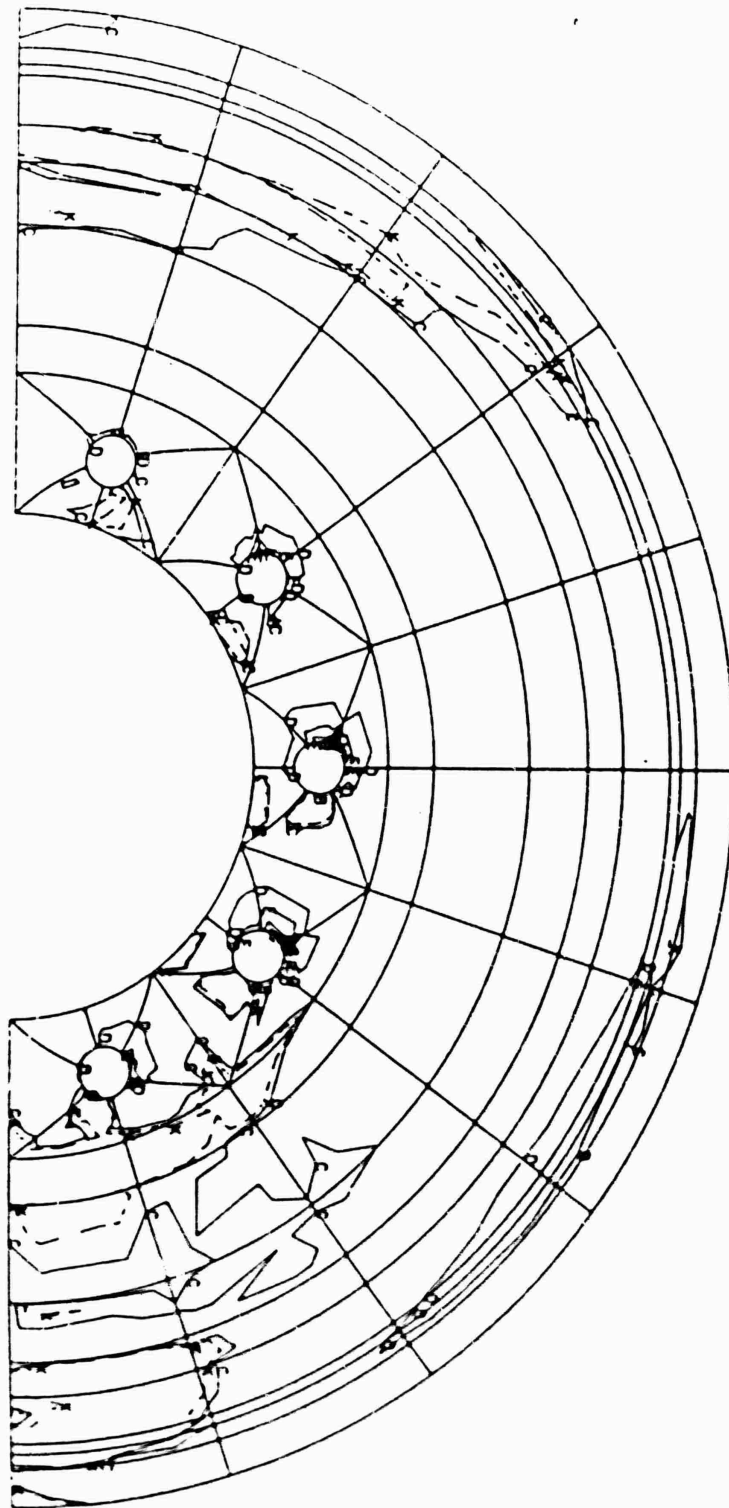
FIGURE A1.2

57

MAXIMUM PRINCIPAL STRESS CONTOURS

FRONT SURFACE
VERTICAL LOAD CASE
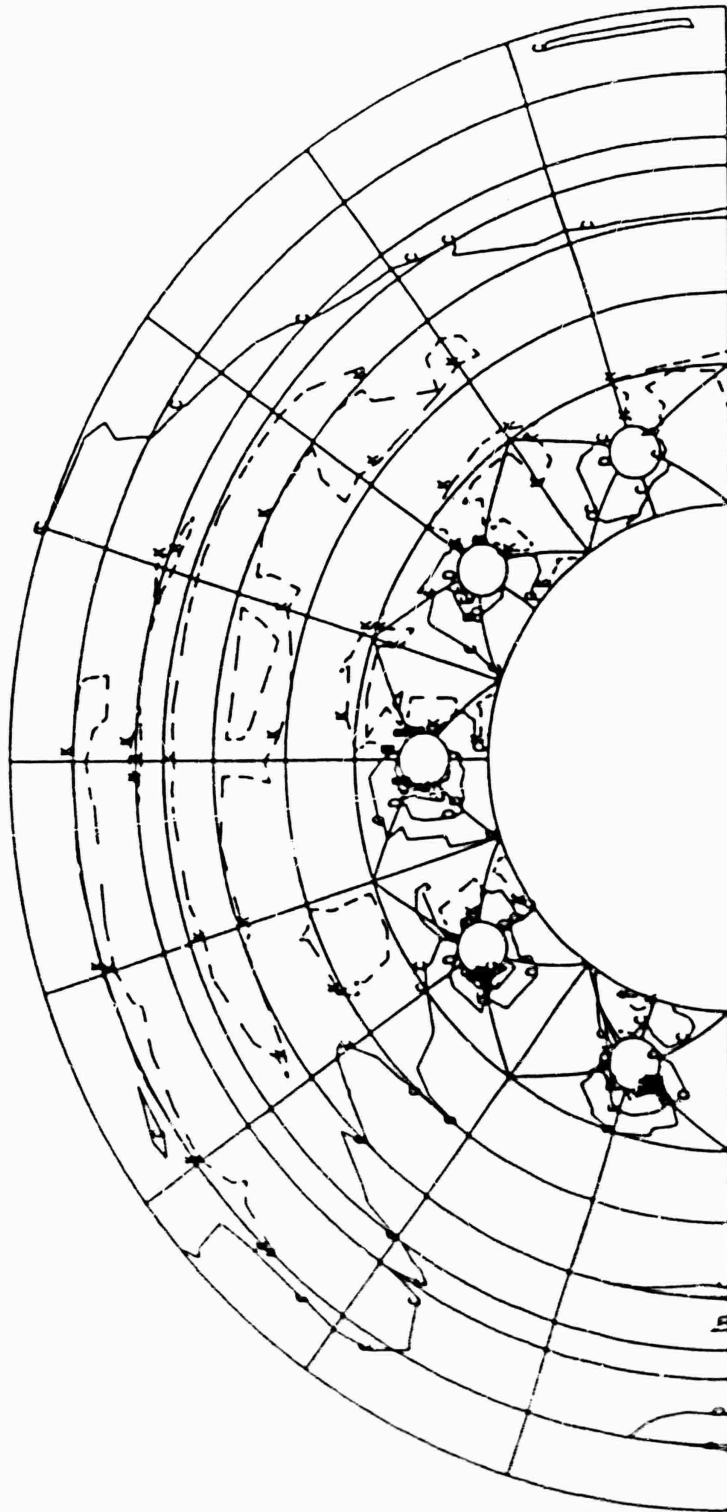
FIGURE A1.3

LEGEND

A = -2.819E+4 psi
B = -1.185E+4
C = -4.465E+3
D = -2.079E+4
E = -3.712E+4
F = -5.344E+4
G = -6.977E+4
H = -8.609E+4
I = -1.024E+5
J = -1.187E+5
K = 0.000E 0

MAXIMUM PRINCIPAL STRESS CONTOURS

BACK SURFACE
VERTICAL LOAD CASE

FIGURE A1.4
59
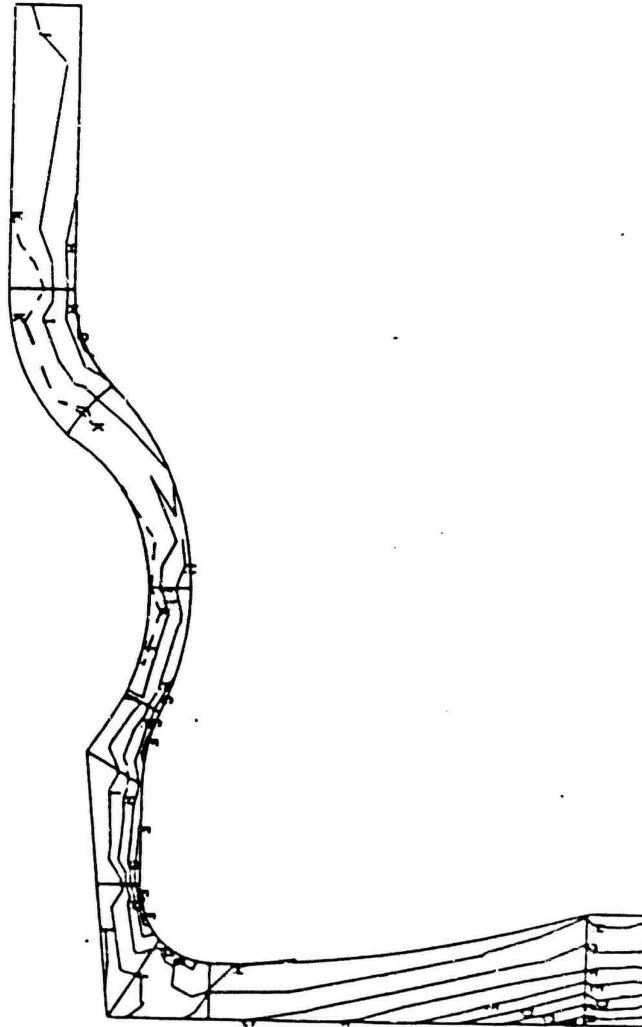
MINIMUM PRINCIPAL STRESS CONTOURS

MID PLANE CROSS SECTION SURFACE
VERTICAL LOAD CASE
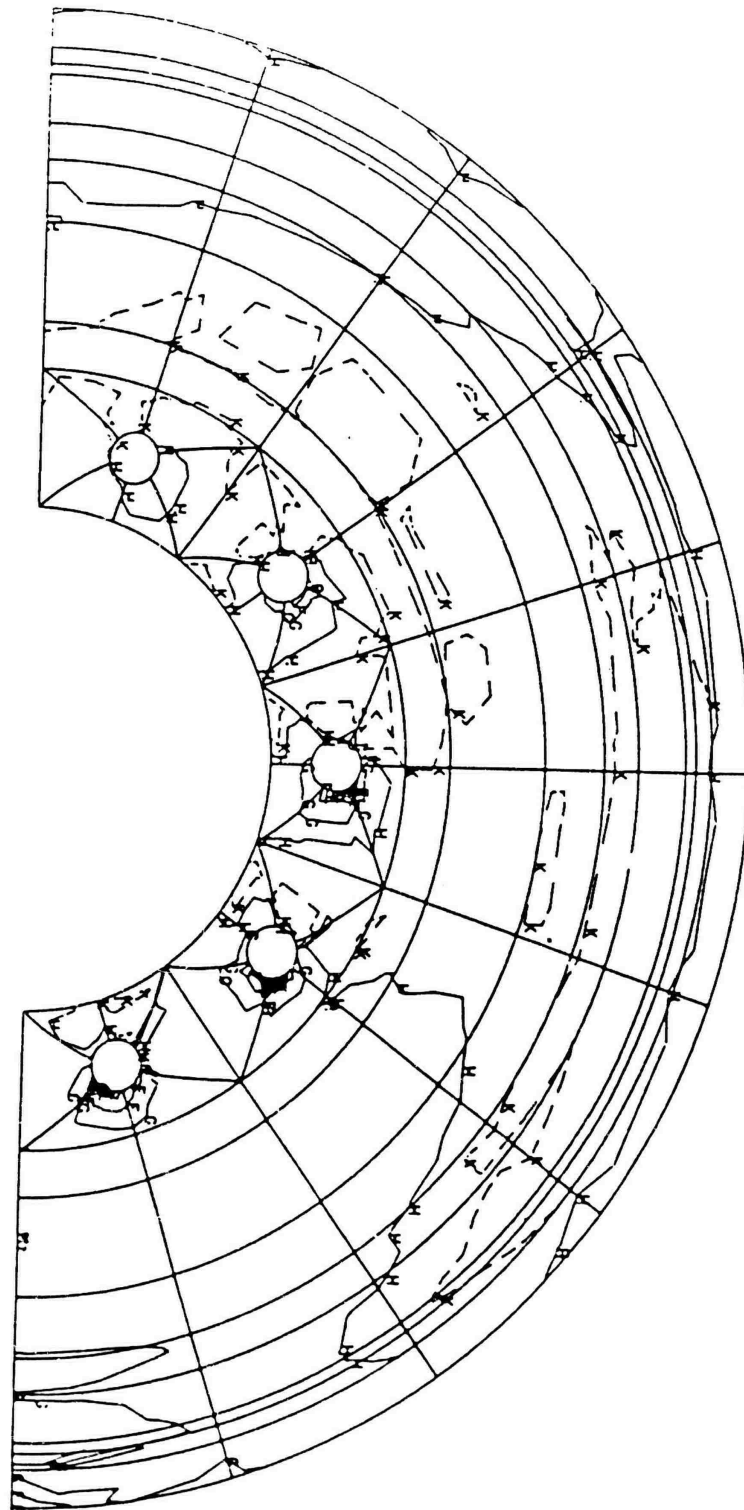
FIGURE A1.5

LEGEND

A = -1.391E+5
B = -1.200E+5
C = -1.009E+5
D = -8.183E+4
E = -6.273E+4
F = -4.363E+4
G = -2.452E+4
H = -5.423E+3
I = +1.368E+4
J = +3.278E+4
K = 0.000E 0

MINIMUM PRINCIPAL STRESS CONTOURS

FRONT SURFACE
VERTICAL LOAD CASE

FIGURE A1.6
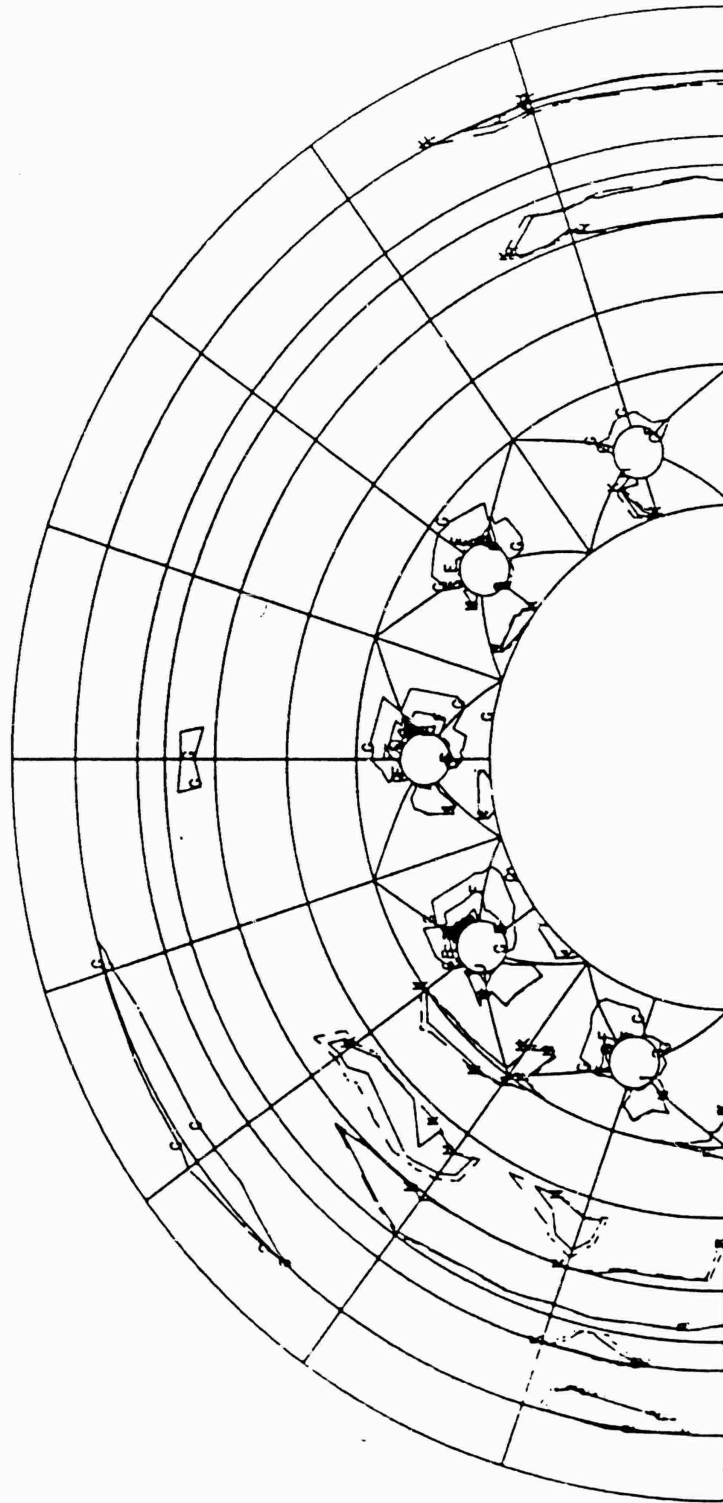
61

MINIMUM PRINCIPAL STRESS CONTOURS

BACK SURFACE
VERTICAL LOAD CASE
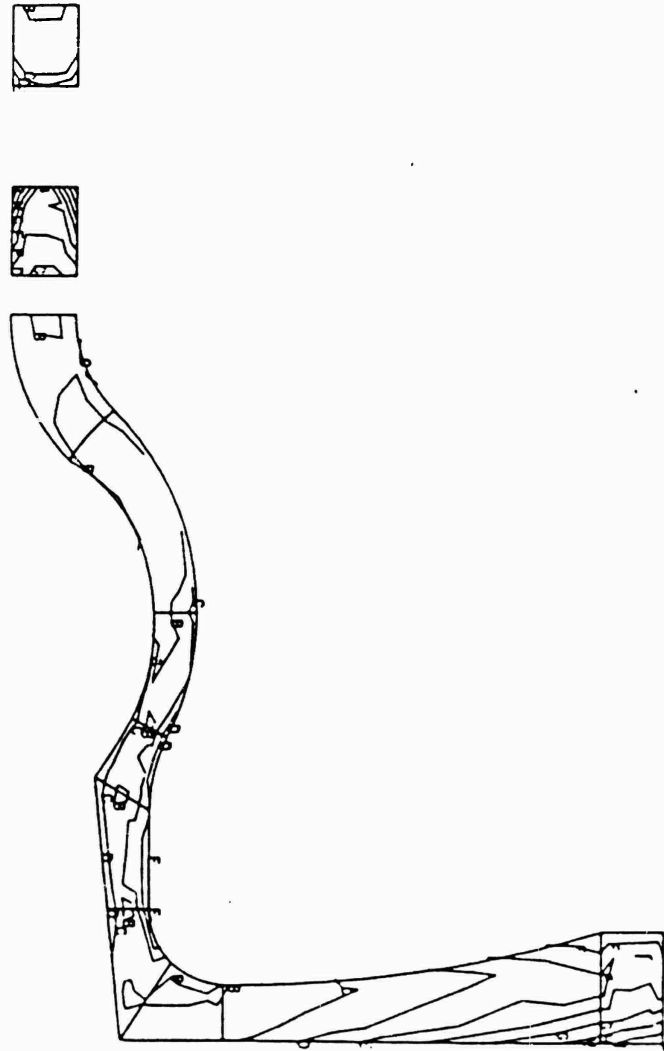
FIGURE A1.7

LEGEND

A = +1.265E+3
B = +7.816E+3
C = +1.437E+4
D = +2.092E+4
E = +2.747E+4
F = +3.402E+4
G = +4.057E+4
H = +4.712E+4
I = +5.366E+4
J = +6.023E+4
K = 0.000E 0

VON MISES EQUIVALENT STRESS CONTOURS

MID PLANE CROSS SECTION SURFACE
VERTICAL LOAD CASE

FIGURE A1.8
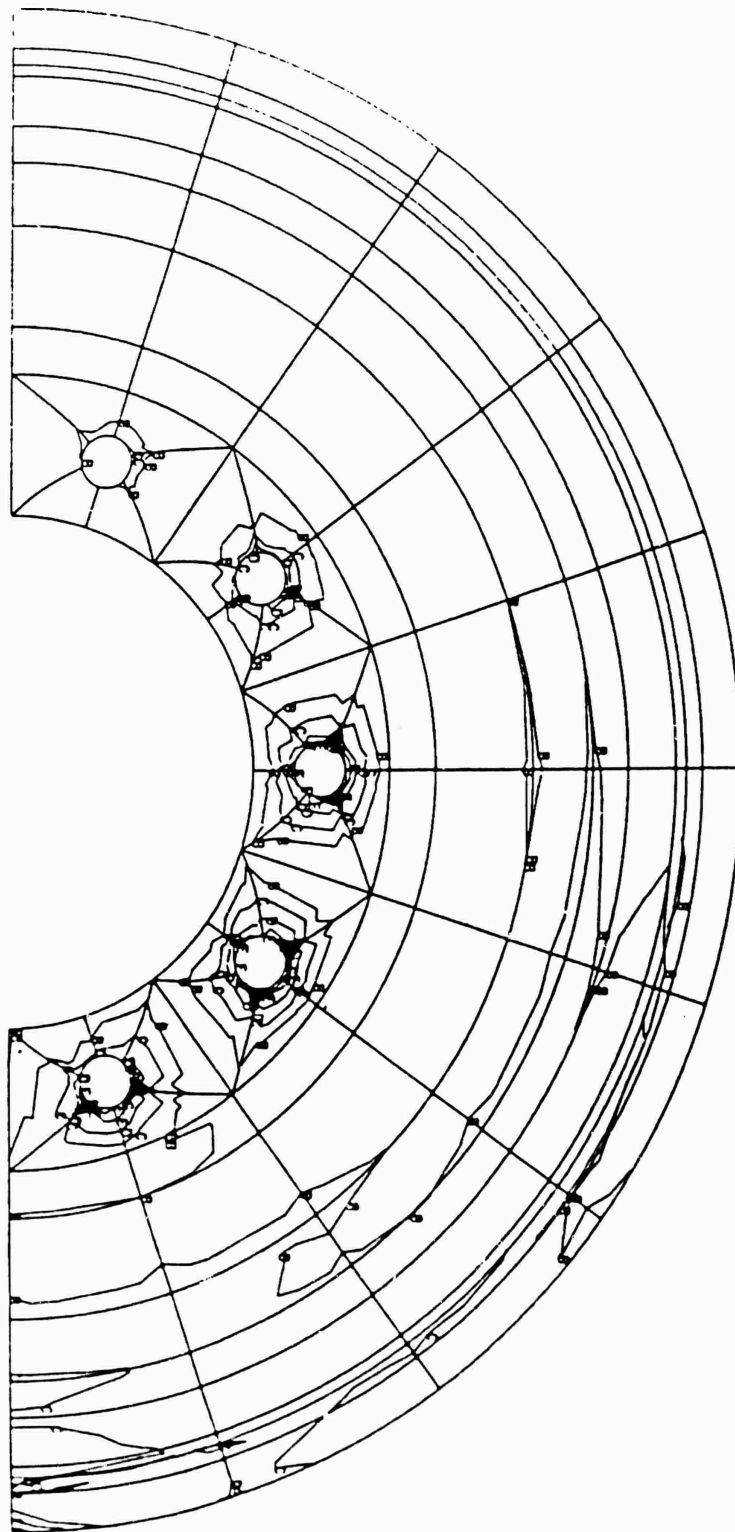
LEGEND

A = +1.256E+3 psi
B = +1.218E+4
C = +2.311E+4
D = +3.404E+4
E = +4.495E+4
F = +5.589E+4
G = +5.662E+4
H = +7.774E+4
I = +8.667E+4
J = +9.959E+4
K = 0.000E 0

VON MISES EQUIVALENT STESSS CONTOURS

FRONT SURFACE
VERTICAL LOAD CASE

FIGURE A1.9
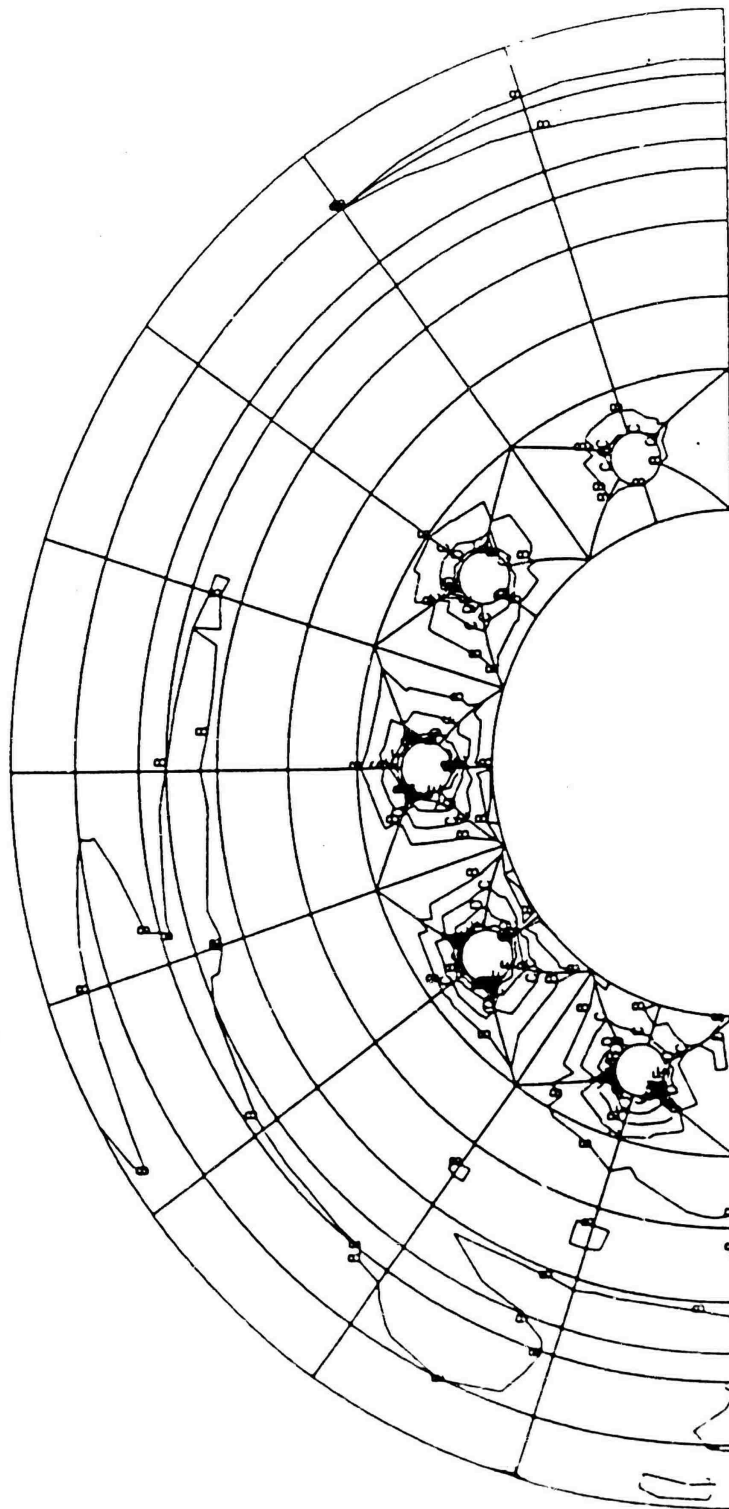
VON MISES EQUIVALENT STRESS CONTOURS

BACK SURFACE
VERTICAL LOAD CASE

FIGURE A1.10

63
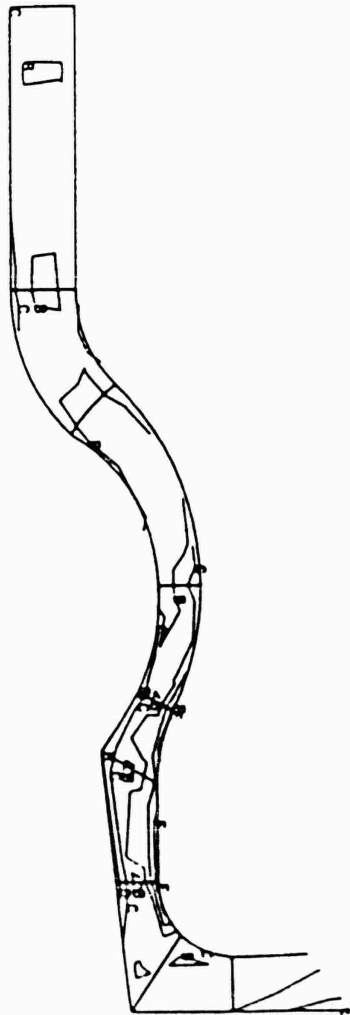
LEGEND

A = +6.930E-2 psi
B = +4.013E+3
C = +7.333E+3
D = +1.065E+4
E = +1.397E+4
F = +1.729E+4
G = +2.051E+4
H = +2.393E+4
I = +2.725E+4
J = +3.057E+4
K = 0.000E 0

MAXIMUM SHEAR STRESS CONTOURS

MID PLANE CROSS SECTION SURFACE
VERTICAL LOAD CASE

FIGURE A1.11

66
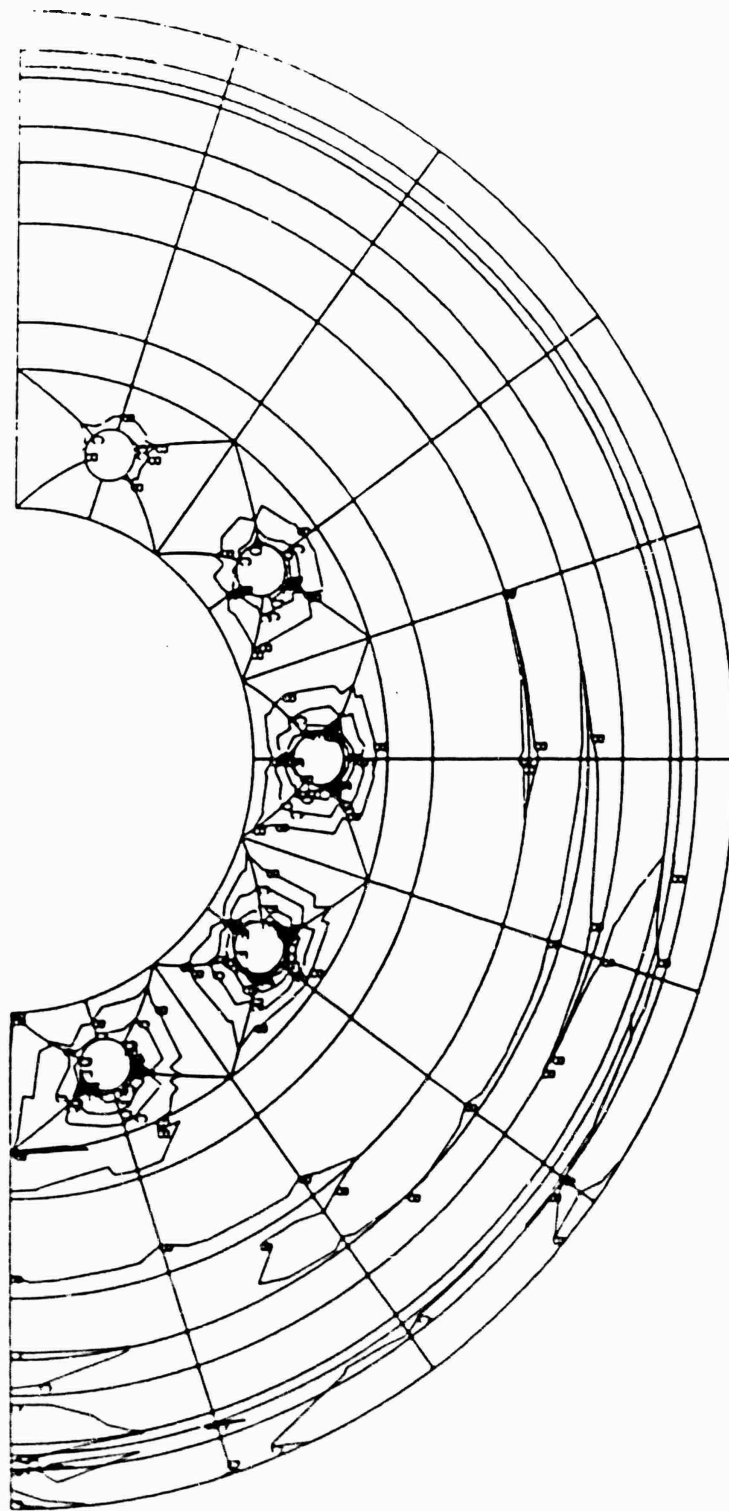
LEGEND

A = +7.219E+2 psi
B = +6.934E+3
C = +1.315E+4
D = +1.936E+4
E = +2.557E+4
F = +3.178E+4
G = +3.799E+4
H = +4.421E+4
I = +5.042E+4
J = +5.663E+4
K = 0.000E 0

MAXIMUM SHEAR STRESS CONTOURS

FRONT SURFACE
VERTICAL LOAD CASE

FIGURE A1.12

67
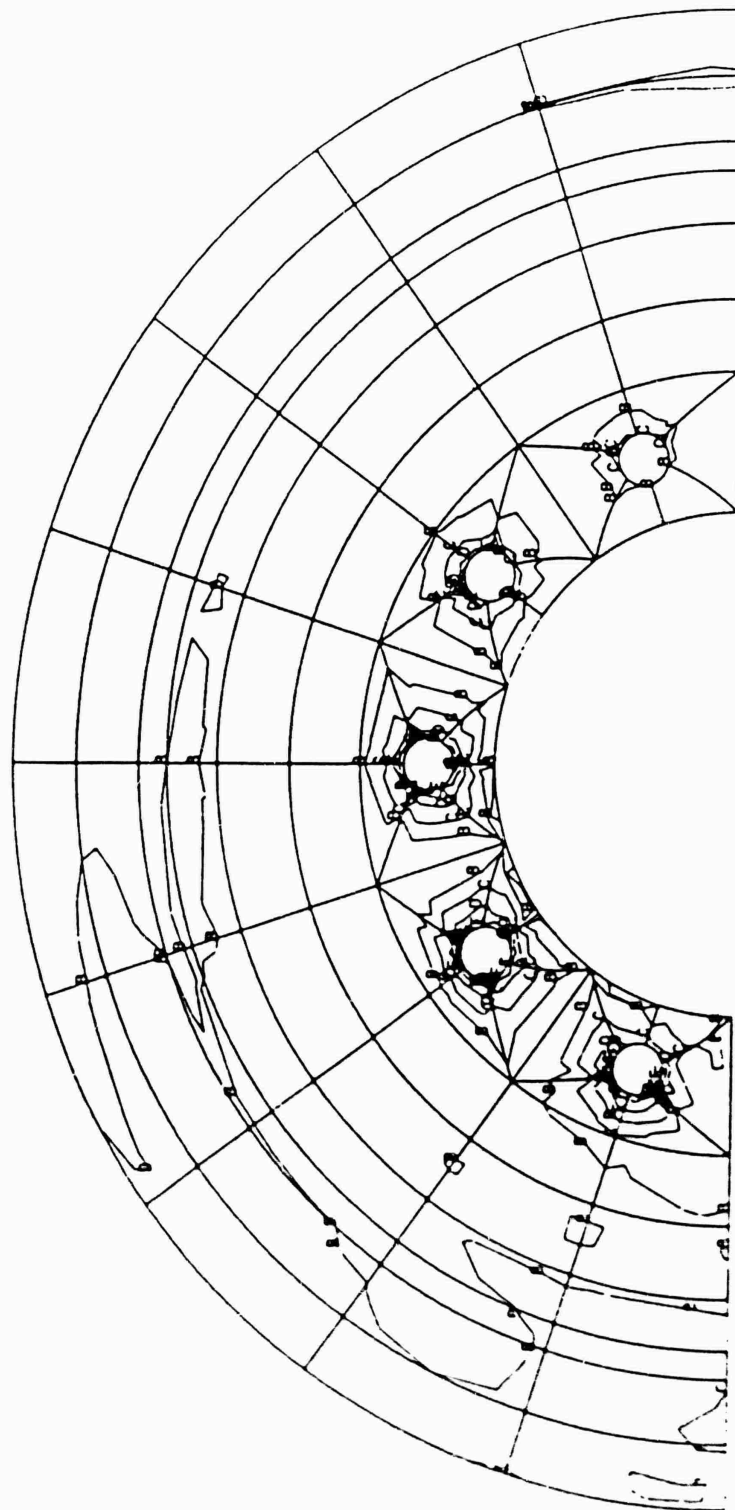
LEGEND

A = +3.101E+2 psi
B = +5.799E+3
C = +1.129E+4
D = +1.678E+4
E = +2.227E+4
F = +2.776E+4
G = +3.324E+4
H = +3.873E+4
I = +4.422E+4
J = +4.971E+4
K = 0.000E 0

MAXIMUM SHEAR STRESS CONTOURS

BACK SURFACE
VERTICAL LOAD CASE

FIGURE A1.13

68

1098 LB. LOAD UNIFORMLY DISTRIBUTED ALONG WEAR RING SEAT

1901 LB. LOAD UNIFORMLY DISTRIBUTED
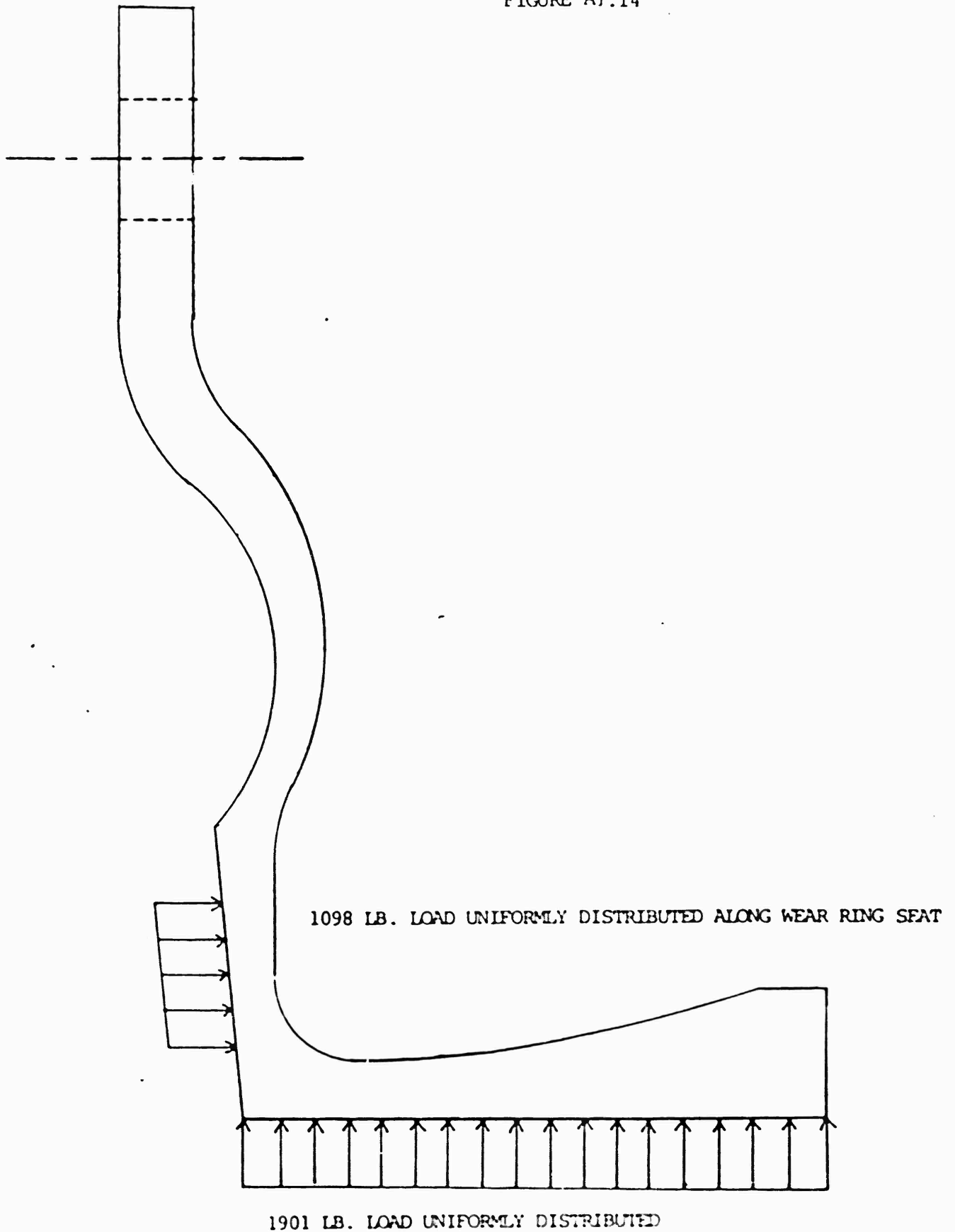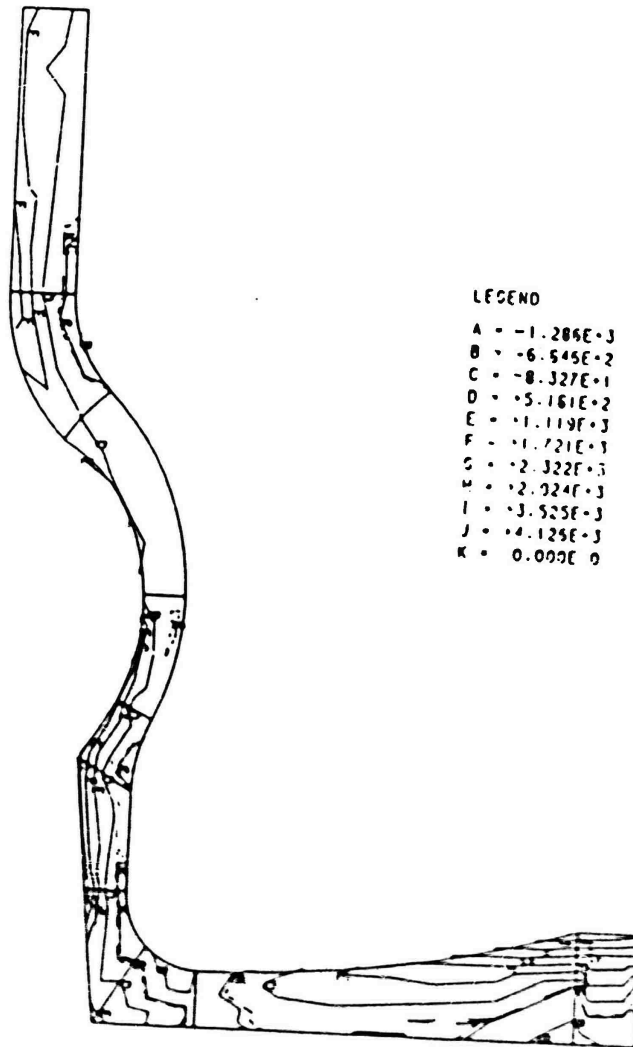
LEGEND

A = -1.285E+3 psi
B = -6.545E+2
C = -8.327E+1
D = +5.161E+2
E = +1.119E+3
F = +1.721E+3
G = +2.322E+3
H = +2.924E+3
I = +3.525E+3
J = +4.125E+3
K = 0.000E+0

MAXIMUM PRINCIPAL STRESS CONTOURS

WHEEL MID PLANE CROSS SECTION SURFACE
COMBINED SIDE AND VERTICAL LOAD CASE

FIGURE A1.15
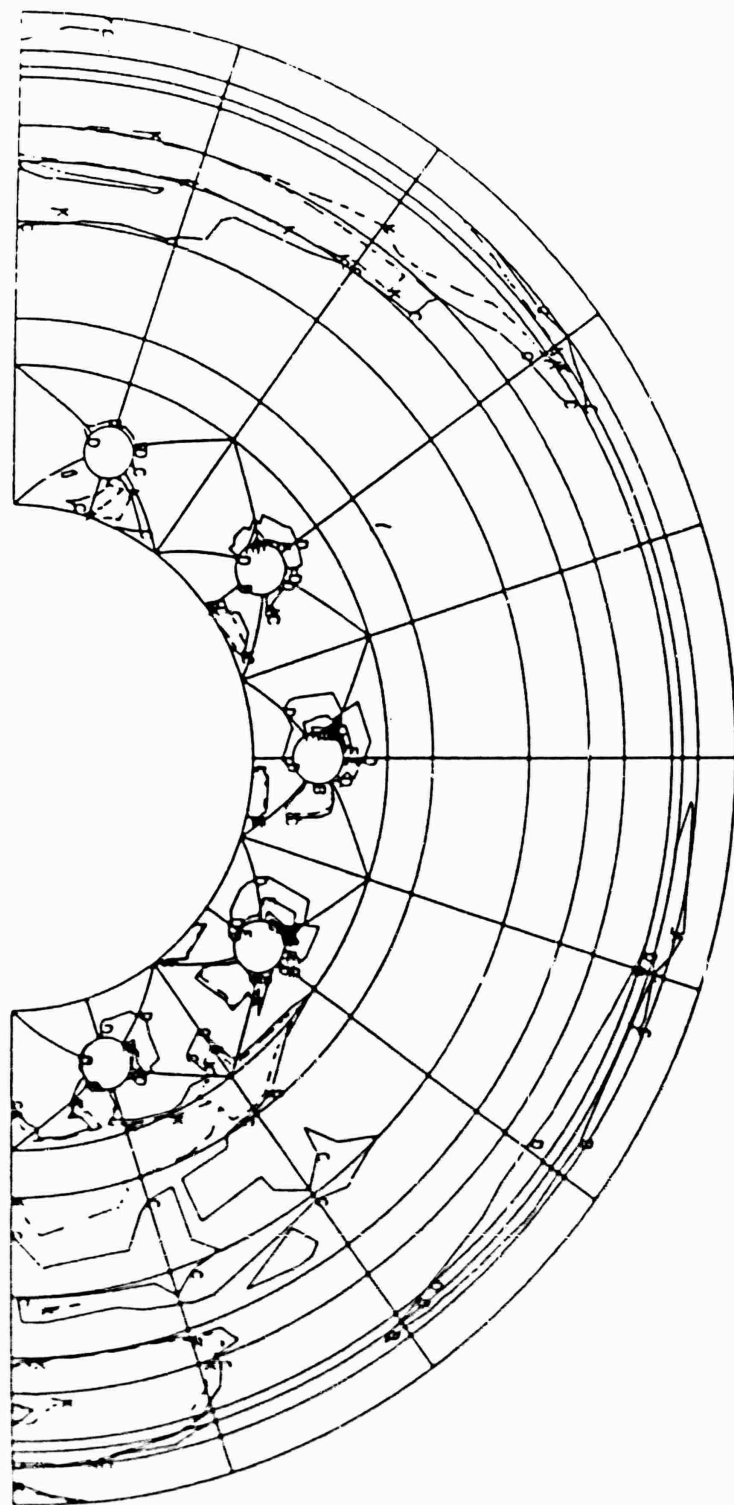
70

MAXIMUM PRINCIPAL STRESS CONTOURS

FRONT SIDE
COMBINED SIDE AND VERTICAL LOAD CASE

FIGURE A1.16

71
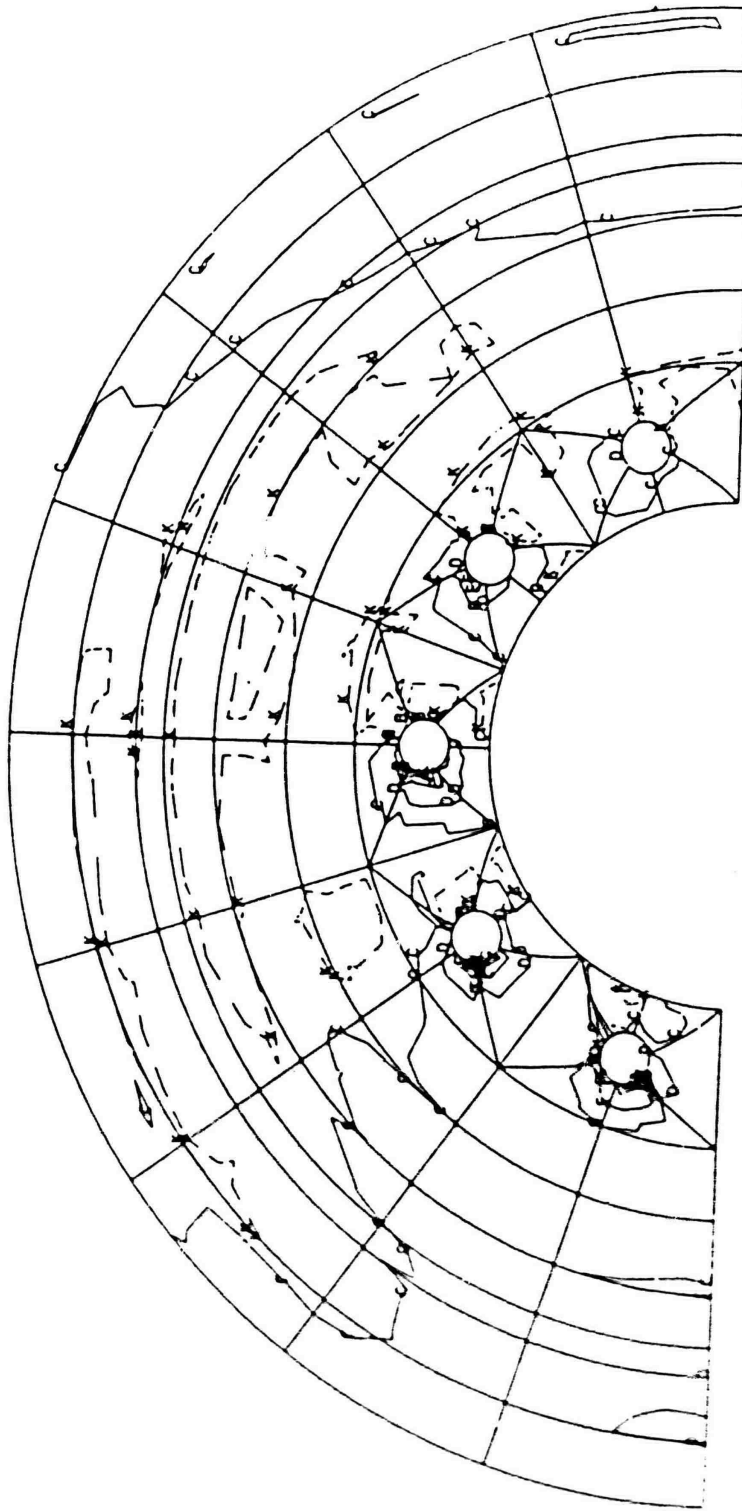
LEGEND

A = 3.416E+3 psi
B = 1.432E+3
C = 5.531E+2
D = 2.537E+3
E = 4.524E+3
F = 5.510E+3
G = 8.495E+3
H = 1.046E+4
I = 1.247E+4
J = 1.445E+4
K = 0.000E 0

MAXIMUM PRINCIPAL STRESS CONTOURS

BACK SURFACE
COMBINED SIDE AND VERTICAL LOAD CASE

FIGURE A1.17
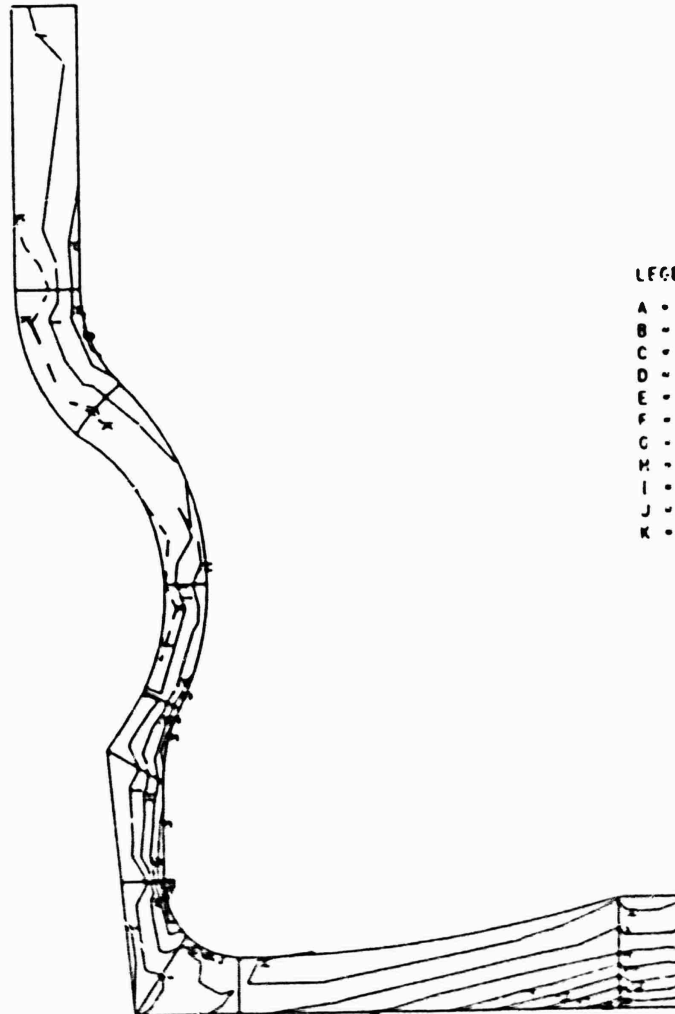
LEGEND

A = -7.639E+3 psi
B = -6.365E+3
C = -6.073E+3
D = -5.161E+3
E = -4.248E+3
F = -3.335E+3
G = -2.423E+3
H = -1.519E+3
I = -5.971E+2
J = +3.156E+2
K = 0.000E 0

MINIMUM PRINCIPAL STRESS CONTOURS

WHEEL MID PLANE CROSS SECTION SURFACE
COMBINED SIDE AND VERTICAL LOAD CASE

FIGURE A1.18

73
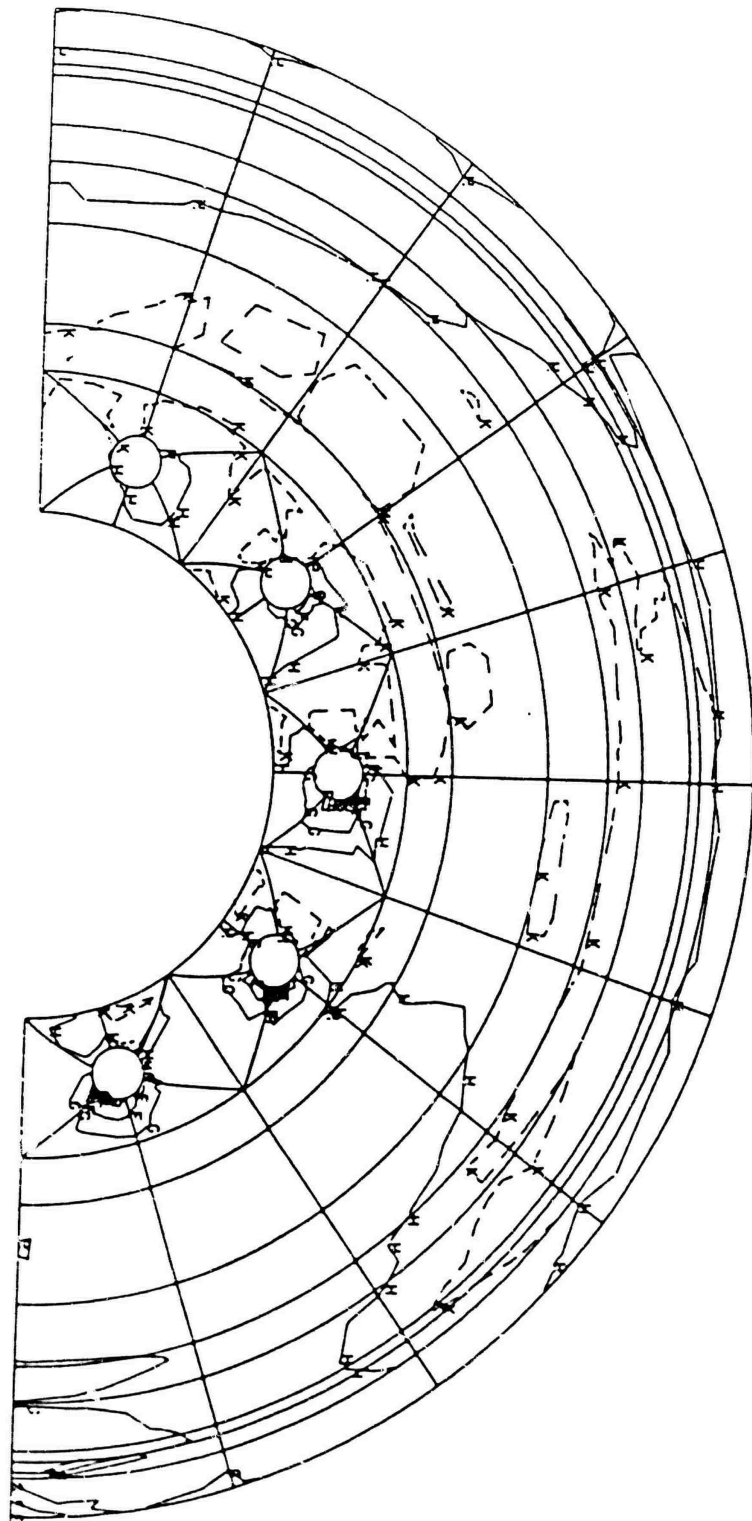
LEGEND

A = -1.700E+4 psi
B. = -1.467E+4
C = -1.234E+4
D = -1.000E+4
E = -7.673E+3
F = -5.341E+3
G = -3.009E+3
H = -6.777E+2
I = +1.654E+3
J = +3.986E+3
K = 0.000E 0

MINIMUM PRINCIPAL STRESS CONTOURS

FRONT SURFACE
COMBINED SIDE AND VERTICAL LOAD CASE

74
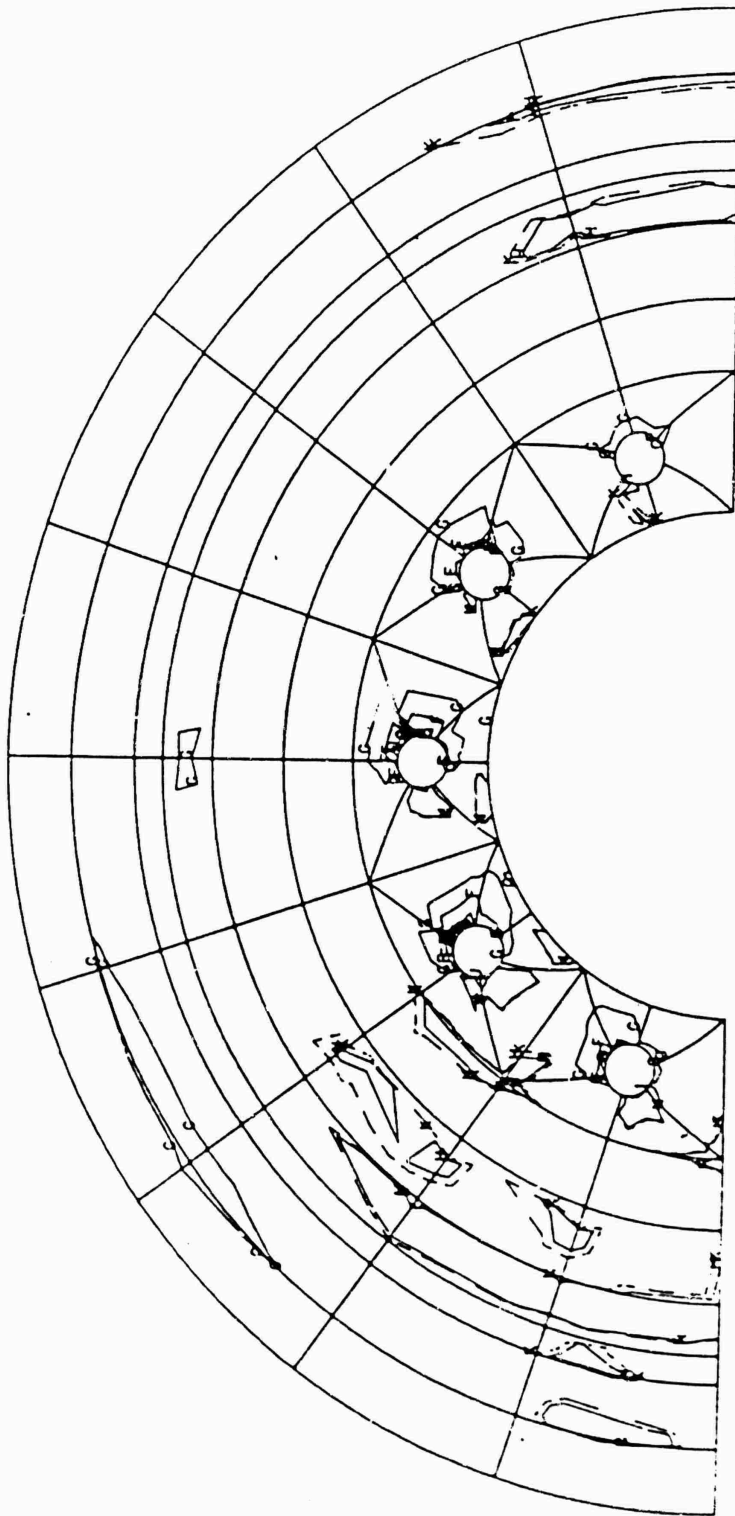
FIGURE A1.19

LEGEND

A = -1.250E+4 psi
B = -1.071E+4
C = -8.917E+3
D = -7.129E+3
E = -5.340E+3
F = -3.551E+3
G = -1.762E+3
H = +2.699E+1
I = +1.816E+3
J = +3.605E+3
K = 0.000E 0

MINIMUM PRINCIPAL STRESS CONTOURS

BACK SURFACE
COMBINED SIDE AND VERTICAL LOAD CASE

75
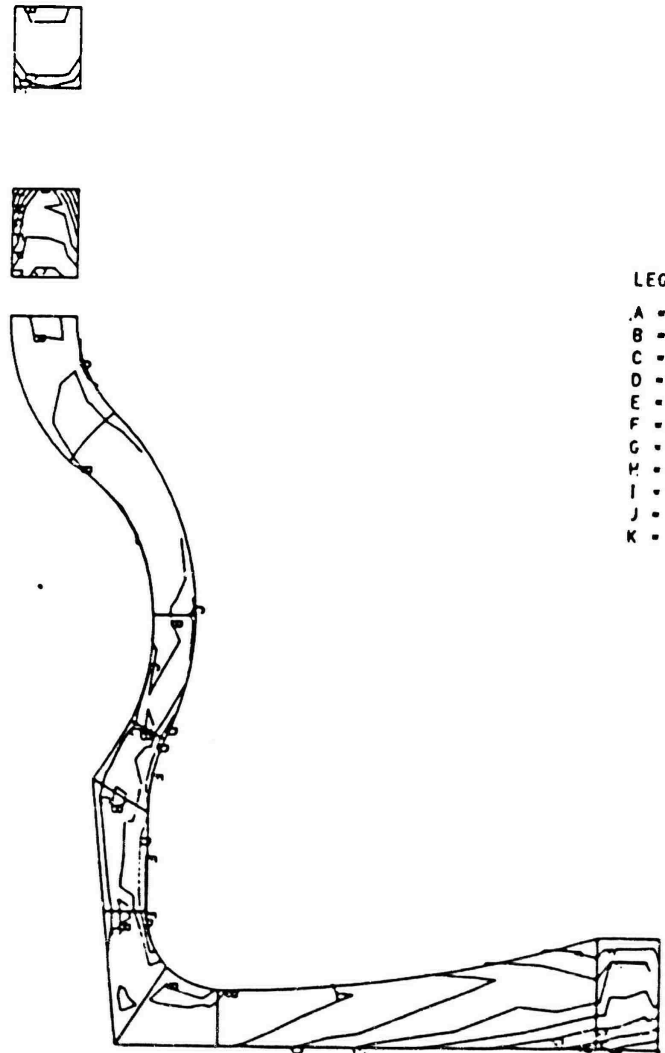
FIGURE A1.20

LEGEND

A = +1.911E+2 psi
B = +9.753E+2
C = +1.759E+3
D = +2.544E+3
E = +3.328E+3
F = +4.112E+3
G = +4.896E+3
H = +5.680E+3
I = +6.464E+3
J = +7.249E+3
K = 0.000E 0

VON MISES EQUIVALENT STRESS CONTOURS

WHEEL MID PLANE CROSS SECTION SURFACE
COMBINED SIDE AND VERTICAL LOAD CASE

FIGURE A1.21

76
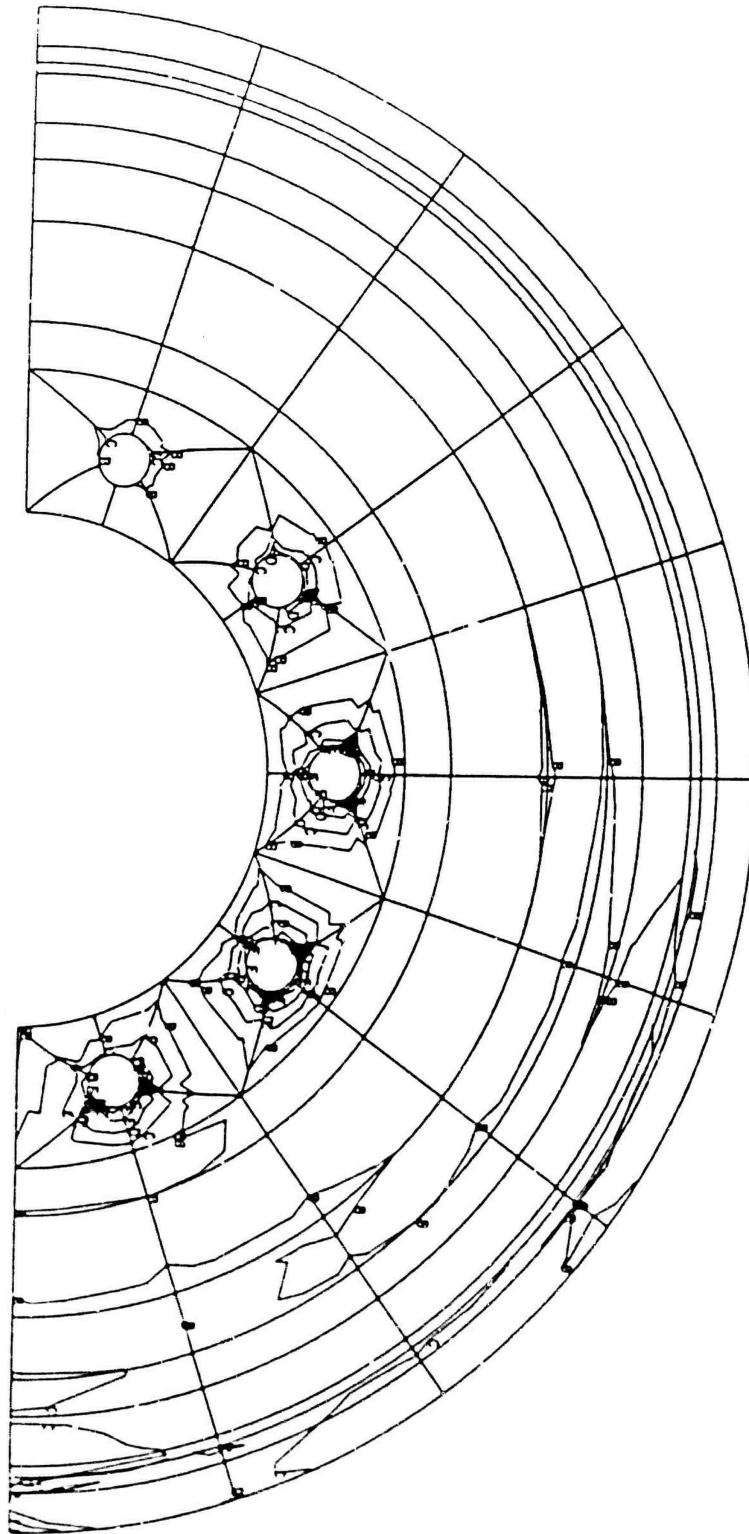
LEGEND
A = +1.516E+2 psi
B = +1.484E+3
C = +2.615E+3
D = +4.147E+3
E = +5.479E+3
F = +6.811E+3
G = +8.142E+3
H = +9.474E+3
I = +1.081E+4
J = +1.214E+4
K = 0.000E 0

VON MISES EQUIVALENT STRESS CONTOURS

FRONT SURFACE
COMBINED SIDE AND VERTICAL LOAD CASE

77
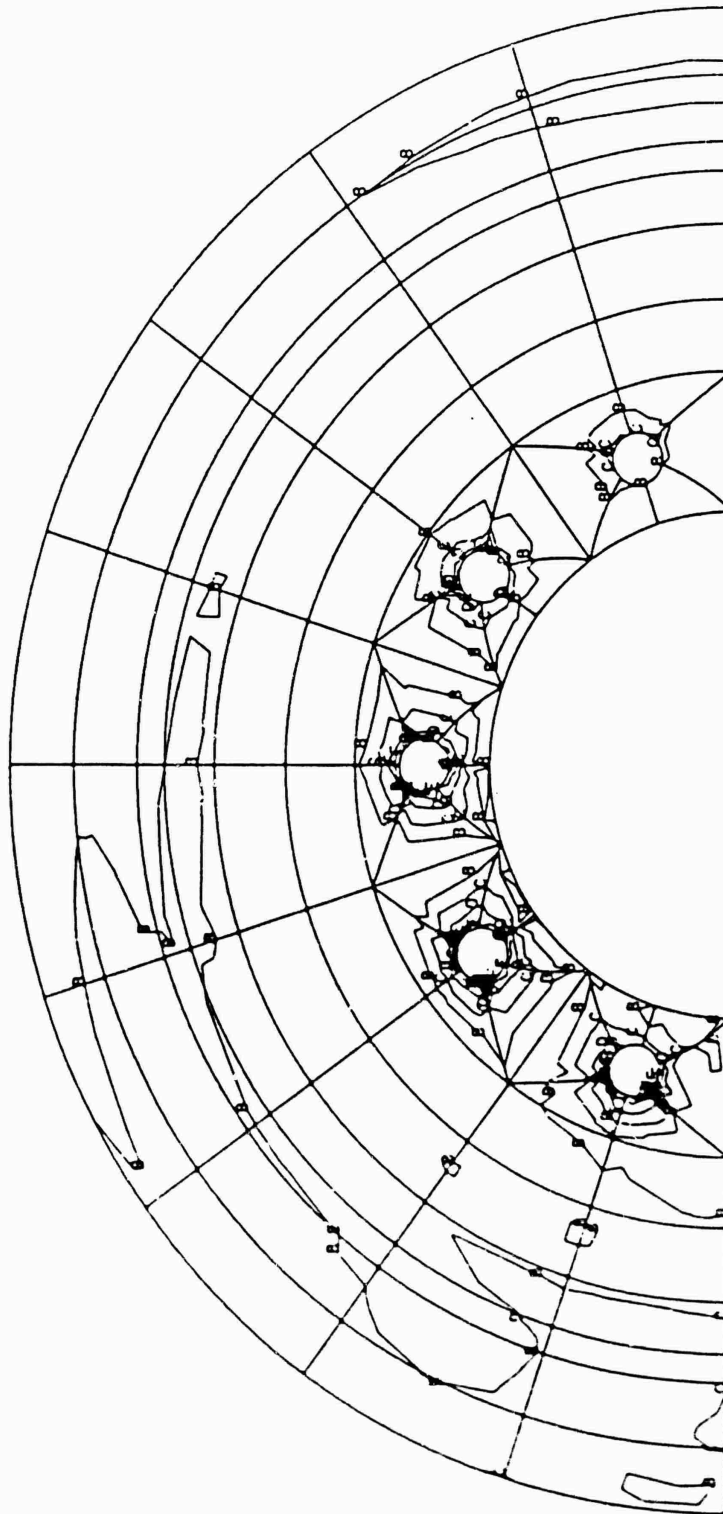
FIGURE A1.22

LEGEND

A = +5.855E+10 ~ 1
B = +1.251E+3
C = +2.434E+3
D = +3.617E+3
E = +4.600E+3
F = +5.983E+3
G = +7.165E+3
H = +8.348E+3
I = +9.531E+3
J = +1.071E+4
K = 0.000E 0

VON MISES EQUIVALENT STESSS CONTOURS

BACK SURFACE
COMBINED SIDE AND VERTICAL LOAD CASE

78

FIGURE A1.23

LEGEND

A = +1.057E+2 psi
B = +5.035E+2
C = +9.019E+2
D = +1.300E+3
E = +1.698E+3
F = +2.095E+3
G = +2.494E+3
H = +2.892E+3
I = +3.290E+3
J = +3.566E+3
K = 0.000E 0
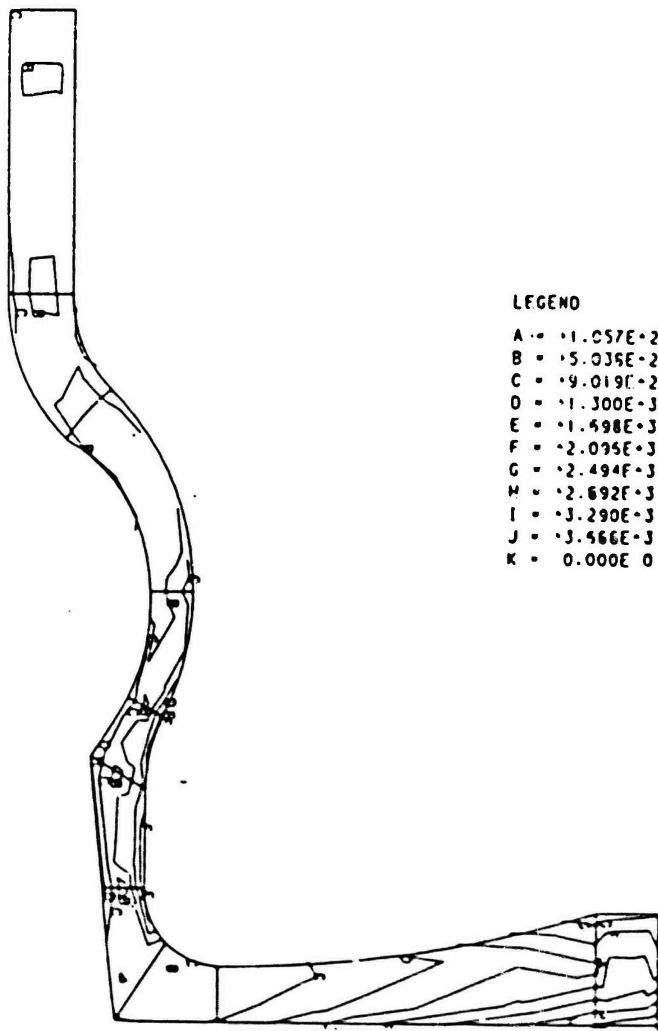
MAXIMUM SHEAR STRESS CONTOURS

WHEEL MID PLANE CROSS SECTION SURFACE
COMBINED SIDE AND VERTICAL LOAD CASE

FIGURE A1.24

79
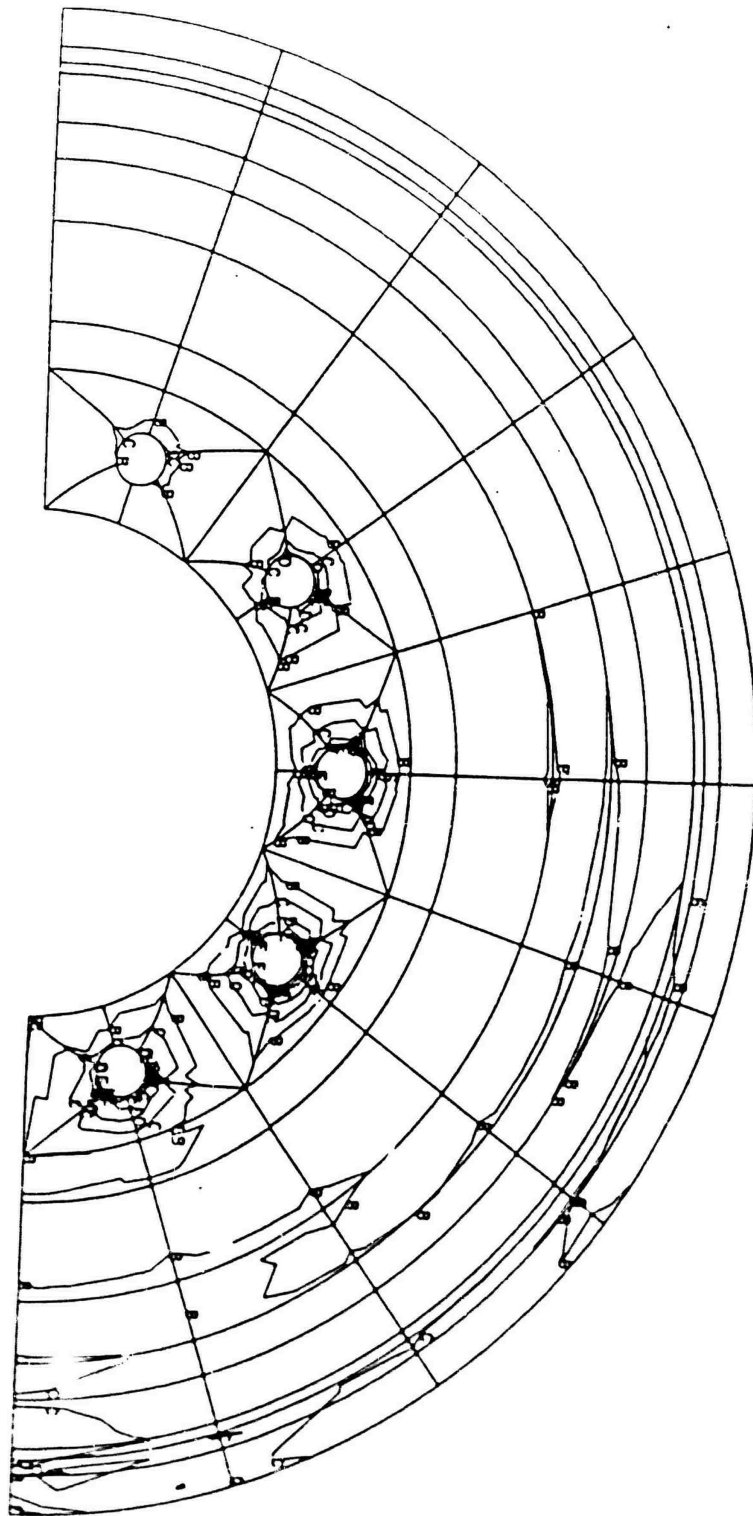
LEGEND

A = ·8.711E·1psi
B = ·8.442E·2
C = ·1.601E·3
D = ·2.356E·3
E = ·3.115E·3
F = ·3.572E·3
G = ·4.630E·3
H = ·5.387E·3
I = ·6.144E·3
J = ·6.901E·3
K = 0.000E 0

MAXIMUM SHEAR STRESS CONTOURS

FRONT SURFACE
COMBINED SIDE AND VERTICAL LOAD CASE

FIGURE A1.25

80
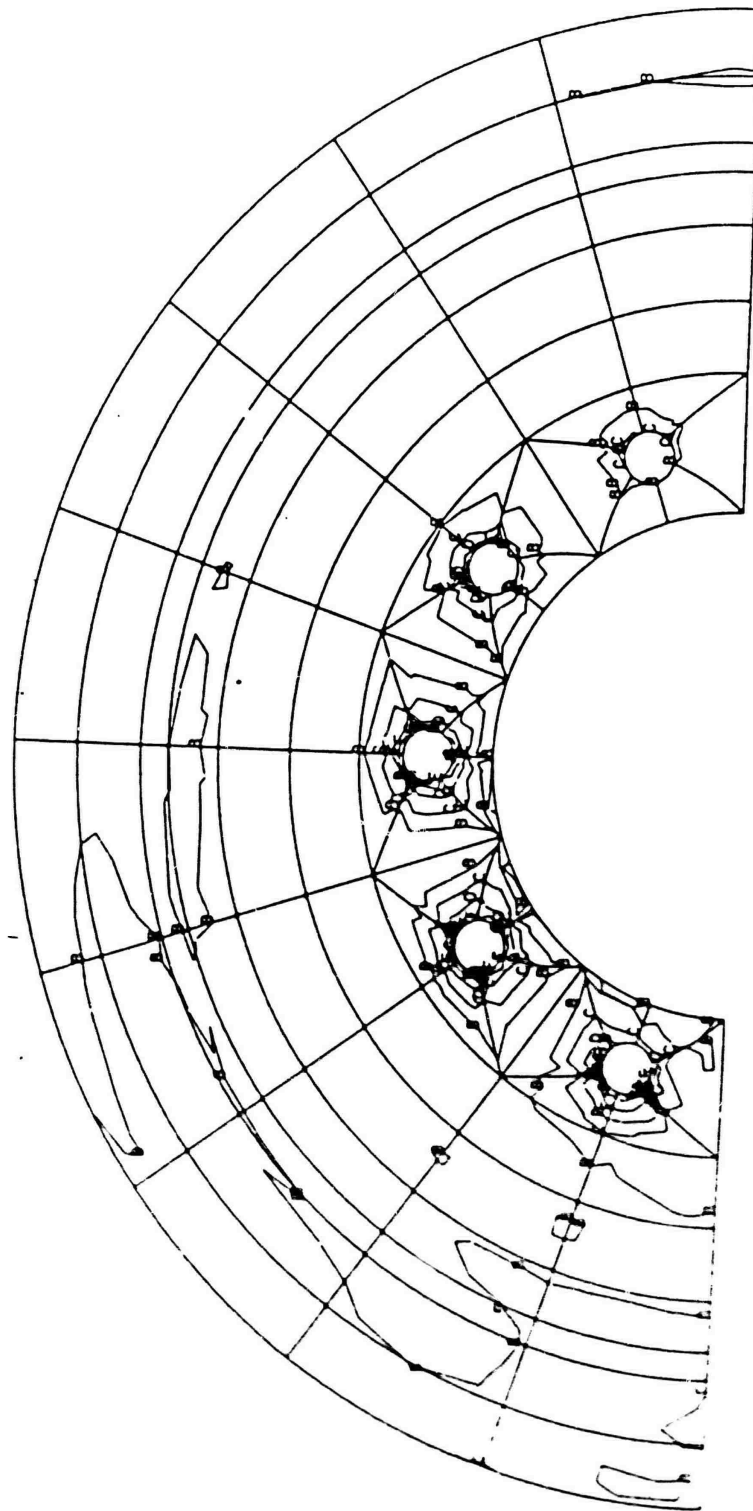
LEGEND

A = ·3.891E·1 psi
B = ·7.091E·2
C = ·1.379E·3
D = ·2.049E·3
E = ·2.720E·3
F = ·3.390E·3
G = ·4.060E·3
H = ·4.730E·3
I = ·5.400E·3
J = ·6.071E·3
K = 0.000E 0

MAXIMUM SHEAR STRESS CONTOURS

BACK SURFACE
COMBINED SIDE AND VERTICAL LOAD CASE

FIGURE A1.26

APPENDIX 2

CALCULATION OF FLEXURAL STIFFNESS COMPONENT
OF LVTP7 WHEEL RIM

APPENDIX 2

CALCULATION OF PRIMARY FLEXURAL MODULUS OF LAMINATE IN RIM OF LVTP7 ROADWHEEL
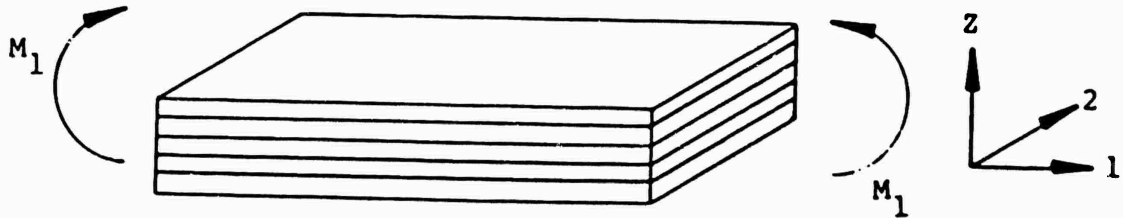
Figure A.2.1

The flexural stiffness of a laminate is given by Tsai and Hahn[1] as:

$$
\begin{array}{c|ccc}
 & K_1 & K_2 & K_6 \\
\hline
M_1 & D_{11} & D_{12} & D_{16} \\
M_2 & D_{21} & D_{22} & D_{26} \\
M_6 & D_{61} & D_{62} & D_{66}
\end{array}
\qquad (A.2.1)
$$

eg. $M_1 = D_{11}K_1 + D_{12}K_2 + D_{16}K_6$

where M_i are the applied movements K_i as the curvatures of the laminate and D_{ij} are the components of flexural modulus which couple curvatures in all in-plane directions to applied moments. For hoop flexure of the composite wheel rim, the curvature components along the longitudinal hoop

83

axis K_2 and in the plane of the laminate K_6 are small compared to K_1. We seek to find D_{11}. For a general laminate:

$$D_{ij} = \frac{h_o^3}{3} \sum_{t=1-n/2}^{n/2} Q_{ij}^{(t)} [t^3 - (t-1)^3] \qquad (A.2.2)$$

where h_o = ply thickness

Q_{ij} = components of in-plane modulus

t = ordinal number of plies as they go from $1-n/2$ to $n/2$

n = total number of plies

D_{11} will be calculated for a 16 ply laminate simulating the fractions of hoop to $\pm 15°$ layers.

PLY	ORIENTATION	$t^3 - (t-1)^3$	Q_{11} x 10^6psi
8	H	169	21
7	15	127	1.7
6	H	91	21
5	H	61	21
4	-15	37	1.7
3	H	19	21
2	H	7	21
1	15	1	1.7 Mid-Plane
1	-15	1	1.7
2	H	7	21
3	15	19	1.7
4	H	37	21
5	-15	61	1.7
6	H	91	21
7	15	127	1.7
8	H	169	21

Figure A.2.2

$$Q_{11} = 21 \times 10^6 \text{ psi for hoop layers}$$

$$Q_{11} = 1.7 \times 10^6 \text{ psi for } \pm 15 \text{ layers}$$

$$h_o = .0625 \text{ in.}$$

$$D_{11} = \frac{h_o^3}{3} \sum_{t=-7}^{8} Q_{11}^{(t)} [t^3 - (t-1)^3]$$

$$D_{11} = 1.164 \times 10^6 \text{ lb-in}$$

The equivalent EI or flexural rigidity of the composite rim, bD_{11} where b = .5 in., an assumed rim width

$$bD_{11} = EI|_{e_r} = .582 \times 10^6 \text{ lb-in}^2$$

For a 1/2 inch width of the outer most portion of the aluminum rim

$$EI_{al} = (10.6 \times 10^6)\frac{(.5)(.9)^3}{12}$$

$$EI_{al} = .339 \times 10^6 \text{ lb-in}^2$$

The ratio of hoop flexural rigidity of the graphite/epoxy to the aluminum rim is 1.72.

APPENDIX 3

DRAWINGS OF LVTP7 AND M113A1
COMPOSITE WHEELS

WEAR RING DETAIL

SECTION A:A
WHEEL DISK DETAIL

FIBER MATERIALS, INC.

LVTP-7 ROADWHEEL

D | 740-0008

SECTION A-A
WHEEL DISC DETAIL

No. of Copies	To
	Commander, Defense Technical Information Center, Cameron Station, Building 5, 5010 Duke Street, Alexandria, VA 20301
12	ATTN: DTIC-TCA
	Director, National Security Agency, Fort George G. Meade, MD 20755
2	ATTN: TDL
	DCA Defense Command Engineering Center, 1860 Wiehle Avenue, Reston, VA 22090
2	ATTN: Code R123, Technical Library
	Defense Command Agency, Technical Library Center, Washington, DC 20375
2	ATTN: Code 204 (P. A. Tolovi)
	Commandant, U.S. Army Infantry School, Fort Benning, GA 31905
1	ATTN: ATSH-CD-MS-E
	Commander, U.S. Army Test & Evaluation Command, Aberdeen Proving Ground, Aberdeen Proving Ground, MD 21005
2	ATTN: DRSTE-CT-C
2	DRSTE-ME
2	Director, U.S. Army Human Engineering Laboratories, Aberdeen Proving Ground, MD 21005
	Director, U.S. Army Materiel Systems Analysis Activity, Aberdeen Proving Ground, MD 21005
2	ATTN: DRXSY-T
2	DRXSY-MP
	Commander, U.S. Army Yuma Proving Ground, Yuma, AZ 85364
1	ATTN: STEYP-MTD (Technical Library)
	Commander, U.S. Army Armament, Munitions & Chemical Command, Dover, NJ 07801
2	ATTN: DRDAR-PML
2	Technical Library
2	Mr. Harry E. Pebly, Jr., Plastec Director
	Commander, U.S. Army Armament, Munitions & Chemical Command, Watervliet, NY 12189
1	ATTN: DRDAR-LCB-S
1	SARWV-PPI
	Commander, U.S. Army Armament, Munitions & Chemical Command, Rock Island, IL 61299
2	ATTN: DRSAR-IRB
1	DRSAR-IMC
2	Technical Library

No. of Copies	To
	Commander, U.S. Army Foreign Science & Technology Center, 220 7th Street N.E., Charlottesville, VA 22901
2	ATTN: DRXST-SD3
	Commander, Rock Island Arsenal, Rock Island, IL 61299
1	ATTN: SARRI-EN
	Commander, Advanced Technology Laboratory, AMRTL, Fort Eustis, VA 23604
1	ATTN: SAVDL-EU-TAS
	Commander, U.S. Army Mobility Equipment Research & Development Command, Fort Belvoir, VA 22060
2	ATTN: DRDME-V, Mr. E. York
2	DRDME-U
	Director, U.S. Army Ballistic Research Laboratory, Aberdeen Proving Ground, Aberdeen Proving Ground, MD 21005
1	ATTN: DRDAR-TSB-S (STINFO)
	Commander, U.S. Army Tank-Automotive Command, Warren, MI 48090
1	ATTN: DRSTA-R
1	DRSTA-RCKM
1	DRCPM-M113
1	DRSTA-RCKT
1	Technical Library
1	DRSTA-EB
1	DRCPM-CVT
1	DRCPM-FVS
1	DRCPM-GCM
1	DRCPM-M60
1	DRCPM-M9
1	DRCPM-LA
	Commander, U.S. Army Natick Research & Development Center, Natick, MA 01760
1	ATTN: DRDNA-Z
	Commander, U.S. Army Materiel Command, 5001 Eisenhower Avenue, Alexandria, VA 22333
2	ATTN: DRCMT
2	DRCLD
2	DRCPM
	Commander, U.S. Army Armament, Munitions & Chemical Command, Dover, NJ 07801
2	ATTN: Mr. Harry E. Pebly, Jr., Plastec Director
	Office of the Under Secretary of Defense for Research and Engineering, The Pentagon, Washington, DC 20301
1	ATTN: Dr. L. L. Lehn, Room 3D 1079

No. of Copies	To

Office of Naval Research, Arlington, VA 22217
1 ATTN: Code 427

Commanding Officer, Naval Research Laboratory, Washington, DC 20375
1 ATTN: Code 2627

Commander, Naval Ocean Systems Center, San Diego, CA 92152
1 ATTN: Library

Commander, Naval Surface Weapons Center, White Oak Laboratory,
Silver Springs, MD 20910
2 ATTN: Library, Code WX-21

Commander, NAVENVPREDRSCHFAC, Monterey, CA 93940
1 ATTN: Technical Library

Office of Naval Research, 800 N. Quincy Street, Arlington, VA 22217
1 ATTN: Dr. T. G. Berlincourt (Code 429)

Headquarters, Naval Material Command, Washington, DC 20360
2 ATTN: Code MAT-042M

Headquarters, Naval Air Systems Command, Washington, DC 20361
1 ATTN: Code 5203

Headquarters, Naval Sea Systems Command, 1941 Jefferson Davis Highway,
Arlington, VA 22376
1 ATTN: Code 035

Commandant, Marine Corps, Headquarters, U.S. Marine Corps,
Washington, DC 20380
2 ATTN: Code LMC

1 Commandant, Control & Communication Division Development Center, Marine Corps
Development & Education Command, Quantico, VA 22134

David W. Taylor Naval, Ship R&D Center, Bethesda, MD 20084
4 ATTN: Mr. E. Wolfe, Code 1129

American Defense Preparedness Association, Rosslyn Center, Suite 900,
1700 N. Moore Street, Arlington, VA 22209
1 ATTN: William G. Gustafson

FMC Corporation, Ordnance Division, 1125 Coleman Avenue, Box 367,
San Jose, CA 95103
1 ATTN: Roland B. Hare

FMC Corporation, Composites Division, 1105 Coleman Avenue, Mail Drop 400,
San Jose, CA 95052
1 ATTN: Dr. James Hill

No. of Copies	To

Textile Fibers Department, EI DuPont DeNemours & Company, Centre Road Building, Wilmington, DE 19898
1 ATTN: William A. Crump

Owens Corning Fiberglas, Composites Development Laboratory, Technical Center, Granville, OH 43023
1 ATTN: Earl M. Zion

Owens Corning Fiberglas, Advanced Composites, Marketing Section, Fiberglas Tower, Toledo, OH 43659
1 ATTN: Larry Dickson

Goodyear Aerospace Corporation, Arizona Division, Litchfield Park, AZ 85340
1 ATTN: Mr. J. D. Locke, D/465A, Building 2

Swedlow, Incorporation, 12122 Western Avenue, Garden Grove, CA 92645
1 ATTN: William Yamaguchi

Director, Army Materials and Mechanics Research Center, Watertown, MA 02172-0001
2 ATTN: DRXMR-PL
1 DRXMR-PAT
1 DRXMR-K
10 DRXMR-OM, P. Dehmer

AD ___UNCLASSIFIED___
UNLIMITED DISTRIBUTION

Army Materials and Mechanics Research Center
Watertown, Massachusetts 02172
DESIGN AND ANALYSIS OF COMPOSITE
ROADWHEEL FOR LVTP7 and M113A1
K.E. Burgess, J. Pepin, S. Biddle
Fiber Materials, Incorporated
Biddeford, Maine 04005

Key Words

Composites
Carbon/Epoxy
Weight Reduction

Technical Report AMMRC TR 84-33 January 1985, 94 pp.
Illus. - tables, Contract DAAG46-83-C-0026
D/A Project: 1L162105AH84
AMCMS Code: 612105. H840011
Final Report, May 83 to October 83

The program goal was to evaluate the feasibility and establish the design criteria for reinforced plastic roadwheels for the LVTP7 and M113A1 armored personnel carriers. Additional objectives included reducing weight and lowering production costs while retaining or increasing the service life as compared to the current metal construction. An analysis of the existing roadwheels was first undertaken to establish areas of high stress and deflection. The data acquired from these analyses was then used to select materials, fiber architecture and geometry of the composite roadwheels. Epoxy reinforced with carbon fibers was selected as the preferred material. A weight reduction of about 30% is predicted for the composite designs relative to the current metal wheels. Manufacturing analyses were done to establish the most suitable production techniques and the estimated costs. Autoclave molding was selected as the preferred construction method.